Spatiotemporal control of clathrin-mediated endocytosis by PI3K C2α and phosphatidylinositol-3,4-bisphosphate

Inaugural-Dissertation

to obtain the academic degree

Doctor rerum naturalium (Dr.rer.nat.)

submitted to the Department of Biology, Chemistry and Pharmacy

of Freie Universität Berlin

by

YORK POSOR

from Berlin, Germany

2013

Period of doctorate studies:	January 2009 to June 2013
Supervisor:	Prof. Dr. Volker Haucke
Institute:	Institute of Chemistry & Biochemistry, Freie Universität Berlin (2009 to August 2012) and Leibniz Institut für Molekulare Pharmakologie (FMP), Berlin-Buch (from September 2012)

1st Reviewer: Prof. Dr. Volker Haucke

2nd Reviewer: Prof. Dr. Christian Freund

Date of defense: November 13th, 2013

Acknowledgements

I am deeply grateful for the excellent training and supervision that I received from **Volker Haucke** during the time of my PhD studies in his lab as well as throughout the time of my undergraduate studies. His enthusiasm for science has been a constant source of motivation and the intense and frequent discussions about my work have been instrumental to the successful research that led to this thesis.

I would like to thank **Marnix Wieffer** and **Michael Krauß** for investing considerable amounts of their time into getting me started in the lab. You helped me overcome numerous experimental problems that I was not sure how to deal with!

I owe sincere thanks to **Marielle Eichhorn-Grünig**. She joined our lab and my project at a time when I was still struggling to find the missing effector protein. Her experimental support and our mutual interest into this project were essential for our ultimate success.

Special thanks go to **Dmytro Puchkov** for support on the ultrastructural side of life. Also, I need to acknowledge the intriguing and furtive collaboration that we set up with the group of **Frank Noé** and would like to thank **Johannes Schöneberg** and **Andreas Ulrich** for our lively and entertaining discussion on how to model maturing pits.

I am also grateful for the support from **Carsten Schultz** and his group at the EMBL in Heidelberg. The retreat at Lago di Como was a true treat indeed!

I would further like to acknowledge all other present and past members of the 'AG Haucke' who contributed to creating a unique atmosphere that has always been cheerful, collaborative, and enjoyable and yet never failed to promote efficiency:
Jelena Bacetic, Katharina Branz, Katrin Diesenberg, Fabian Feutlinske, Uwe Fink, Niclas Gimber, Claudia Gras, Isabelle Grass, Kira Gromova, Sabine Hahn, Burkhard Jakob, Lisa Jerndal, Natalie Kaempf, Christina Kath, Nina Kahlfeldt, Peter Koch, Gaga Kochlamazashvili, Natalia Kononenko, Seong Joo Koo, Ludwig Krabben, André Lampe, Wen-Ting Lo, Martin Lehmann, Gregor Lichtner,

Andrea Marat, Tanja Maritzen, Julia Mössinger, Maria Mühlbauer, Arndt Pechstein, Jasmin Podufall, Yijian Rao, Christine Rückert, Jan Schmoranzer, Irene Schütz, Wiebke Stahlschmidt, Susanne Thomsen, Anela Vukoja, Ingeborg Walther and Susanne Wojtke.

Lastly, but most importantly, I want to express my gratitude to **Gala Claßen** and **my parents** for being true pillars of strength to me. After all, no matter how consuming my work turned out to be, you never failed to support and reinvigorate me.

I. Table of Contents

II. Abstract

Phosphoinositides (PIs) are rare lipids of the cytoplasmic leaflet of eukaryotic membranes that have emerged as key organizers of the endomembrane system. PIs serve as spatiotemporal signposts directing proteins to distinct subcellular compartments or membrane domains and thereby contribute to defining membrane identity. Of the seven PI species, phosphatidylinositol-4,5-bisphosphate [PI(4,5)P_2] has been most extensively characterized while comparatively little is known about other PIs, in particular phosphatidylinositol-3,4-bisphosphate [PI(3,4)P_2]. PI(4,5)P_2 is most abundant at the plasma membrane where it regulates signaling, ion channels, actin dynamics, and clathrin-mediated endocytosis (CME). The nucleation and assembly of clathrin-coated pits (CCPs) depends on PI(4,5)P_2 as it is critical for the membrane association of several endocytic adaptor proteins. During late stages of endocytosis, PI(4,5)P_2 is hydrolyzed, the endocytic protein coat is shed, and newly formed vesicles fuse with the early endosomal compartment. Endosomes are highly enriched in phosphatidylinositol-3-phosphate [PI(3)P] and maintenance and functionality of these organelles both require PI(3)P. However, the mechanism of PI conversion on the endocytic route from a PI(4,5)P_2 to a PI(3)P enriched membrane is still enigmatic.

Here, we show that PI(3,4)P_2 is a novel lipid regulator of CME that is required for the maturation of CCPs. Cells depleted of PI(3,4)P_2 by means of the PI(3,4)P_2-specific 4-phosphatase INPP4B display endocytic defects characterized by long-lived CCPs that successfully assemble but fail to proceed to a fission-competent state. This effect is different from PI(4,5)P_2-controlled initiation of CCP formation and demonstrates a dual lipid requirement for the sequential generation of PI(4,5)P_2 and PI(3,4)P_2 during CME. We further identify the clathrin-associated class II phosphatidylinositol-3-kinase, PI3K C2α, as the enzyme that synthesizes PI(3,4)P_2 at CCPs. RNA interference-mediated depletion of PI3K C2α phenocopies effects seen in cells enzymatically depleted of PI(3,4)P_2 and results in a partial loss of PI(3,4)P_2 from the plasma membrane. Detailed characterization of this endocytic defect by ultrastructural analysis of the accumulating endocytic intermediates and analysis of the recruitment dynamics of PI3K C2α suggested a late maturation defect preceding dynamin-mediated fission.

A comprehensive analysis of endocytic proteins revealed the PX-BAR domain protein sorting nexin 9 (SNX9) as the only protein tested that fails to localize to the accumulating endocytic intermediates in PI3K C2α-depleted cells. Consistently, the recruitment of SNX9 to CCPs arrested at a late stage due to dynamin2-depletion strictly depended on both PI3K C2α and $PI(3,4)P_2$, suggesting that SNX9 is an effector of $PI(3,4)P_2$ at CCPs. Furthermore, depletion of SNX9 and its close homolog SNX18 causes endocytic defects akin to loss of PI3K C2α that could not be rescued by PI-binding deficient mutants of SNX9.

Taken together, these observations identify a novel lipid requirement in CME and suggest a revised model of PI conversion on the endocytic route. Instead of *de novo* formation of PI(3)P on early endosomes by the class III PI3K hVps34, it appears that a continuous conversion mechanism operates. As vesicle formation is coupled to $PI(3,4)P_2$ synthesis, dephosphorylation at the 4-position by INPP4A, an effector of the early endosomal GTPase Rab5, would directly generate PI(3)P on membranes about to fuse with the early endosomal compartment. These findings establish a novel role of $PI(3,4)P_2$ as a product of a class II PI3K in a central cell physiological process and thus significantly advance our understanding of membrane traffic, the roles of class II PI3Ks, and the physiological importance of $PI(3,4)P_2$.

III. Zusammenfassung

Phosphoinositide (PIs) sind seltene Lipide der zytoplasmatischen Seite eukaryotischer Membranen, die als zentrale Organisatoren des Endomembransystems hervorgetreten sind. PIs dienen als räumliche und zeitliche Orientierungspunkte für Proteine und steuern deren Assoziation mit bestimmten subzellulären Kompartimenten oder Membrandomänen, wodurch sie einen wesentlichen Beitrag zur Schaffung der Identität distinkter zellulärer Membranen leisten. Von den sieben bekannten PI Spezies ist Phosphatidylinositol-4,5-bisphosphat [PI(4,5)P_2] am besten beschrieben, während vergleichsweise wenig über andere PIs bekannt ist, insbesondere über Phosphatidylinositol-3,4-bisphosphat [PI(3,4)P_2]. PI(4,5)P_2 ist in der Plasmamembran konzentriert und dort von essentieller Bedeutung für die Signaltransduktion, die Regulierung von Ionenkanälen, die Actin-Dynamik sowie für die Clathrin-vermittelte Endozytose (CME). Für die Nukleation und Assemblierung Clathrin-ummantelter Vertiefungen in der Plasmamembran (CCPs) ist PI(4,5)P_2 unverzichtbar, da die Membranbindung vieler endozytischer Proteine von diesem Lipid abhängt. Während später Stadien der Endozytose wird PI(4,5)P_2 hydrolysiert, die Hülle endozytischer Protein wird entfernt und das Vesikel fusioniert mit dem frühen endosomalen Kompartiment. In Endosomen ist Phosphatidylinositol-3-phosphat [PI(3)P] die dominierende PI Spezies und für den Erhalt und die Funktion dieser Organellen unabdingbar. Jedoch ist der Mechanismus der PI Konversion auf der endozytischen Route, die Umwandlung einer PI(4,5)P_2- zu einer PI(3)P-reichen Membran, bisher nur unzureichend verstanden.

In der vorliegenden Arbeit etablieren wir PI(3,4)P_2 als neuen Lipidregulator der CME, der für die Reifung der CCPs von Bedeutung ist. Durch die Expression der PI(3,4)P_2-spezifischen 4-Phosphatase INPP4B von PI(3,4)P_2 depletierte Zellen zeigen einen endozytischen Defekt, der durch lang-lebige CCPs charakterisiert ist, die sich erfolgreich assemblieren, aber nicht bis zu einem Membran-Fission kompetenten Stadium fortschreiten. Dieser Effekt unterscheidet sich von der PI(4,5)P_2-kontrollierten Initiation der CCP Bildung und zeigt ein Erfordernis der sequentiellen Generierung von PI(4,5)P_2 und PI(3,4)P_2 auf. Weiterhin identifizieren wir die Clathrin-assoziierte Klasse II Phosphatidylinositol-3-Kinase (PI3K) PI3K C2α als das Enzym, das für die Synthese von PI(3,4)P_2 an CCPs verantwortlich ist. Die RNA Interferenz-vermittelte Depletion von PI3K C2α führte zu einer Phänokopie der Effekte, die in PI(3,4)P_2-defizienten

Zellen auftraten und führte zu einem partiellen Verlust PI(3,4)P_2s von der Plasmamembran. Eine detaillierte Untersuchung dieses endozytischen Defekts mittels ultrastruktureller Analyse der akkumulierenden endozytischen Intermediate sowie einer Analyse der Rekrutierungsdynamik von PI3K C2α zu CCPs lieferte klare Hinweise, dass es sich um einen Maturierungsdefekt in einem späten Stadium der CCP-Bildung handelt, der jedoch deutlich vor der Dynamin-vermittelten Membranspaltung liegt.

Eine umfassende Analyse endozytischer Proteine zeigte das PX-BAR-Domänen Protein sorting nexin 9 (SNX9) auf, das als einziges der getesteten Proteine nicht zu den akkumulierenden endozytischen Intermediaten in PI3K C2α-depletierten Zellen lokalisierte. Die Rekrutierung von SNX9 zu arretierten Spätstadium-CCPs in Dynamin2-depletierten Zellen war strikt von PI3K C2α und PI(3,4)P_2 abhängig, was stark auf SNX9 als einen Effektor von PI(3,4)P_2 an CCPs hindeutet. In Übereinstimmung damit führen die Depletion von SNX9 und dessen eng verwandtem Protein SNX18 zu einem endozytischen Defekt ähnlich dem in PI3K C2α-depletierten Zellen beobachteten Effekt, der nicht von PI-Bindungs-defizienten Mutanten von SNX9 kompensiert werden kann.

Zusammengenommen identifizieren diese Daten ein neues Lipid-Erfordernis in der CME und legen ein revidiertes Modell der PI Konversion auf der endozytischen Route nahe. Anstatt der *de novo* Bildung von PI(3)P in frühen Endosomen durch die Klasse III PI3K hVps34 scheint ein Mechanismus der kontinuierlichen Konversion zu operieren. Da die Vesikelbildung an PI(3,4)P_2-Synthese gekoppelt ist, würde Dephosphorylierung an der 4-Position durch INPP4A, einen Effektor der früh-endosomalen GTPase Rab5, zur direkten Generierung von PI(3)P auf Membranen führen, deren Fusion mit dem frühen endosomalen Kompartiment unmittelbar bevorsteht. Diese Ergebnisse etablieren eine neue Rolle von PI(3,4)P_2 als Produkt einer Klasse II PI3K in einem zentralen zellphysiologischen Prozess und tragen daher signifikant zu unserem Verständnis des Membranverkehrs, der Rollen der Klasse II PI3Ks und der physiologischen Bedeutung von PI(3,4)P_2 bei.

1 Introduction

1.1 Cellular membranes

The origin of all organisms traces back to the formation of a barrier between an ensemble of primitive biomolecules and their surrounding environment, thereby rendering the properties of this ensemble an exclusive and selective advantage. This barrier is now termed a cellular membrane and has proven to be a hallmark feature of all organisms. Cellular membranes are lipid bilayers with a hydrophobic core and hydrophilic head groups facing the aqueous surroundings. In mammalian cells, their main constituents are glycerophospholipids, sphingolipids, cholesterol, and membrane-integral proteins (van Meer et al., 2008).

While prokaryotes such as bacteria have one outer membrane, eukaryotes have evolved a system of subcellular, membrane-delimited compartments that within one cell create a number of distinct environments. These are functionally specialized organelles where processes as diverse as DNA- / RNA-synthesis (the nucleus), energy generation (mitochondria), or hydrolytic degradation of biomolecules (lysosomes) take place, to name just a few (Lodish et al., 2003). Their coordinated interplay requires a restricted exchange of membrane proteins and lumenal content that is mediated by tubulovesicular carriers, a process referred to as membrane traffic. The complexity and dynamic nature of this endomembrane system required means of organizing and regulating processes that occur at membranes. One solution to this problem is the spatiotemporally regulated modification of the membrane itself that allows associated proteins to distinguish one site in the membrane from another. The reversible phosphorylation and dephosphorylation of phosphatidylinositol lipids (phosphoinositides) has been recognized as a central regulatory element of a plethora of cell biological pathways (Di Paolo and De Camilli, 2006).

1.2 Phosphoinositides

The discovery of phosphoinositides (PIs) as regulators of cell physiology dates back to the 1950s when Mabel and Lowell Hokin reported the agonist-induced

incorporation of ^{32}P into a specific class of phospholipids (Hokin and Hokin, 1953; Hokin and Hokin, 1958). PIs are derivatives of phosphatidylinositol, a glycerophospholipid with the cyclohexanehexol *myo*-inositol as a headgroup that can be reversibly phosphorylated at positions 3, 4, and 5, giving rise to a total of seven PI species (Figure 1-1; (De Matteis and Godi, 2004)). The hydroxyl groups of the *myo*-inositol ring display distinct stereochemical orientations, with positions 4 and 6 being oriented in *trans* of the plane of the inositol ring and position 2 being the only axial substituent. Paired with the negative charge introduced by phosphoryl groups this allows for specific recognition of PIs as signaling molecules and denominators of membrane identity (Di Paolo and De Camilli, 2006; Lemmon, 2008). PIs are rare lipids when compared to structural glycerophospholipids, such as phosphatidylcholine and phosphatidylethanolamine; phosphatidylinositol-4,5-bisphosphate [$PI(4,5)P_2$] as the most abundant PI is estimated to comprise only about 1% of the lipids of the inner leaflet of the plasma membrane (McLaughlin et al., 2002).

The interconversion of PI species is mediated by PI kinases and phosphatases that catalyze the transfer of the γ-phosphoryl group of ATP onto or the hydrolysis of a phosphate from a hydroxyl group of the inositol ring, respectively. Both classes of enzymes have been found to be highly stereoselective, i.e. to catalyze the reaction at

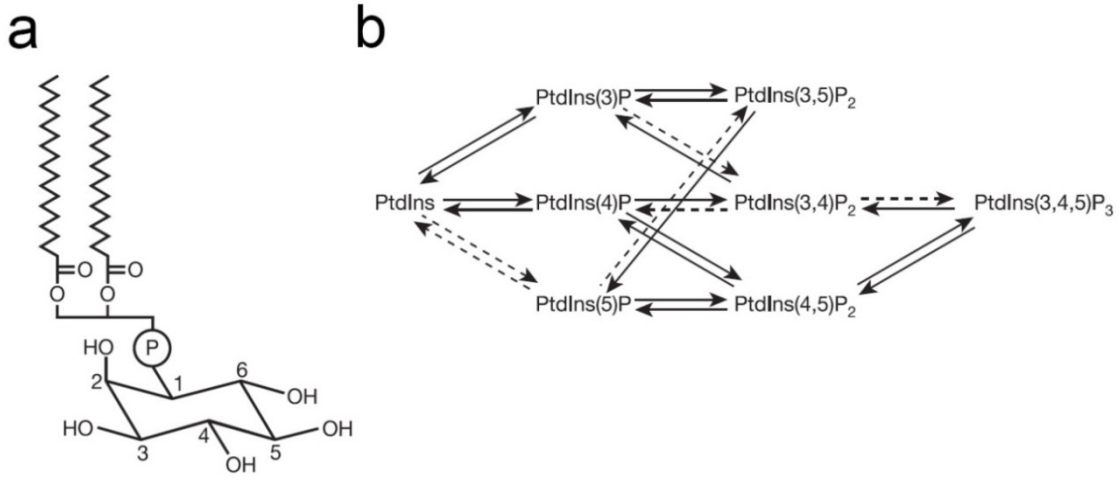

Figure 1-1: Phosphoinositides. a) Chemical structure of phosphatidylinositol. The fatty acid esterified with the 2-OH group of the glycerol moiety is commonly unsaturated (not depicted). **b)** Schematic diagram of phosphoinositide metabolism. Dotted arrows represent reactions that have been demonstrated *in vitro* but whose importance *in vivo* remains unclear. PtdIns, phosphatidylinositol. Adapted from (Di Paolo and De Camilli, 2006).

exclusively one position, yet may accept more than one PI species as substrate (De Matteis and Godi, 2004; Krauss and Haucke, 2007). In mammalian cells, the diversity of PI metabolizing enzymes covers most of the conceivable PI interconversions (Figure 1-1b); a comprehensive overview of PI metabolizing enzymes, their preferred substrate, and subcellular localization is given in Table 1-1.

Table 1-1: Phosphoinositide metabolizing enzymes. Overview of mammalian PI kinases and phosphatases, their preferred substrate and subcellular localization. Note that the 4-phosphatase activity of Synaptojanin 1 / 2 relates to a second, Sac1-like phosphatase domain that has not been characterized *in vivo*. [Substrate] denotes that this preference has so far been shown *in vitro* only. PM, plasma membrane; TGN, *trans*-Golgi network; E, endosomes; GC, Golgi complex; ER, endoplasmic reticulum; ND, not determined.

PI kinases	**Substrate**	**Localization**
3-kinases		
p110α – δ (class I)	$PI(4,5)P_2$	PM
PI3K C2 α - γ (class II)	PI, PI(4)P, $[PI(4,5)P_2]$	PM, TGN, E
hVps34 (class III)	PI	E
4-kinases		
PI4K II α / β	PI	TGN, E, PM
PI4K III α / β	PI	PM / TGN
PIP(4)K α - γ	PI(5)P	PM
5-kinases		
PIKfyve	PI(3)P	E
PIP(5)K I α - γ	PI(4)P	PM

PI phosphatases	**Substrate**	**Localization**
3-phosphatases		
PTEN	$PI(3,4,5)P_3$, $[PI(3,4)P_2]$	PM
MTM1, MTMR1-13	PI(3)P, $PI(3,5)P_2$	E or ND
TPIPα (TPTE2)	$[PI(3,4,5)P_3]$	PM
4-phosphatases		
Sac1-3	PI(4)P	ER, GC
INPP4A / B (type I / II)	$PI(3,4)P_2$	E / ND
Synaptojanin 1/2	[PI(4)P]	PM
5-phosphatases		
Synaptojanin 1/2	$PI(4,5)P_2$	PM
OCRL	$PI(4,5)P_2$	PM, E
SHIP1 / 2	$PI(3,4,5)P_3$	PM
INPP5E (72kDa-5-phosphatase)	$PI(4,5)P_2$, $[PI(3,4,5)P_3$, $PI(3,5)P_2]$	GC
PIPP (INPP5J)	$PI(4,5)P_2$	PM
SKIP (INPP5K)	$PI(4,5)P_2$	ER, PM

1.3 Phosphoinositides as regulators of cellular function

PIs are limited to the cytoplasmic leaflet of cellular membranes and are not equally abundant in all membranes but instead display a characteristic pattern of enrichment in specific compartments. This is largely a consequence of the localization and spatially regulated activity of PI metabolizing enzymes (Table 1-1;(Krauss and Haucke, 2007)). Phosphatidylinositol, synthesized from activated diacylglycerol and *myo*-inositol in the endoplasmic reticulum (ER) or in ER-derived mobile organelles (Michell, 2008; Kim et al., 2011), is present in all cellular membranes at levels of about 5% (plasma membrane) to 15% (ER) of total phospholipids (van Meer et al., 2008). Phosphatidylinositol-4-kinase (PI4K) IIIβ and IIIα synthesize PI(4)P at the Golgi complex and at the plasma membrane, respectively (Nakatsu et al., 2012). Plasma membrane PI(4)P serves as a substrate for phosphatidylinositol-4-phosphate

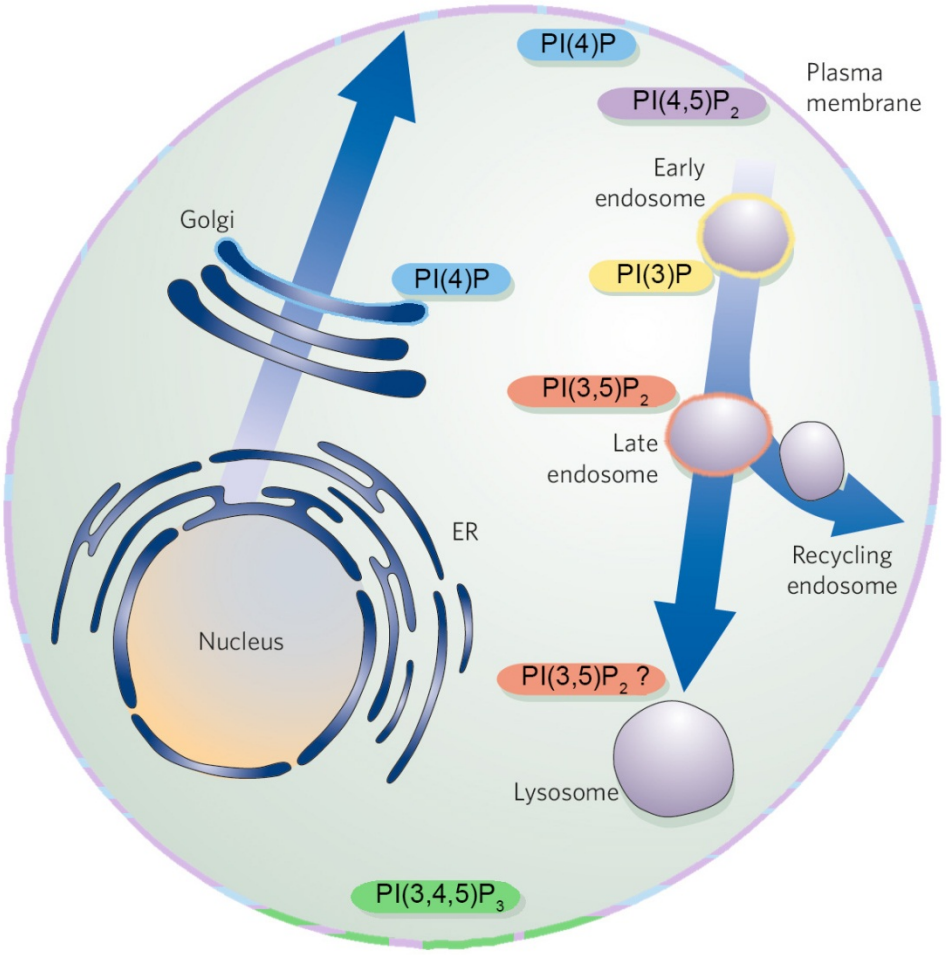

Figure 1-2: Phosphoinositides are enriched in distinct subcellular compartments. Schematic representation of the subcellular localization of PI pools. Modified from (Behnia and Munro, 2005).

5-kinases (PIP5K) to produce PI(4,5)P_2, the dominating PI species in the plasmalemma. Endosomal compartments are enriched in 3-phosphorylated PIs; early endosomes contain mainly PI(3)P, whereas the maturation to late endosomes is accompanied by a conversion of PI(3)P to PI(3,5)P_2. This selective enrichment of PI species, illustrated in Figure 1-2 as a 'PI map', is now recognized as a major determinant of membrane identity and membrane flux in eukaryotic cells (Behnia and Munro, 2005; Di Paolo and De Camilli, 2006).

The regulation of cellular functions by PIs is characterized by certain recurring themes. Both synthesis and degradation of PIs are fast and highly regulated processes that usually occur in a spatiotemporally defined manner. This allows for the dynamic generation of membrane subdomains dedicated to a distinct function, such as signaling or vesicular carrier formation (Behnia and Munro, 2005). PI metabolizing enzymes are frequently recruited and activated by key regulators of cellular pathways, especially small GTPases of the Rab and Arf families, to locally produce or degrade a distinct PI (Krauss and Haucke, 2007). Further, many PI-protein interactions are of moderate affinity and alone may be insufficient to recruit individual proteins (DiNitto et al., 2003; Lemmon, 2008). Instead, PIs commonly operate according to a coincidence detection mechanism that requires additional factors, such as activated small GTPases, in order to recruit effector proteins: Only the combined protein and lipid interactions result in sufficient total avidity (Di Paolo and De Camilli, 2006). This combinatorial gate diversifies the effector proteins that can be recruited, as two sets of effectors may require the same lipid but different protein partners.

The cellular functions of PIs have turned out to encompass a plethora of pathways and processes; a comprehensive overview is beyond the scope of this introduction. We will instead focus on the regulation of membrane traffic by PIs and the roles of phosphatidylinositol-3-kinase (PI3K) products, as these subjects are of immediate relevance to this work. In section 1.4, clathrin-mediated endocytosis will then be introduced as an example of a PI-controlled process in detail.

1.3.1 *Membrane traffic*

The budding of vesicular carriers from a donor compartment and their subsequent fusion with an acceptor compartment requires the specific recognition of the respective membranes by the protein machinery mediating transport. For this reason, the characteristic PI composition of the different subcellular compartments as well as the

acute and local modulation of PI levels is of central importance for membrane trafficking.

Plasma membrane identity is defined by $PI(4,5)P_2$ and consequently, both endocytic and exocytic processes are regulated by this lipid. The assembly of endocytic structures during clathrin-mediated endocytosis entirely depends on $PI(4,5)P_2$ (see section 1.4 for a detailed description). The engulfment and subsequent uptake of larger particles by phagocytosis likewise relies on $PI(4,5)P_2$ and local $PI(3,4,5)P_3$ synthesis (Di Paolo and De Camilli, 2006). Conversely, exocytosis uses $PI(4,5)P_2$ as an identifier of the target membrane. Several proteins mediating exocytic vesicle priming, docking or fusion have been found to associate with $PI(4,5)P_2$, among them synaptotagmin I (synaptic vesicle exocytosis) and VII (secretion in chromaffin cells), CAPS, an essential factor for Ca^{2+}-triggered fusion of large dense core vesicles in neuroendocrine cells, and a modulator of secretory granule exocytosis in pancreatic β-cells, granuphilin (Wen et al., 2011).

Following internalization, endocytic vesicles fuse with the endosomal compartment whose functions depend on 3-phosphorylated PIs in several aspects. To begin with, homotypic endosomal fusion requires PI(3)P (Ohya et al., 2009). Proteins involved in this step, such as the tethering factors early endosomal antigen 1 or rabenosyn-5, typically interact with the small GTPase Rab5 and additionally bind to PI(3)P using either FYVE- (Fab1, YOTB, Vac1, EEA1) or PX- (phox homology) domains (Simonsen et al., 1998; Nielsen et al., 2000). This represents a classical example of coincidence detection as presence of Rab5 alone leads to the recruitment of different effector proteins, such as APPL1, which are associated with pre-endosomal vesicle stages (Zoncu et al., 2009). Only upon generation of a PI(3)P pool can the early endosomal fusion and tethering factors associate with the vesicle. The group of Rab5 effector proteins comprises several PI metabolizing enzymes that may take part in generating PI(3)P, among them the class III PI3K hVps34/Vps15 complex (Shin et al., 2005). Hence, Rab5-dependent PI(3)P formation is essential for both biogenesis and maintenance of the early endosomal compartment (Zerial and McBride, 2001; Zeigerer et al., 2012).

The early endosome acts as the central sorting station on the endocytic route from where cargo proteins can either be recycled back to the plasma membrane, undergo retrograde transport towards the Golgi, or embark on the degradative pathway towards lysosomes (Grant and Donaldson, 2009). Degradative sorting is regulated by

PIs: The adaptor recognizing ubiquitinated cargo, the endosomal complex required for transport (ESCRT) 0 component Hrs, binds PI(3)P via its FYVE-domain. Also ESCRT II which mediates a subsequent step of multi-vesicular body (MVB) formation associates with PI(3)P (Henne et al., 2011). This coincidence detection of ubiquitinated cargo and PI(3)P ensures that MVBs are generated exclusively from early endosomal membranes. It has been noted that the sole PI(3)P 5-kinase, PIKfyve, localizes to late endosomal / lysosomal compartments, converting PI(3)P to $PI(3,5)P_2$ during endosomal maturation. $PI(3,5)P_2$ has been implicated in late steps of MVB formation (an ESCRT-III subunit may associate with $PI(3,5)P_2$) and PIKfyve inhibition causes a dilation of the endolysosomal compartment (Ho et al., 2012). However, the molecular function of $PI(3,5)P_2$ is poorly understood to date.

Regulation of membrane traffic by PIs is not restricted to the endocytic pathway. The *trans*-Golgi network (TGN) has long been known to be enriched in PI(4)P and molecular details of its function have emerged (Santiago-Tirado and Bretscher, 2011). PI(4)P together with the small GTPase ADP-ribosylation factor 1 (Arf1) defines TGN membrane identity and serves as a recruitment platform for the clathrin adaptors AP-1 and GGA-1/2 as well as for the PH-domain proteins FAPP-1/2 (Wang et al., 2003; Godi et al., 2004; Szentpetery et al., 2010); all of these proteins are directly or indirectly involved in secretory traffic from the TGN. Moreover, the observed dilation of the Golgi apparatus upon genetic perturbation of PI(4)P levels was recently rationalized by the discovery of the PI(4)P- and myosin MYO18a-binding protein GOLPH3 that provides Golgi-membranes with actin / myosin-derived tension and thereby supports Golgi morphology (Dippold et al., 2009).

1.3.2 *Cellular roles of phosphatidylinositol-3-kinase products*

While the products of the three classes of PI3Ks (for a detailed description of this enzyme family, see section 1.5) comprise PI(3)P, $PI(3,4)P_2$, and $PI(3,4,5)P_3$, the vast majority of research has focused on the generation of $PI(3,4,5)P_3$ by class I PI3Ks in the context of growth factor signaling (Vanhaesebroeck et al., 2012). Receptor tyrosine kinase (RTK) or G protein coupled receptor (GPCR) ligation activates class I PI3Ks to synthesize $PI(3,4,5)P_3$ from $PI(4,5)P_2$ at the plasma membrane. $PI(3,4,5)P_3$ directly transmits the signal by recruiting proteins to the plasma membrane that specifically bind this lipid, in many cases via pleckstrin-homology (PH) domains. $PI(3,4,5)P_3$ effectors include several regulators of small GTPases (Rac, Ras, and Arf)

and other scaffolding adaptor proteins, but the most prominent effector is the protein kinase Akt. Upon recruitment to the plasma membrane by $PI(3,4,5)P_3$ or its degradation product $PI(3,4)P_2$, Akt gets phosphorylated and activated at Thr^{308} by the likewise $PI(3,4,5)P_3$-regulated PI-dependent kinase 1 (PDK1). Akt has been found to be a central regulator of cell survival (by inhibiting the pro-apoptotic Bcl-2 antagonist of cell death, BAD), proliferation (e.g. by phosphorylating the cell cycle regulators p21 and p27) and metabolism, e.g. by phosphorylating glucogen synthase kinase 3, part of the insulin receptor signaling pathway (Engelman et al., 2006; Vanhaesebroeck et al., 2012). Moreover, Akt stimulates mechanistic target of rapamycin (mTOR)-dependent growth signals by inhibiting the tuberous sclerosis proteins 1/2 (TSC1/2), two inhibitors of the mTOR complex 1 (Laplante and Sabatini, 2012). In summary, $PI(3,4,5)P_3$ is a second messenger of paramount importance for cell growth and survival and for reasons of its implication in disease (Vanhaesebroeck et al., 2010) has drawn most of the attention directed towards PI3K products.

The view on $PI(3,4)P_2$ has largely been dominated by its role as the breakdown product of the signaling lipid $PI(3,4,5)P_3$ generated by SH2 domain-containing inositol 5-phosphatase (SHIP) 1/2. Since the major PI3K-signaling effectors PDK1 and Akt are activated by both $PI(3,4,5)P_3$ and $PI(3,4)P_2$, SHIP1/2-dependent $PI(3,4)P_2$ synthesis has been proposed to contribute to sustained PI3K signaling, as opposed to the termination of signaling by 3-phosphate removal by phosphatase and tensin homologue deleted on chromosome 10 (PTEN; (Bunney and Katan, 2010)). This is supported by the finding that the $PI(3,4)P_2$-specific 4-phosphatase INPP4B acts as a tumor suppressor (Gewinner et al., 2009). $PI(3,4)P_2$ has further been found to be enriched at platelet-derived growth factor- (PDGF) induced membrane ruffles where it may recruit the actin regulatory protein lamellipodin (Krause et al., 2004). Likewise, formation of podosomes (circular dorsal ruffles) has been associated with increased local $PI(3,4)P_2$ levels (Oikawa et al., 2008). However, in all these settings presence of $PI(3,4)P_2$ appears to be a secondary consequence of class I PI3K-mediated $PI(3,4,5)P_3$ formation. Class I PI3K-independent synthesis as well as autonomous functional roles of $PI(3,4)P_2$ have not been demonstrated yet.

1.4 Clathrin-mediated endocytosis

Clathrin-mediated endocytosis (CME) regulates the cell surface levels of membrane proteins through incorporation into coated vesicles that bud from the plasma membrane into the interior of the cell. Essential aspects of cell physiology such as nutrient uptake, modulation of signal transduction, synaptic transmission, and membrane turn-over rely on this fundamental process (Conner and Schmid, 2003; McMahon and Boucrot, 2011). The initial observation of internalized material in coated vesicles by electron microscopy (EM) in the 1960s was followed by the identification of clathrin as the major protein constituent of these vesicles in 1975 (Roth and Porter, 1964; Pearse, 1976). Subsequent EM analyses provided snapshots of flat, curved, and deeply invaginated clathrin-coats at the plasma membrane, giving rise to an early model of the process of CME (Heuser, 1980). By now, a complex machinery of proteins has been identified that transiently associates with the cytoplasmic face of the membrane in a spatiotemporally coordinated manner that ultimately brings about vesicle formation. At the core of this machinery are clathrin itself and the heterotetrameric adaptor protein complex 2 (AP-2). Three clathrin heavy chains and three light chains associate to form a three-legged structure termed triskelion. At the distal end of each leg, a globular clathrin terminal domain (CTD) consisting of a 7-bladed β-propeller fold serves as a binding module for 'clathrin-box' ligands (Ter Haar et al., 2000; Miele et al., 2004), short peptide motifs present in unstructured regions of numerous endocytic proteins.

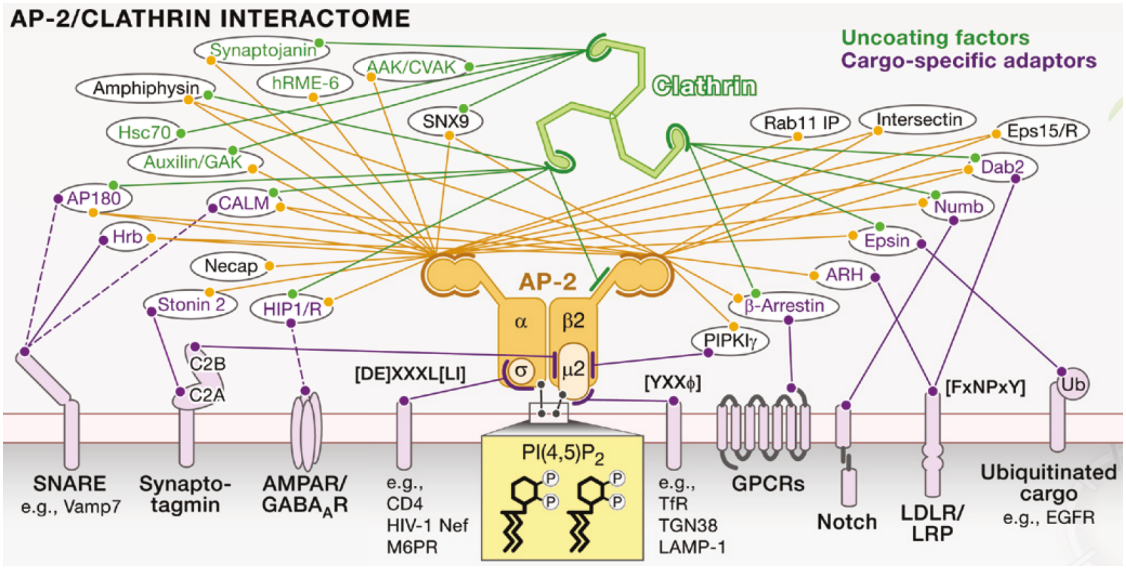

Figure 1-3: Clathrin and AP-2 are the central interaction hubs of the endocytic network. Taken from (Wieffer et al., 2009).

The AP-2 complex consists of two large (α, β2), a medium (μ2), and a small (σ2) adaptin subunit that together form a trunk-like structure from which, linked via unstructured hinge regions, the appendage domains of α- and β2-adaptin extend (Edeling et al., 2006). Akin to the CTD, the appendage domains serve as recognition modules for short peptide ligands found in a large number of endocytic proteins. Hence, clathrin and AP-2, connecting to each other through interactions between CTD and β2-hinge as well as β2-appendage and clathrin leg, constitute the central interaction hub of the endocytic protein network (Figure 1-3; (Wieffer et al., 2009)). For clarity, CME can be subdivided into five loosely defined stages: nucleation, cargo selection, maturation, scission, and uncoating (Figure 1-4; (McMahon and Boucrot, 2011)).

1.4.1 *Nucleation*

Clathrin-coated pit (CCP) formation initiates with the $PI(4,5)P_2$-dependent recruitment of endocytic adaptors. The identity of the very first molecules demarcating the site of a newly forming CCP is a matter of intense debate. A CCP nucleation module, consisting of FCHo1/2 (Fer/Cip4 homology domain-only proteins 1 / 2), intersectin and Eps15 that precedes arrival of AP-2 and clathrin has been proposed (Henne et al., 2010); others have questioned these data (Cocucci et al., 2012; Umasankar et al., 2012). Still, the early events of CCP formation have been described in great detail. For example, membrane association of AP-2 involves initial low-affinity interactions of the α and β2 subunits with $PI(4,5)P_2$. Upon encountering cargo proteins displaying tyrosine- (Yxxϕ, where x is any and ϕ a bulky hydrophobic amino acid) or dileucine-based ([DE]xxxL[LI]) sorting motifs that bind to the μ2-subunit or to an interface between α and σ2 (Doray et al., 2007), respectively, the AP-2 complex adopts an open confirmation with two additional $PI(4,5)P_2$ binding sites on μ2 (Rohde et al., 2002; Höning et al., 2005; Jackson et al., 2010), leading to tight membrane association. AP-2-cargo complexes have further been found to interact with and to potently stimulate type I PIP(5)K, thereby causing a local increase in $PI(4,5)P_2$ that presumably drives CCP assembly by a feed-forward loop (Krauss et al., 2006). The pivotal role of $PI(4,5)P_2$ in CCP initiation is demonstrated by the acute and specific depletion of $PI(4,5)P_2$ causing a near complete loss of CCPs from the plasma membrane (Zoncu et al., 2007).

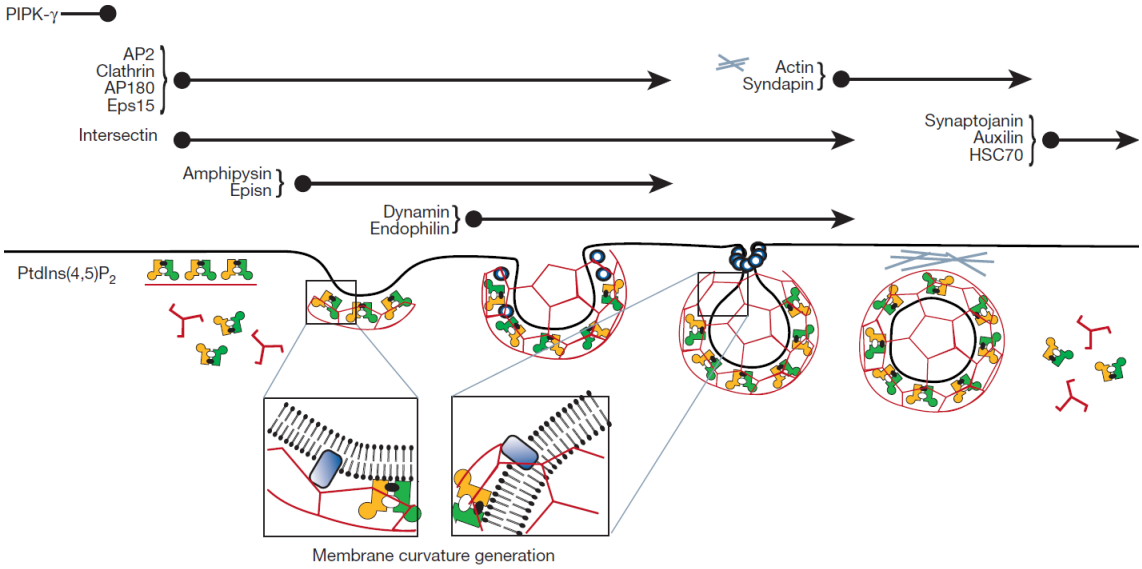

Figure 1-4: Schematic representation of clathrin-mediated endocytosis. The successive recruitment of functionally distinct endocytic proteins gives rise to a growing vesicle that finally pinches off. Yellow / green trunks represent AP-2, red triskelia represent clathrin and blue spheres dynamin. Taken from (Conner and Schmid, 2003).

1.4.2 *Cargo selection*

Nucleation of CCPs is intimately linked to the recruitment of cargo proteins that may promote CCP maturation and preclude abortive disassembly (Loerke et al., 2009). The AP-2 complex directly associates with proteins displaying tyrosine- or dileucine-based sorting motifs, but coverage of the entire spectrum of cargo proteins requires a host of clathrin-associated sorting proteins (CLASPs, see 'cargo specific adaptors' in Figure 1-3). Most CLASPs are integrated into the endocytic network by interactions with both CTD and the AP-2 appendage domains (Wieffer et al., 2009). Cargo sorting frequently relies on the recognition of a sorting signal present in a number of cargo proteins by one or a few CLASPs. Examples include the recognition of ubiquitinated proteins by epsins and Eps15, of phosphorylated GPCRs by β-arrestins, and of NPXY-motif containing proteins, e.g. integrins and LDL receptors, by Dab2, ARH and Numb (Traub, 2009). Also adaptors specifically recognizing one cargo protein have been reported, such as stonin2 for the internalization of synaptotagmin 1 (Diril et al., 2006) or AP180 /CALM for the sorting of synaptobrevin 2 at synapses (Koo et al., 2011), yet the existence of further cargo proteins for these adaptors cannot be excluded. Besides cargo, CLASPs often bind to PI(4,5)P_2 as well, e.g. epsins and AP180 / CALM, suggesting a coincidence detection mechanism for ensuring compartmental specificity and once again emphasizing the importance of PI(4,5)P_2 for early stages of CME.

1.4.3 *Maturation*

An essential aspect of CCP maturation is the acquisition of curvature and the progressive invagination of the membrane. Peripheral membrane proteins may affect the shape of the membrane by five distinct mechanisms: (1) Scaffolding of the membrane by intrinsically curved protein domains or assemblies, (2) insertion of amphipathic folds that increase the surface of the cytoplasmic leaflet, (3) enzymatic activity generating cone-shaped lipids that also increase the surface area of the inner leaflet, (4) remodeling of the membrane by the cytoskeleton (1-4: (McMahon and Gallop, 2005)), and (5) crowding of peripherally attached proteins on the membrane (Stachowiak et al., 2012). At least two of these mechanisms, (1) and (2), operate in CME.

Several members of the BAR-domain (Bin1 / amphiphysin / Rvs) family participate in CME. BAR-domains are dimerizing coiled-coil folds that via their curved and positively charged surface associate with cognate membranes and can oligomerize into helical assemblies to generate membrane tubules (Frost et al., 2009). In early stages of CME, the F-BAR domains of FCHo proteins are believed to provide a scaffold to accommodate shallow curvature (Henne et al., 2007; Henne et al., 2010). Endophilin and amphiphysin are N-BAR (N-terminal amphipathic helix BAR) domain proteins with a high degree of intrinsic curvature and consistently are recruited late during CCP maturation (Taylor et al., 2011). Additionally, amphipathic helix insertion by N-BAR domains leads to a further induction of membrane curvature. Hence, the time point of recruitment of BAR-domain proteins to CCPs appears to correlate with their ability to induce or accommodate increasing degrees of curvature.

A second class of proteins that uses amphipathic helix insertion to remodel the membrane during CME are epsins. Contrasting BAR-domains, the ENTH (epsin N-terminal homology) domain of epsins is a small globular fold that specifically binds $PI(4,5)P_2$ but does not act as a scaffold (Ford et al., 2002). In spite of their potent curvature-inducing properties, epsins arrive early at CCPs (Taylor et al., 2011), possibly reflecting lower curvature sensitivity of the flexible ENTH-domains as compared to the more rigid BAR-domains scaffolds. Based on this lack of a domain stabilizing the curved membrane, epsins have recently been proposed to support not only bending but also fission of lipid bilayers (Boucrot et al., 2012).

Finally, the capability of the clathrin lattice itself to remodel the membrane has been debated. Initially, the description of clathrin assembling into cages *in vitro* gave rise to the notion that clathrin itself would drive CCP budding (Keen et al., 1979). The

observation of flat clathrin assemblies by EM and the fact that clathrin does not directly associate with the membrane but mostly interacts with the unstructured and flexible regions of adaptor proteins have challenged this hypothesis (McMahon and Boucrot, 2011). However, recent evidence from *in vitro* reconstitution experiments demonstrated that assembly of a clathrin cage alone is sufficient to drive budding of CCPs, suggesting a direct contribution of clathrin to curvature generation (Dannhauser and Ungewickell, 2012).

Before scission, deeply invaginated CCPs must first undergo constriction until only a narrow stalk, the neck, connects them to the plasma membrane (Figure 1-4). This requires a further local increase of membrane curvature at the rim of invaginated CCPs, a process in which both BAR-domain proteins and the actin cytoskeleton have been implicated but that remains poorly defined mechanistically (Ferguson et al., 2009). Especially the spatial regulation of this process, i.e. the determination of the rim of an invaginated CCP as the site for constriction and formation of the neck, has not been elucidated. The N-BAR domain proteins amphiphysin / Bin1 and endophilin, as well as the PX-BAR domain protein sorting nexin 9 (SNX9), are recruited to late stage CCPs (Taylor et al., 2011) and via their src homology 3 (SH3)- domains interact with the large GTPase dynamin, the main catalyst of membrane fission in mammalian cells ((Ferguson and De Camilli, 2012); see section 1.4.4). In cells lacking dynamin, these BAR-domain proteins accumulate on elongated necks of arrested endocytic intermediates that cannot undergo fission. The long tubular necks are scaffolded by filamentous actin and do not form if actin polymerization or branching are perturbed. These data indicate a cooperative function of BAR-domain proteins and the actin machinery in the constriction of CCPs (Ferguson et al., 2009). Further support for a role of branched actin networks in this process came from ultrastructural analyses using platinum replica EM (Collins et al., 2011). However, there have been conflicting reports regarding the principal requirement of actin in CME. Recent evidence suggests that actin may specifically be required for CME under conditions of high membrane tension (Merrifield et al., 2002; Yarar et al., 2005; Boulant et al., 2011).

Compared to the early stages of CCP formation, the role of PIs during the maturation of CCPs is less well characterized. As type I PIP(5)Ks are not enriched at maturing CCPs or in CCVs, the local formation of $PI(4,5)P_2$ is likely restricted to the initial phase (Borner et al., 2006; Krauss et al., 2006). Furthermore, the 5-phosphatases SHIP2 and the 170 kDa isoform of synaptojanin 1 (Sjn1) have been reported to localize

to CCPs during early stages (SHIP2) and throughout maturation (Sjn1). Whereas the 5-phosphatase activity of Sjn1 was shown to be required for normal maturation, small interfering RNA (siRNA) mediated depletion of SHIP2 caused a decrease in the lifetime of CCPs (Perera et al., 2006; Nakatsu et al., 2010). This indicates tight control of $PI(4,5)P_2$ levels at CCPs and suggests that dephosphorylation of $PI(4,5)P_2$ at the 5-position plays a role already during maturation. However, the underlying mechanisms are not yet understood.

1.4.4 *Scission*

Once a CCP has constricted, the tubular membrane stalk at the neck of the pit serves as a template for the assembly of dynamin oligomers (Roux et al., 2010). Dynamin is present at low levels during the maturation of CCPs while a burst of dynamin recruitment coincides with the fission reaction (Perera et al., 2006; Loerke et al., 2009). This recruitment behavior is largely attributed to the high avidity interaction between dynamin's proline rich domain (PRD) and the SH3 domains of BAR-domain proteins, Sjn and possibly components of the actin machinery (i.e. cortactin) that accumulate at the neck of CCPs. Consistently, dynamin was shown to localize specifically to the neck of CCPs when scission was blocked by GTPγS (Wu et al., 2010).

The mechanism of dynamin-mediated membrane fission has been subject to intense investigation over the last decade and biophysical and structural insights have now led to an elaborate model of dynamin function (Roux et al., 2006; Chappie et al., 2010; Faelber et al., 2011). Dynamin is composed of the GTP-binding G domain that via the closely apposed helical bundle signaling element (BSE) connects to the extended stalk region, at the bottom of which the membrane binding PH-domain is attached (Figure 1-5a); the unfolded carboxy-terminal PRD emerges between G domain and BSE. This modular organization allows dynamin to oligomerize in a criss-cross pattern via interactions between the stalk domains. These involve three distinct interfaces that connect dynamin to dimers (interface 2) and further dimers to tetramers (interfaces 1 and 3) (Faelber et al., 2011). In this manner, a helical assembly of dynamin tetramers forms around a lipid tubule in which the PH-domains face the membrane and the G

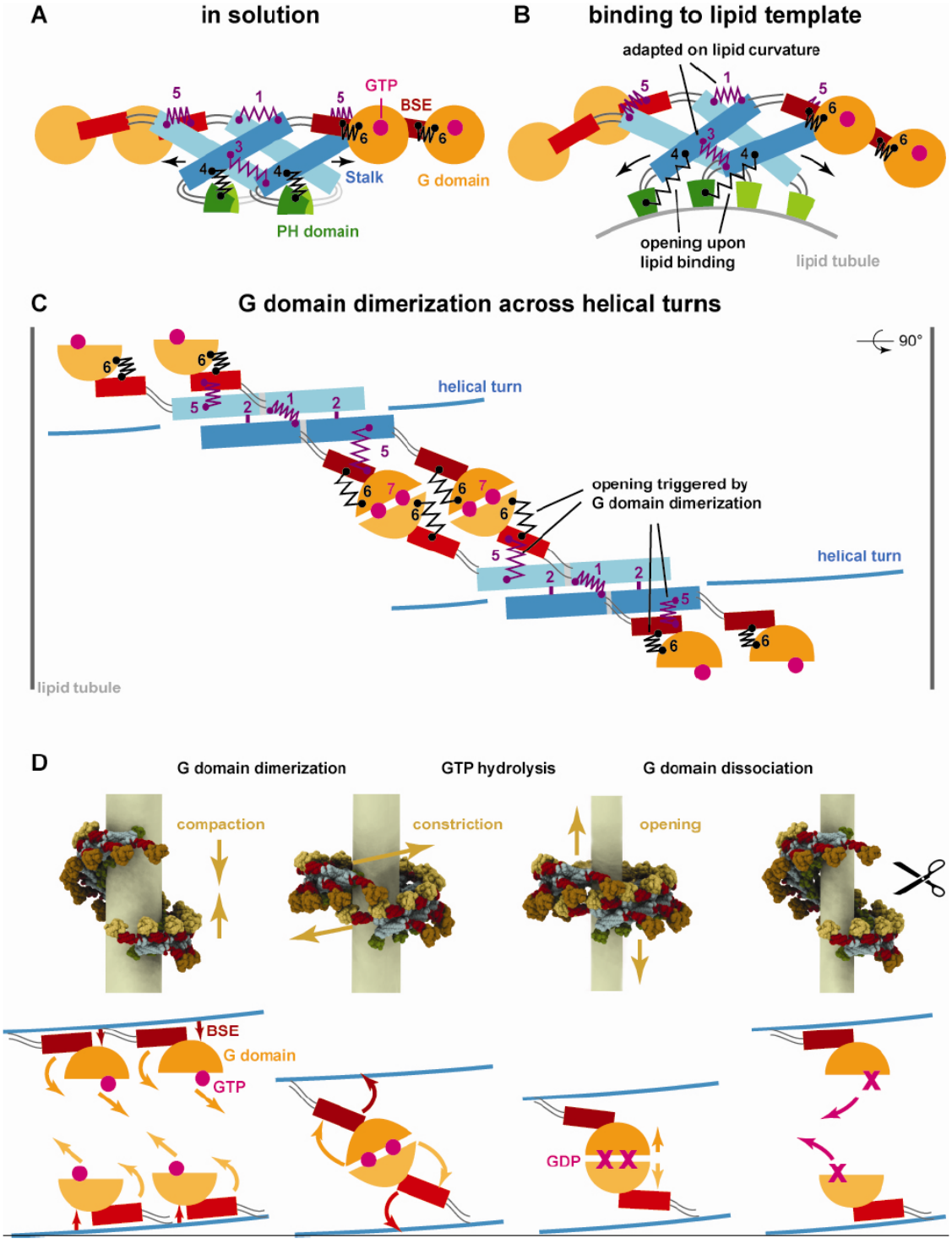

Figure 1-5: Structural model of dynamin-mediated membrane scission. a, b) Intermolecular domain interactions within dynamin tetramers in solution and upon membrane binding. **c)** G domain dimerization of dynamin tetramers across adjacent turns of the helix. Note the opening of interfaces 5 (stalk-BSE) and 6 (G domain-BSE) upon GTP-G domain dimerization. **d)** for GTP-G domain dimerization, neighboring turns have to move towards each other, leading to compaction of the helix. Upon GTP-hydrolysis, closing of interfaces 5 and 6 causes anti-parallel sliding and constriction of the helix. GDP-G domain dissociation leads to opening of the helix and extension along its axis. Taken from (Faelber et al., 2012).

domains point outwards (Figure 1-5b; (Faelber et al., 2012)). Dimerization of GTP-loaded G domains of dynamin molecules in neighboring turns of the helix requires compaction of the helix along its axis and leads to an opening of the G domain-BSE and the BSE-stalk interfaces (Figure 1-5c). Upon dimerization-stimulated GTP-hydrolysis, this conformational change reverts and thereby causes anti-parallel sliding of dynamin rungs and constriction of the dynamin helix (Figure 1-5d). GDP-G domain dissociation may then cause the helix to extend along its axis. In this model, the strain exerted on the underlying membrane is thought to catalyze membrane scission, reconciling earlier proposed modes of dynamin acting as a "twistase", "constrictase" or "poppase" (Ferguson and De Camilli, 2012).

1.4.5 *Uncoating*

Newly formed vesicles rapidly uncoat to allow recycling of the coat components and subsequent fusion of the vesicle with the target membrane, i.e. the early endosomal compartment. The key mediators of CCV uncoating were identified in early biochemical studies on purified CCVs to be the ATPase heat shock cognate 70 (Hsc70, (Schlossman et al., 1984)) and its recruiting cofactor, the DNAJ-domain protein auxilin (cyclin G associated kinase or auxilin 2 in non-neuronal cells, (Ungewickell et al., 1995)). In a clathrin cage seen from the outside, each vertex comprises the central hub of one triskelion as the outmost layer, followed by three intersecting distal leg segments of neighboring triskelia and finally three CTDs and ankle segments of triskelia centered two vertices away. Auxilin associates with this innermost layer of the vertex and in doing so slightly displaces the carboxy-terminal clathrin heavy chain peptide, of which three emerge beneath each hub, from its association with an ankle segment (Fotin et al., 2004). Upon recruitment by the auxilin J-domain, Hsc70 can bind to a substrate sequence in this carboxy-terminal peptide. Occupation of about every second clathrin heavy chain carboxy-terminus causes a cumulative destabilization of the clathrin lattice, possibly by trapping of conformationally distorted states, and thus initiates concerted ATP-dependent disassembly (Böcking et al., 2011). In this model, triggering of uncoating depends on the recruitment of auxilin, which indeed peaks shortly after dynamin recruitment (Massol et al., 2006; Taylor et al., 2011). However, what determines the timing of auxilin recruitment has not been clarified yet, although this property appears to be encoded in the PTEN-like domain of auxilin that is essential for the burst of auxilin recruitment to CCVs. This PTEN-like domain was reported to

associate with PI(4)P though the experimental evidence for this appears weak (Massol et al., 2006). The observed accumulation of intact CCVs in synaptic terminals of mice deficient of Sjn1 suggests a requirement for PI(4,5)P_2 dephosphorylation for vesicle uncoating (Cremona et al., 1999). Moreover, loss of endophilins, BAR- and SH3-domain proteins that are essential for recruitment of Sjn, causes defects in uncoating (Milosevic et al., 2011). These findings are consistent with a role for PI(4)P in auxilin recruitment which however lacks confirmation by clear-cut *in vitro* data.

After this introduction into the molecular mechanisms of CME and the roles of PIs in this process, the following two sections will address the protein families of PI3Ks and sorting nexins. Two representatives of these, PI3K C2α and sorting nexin 9, have proven to be connected with the regulation of CME by PIs and hence are of immediate relevance to this work.

1.5 Phosphoinositide-3-kinases

Several PI metabolizing enzymes participate in regulating CME, mostly by producing or degrading PI(4,5)P_2. The sole enzyme modifying the 3-position of the inositol ring that has been implicated in CME is PI3K C2α, a member of the still enigmatic class II PI3Ks.

1.5.1 *PI3K subfamilies*

Mammalian genomes encode a total of eight PI3Ks that fall into three subfamilies termed class I, II, and III. Class I PI3Ks are heterodimeric enzymes consisting of a catalytic p110α, β, γ, or δ and a smaller regulatory subunit p85, p87, or p101(Figure 1-6; (Engelman et al., 2006)). Cytosolic class I PI3Ks are kept inactive by the regulatory subunit, which upon recruitment to activated signaling receptors, e.g. by the p85 SH2 domains binding to phospho-tyrosines of activated RTKs, simultaneously localizes and activates the catalytic subunit to produce PI(3,4,5)P_3. Of all PI3Ks, the class I isoforms have been most extensively studied and their roles in signal transduction downstream of RTKs and GPCRs are well characterized (see section 1.3.1; (Vanhaesebroeck et al., 2010)).

The single class III PI3K hVps34 exists as a heteromer with myristoylated Vps15 and is thereby constitutively tethered to cellular membranes. hVps34 exclusively

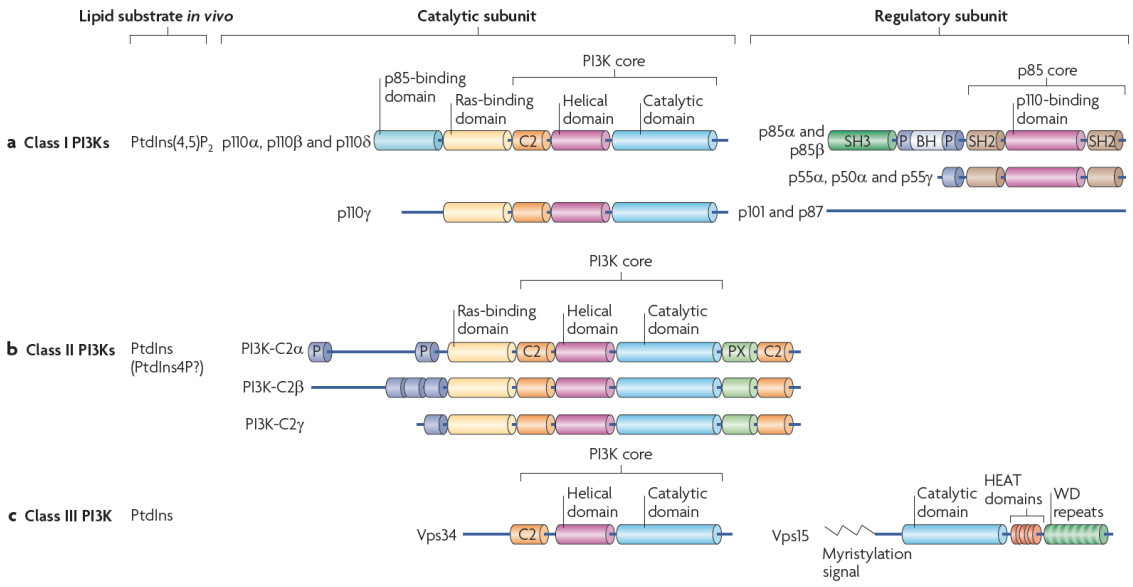

Figure 1-6: Domain structure of mammalian PI3Ks. The PI3K core is conserved throughout all PI3K subfamilies but lipid product specificity and regulatory subunits and domains differ. P, proline-rich domain; BH, B cell receptor homology domain. Taken from (Vanhaesebroeck et al., 2010).

produces PI(3)P and has been shown to regulate endosomal trafficking (see section 1.3.3) and the formation of the phagophore during autophagy (Simonsen and Tooze, 2009).

Contrasting the class I and III PI3Ks, the physiological roles and cellular functions of the class II PI3Ks are just beginning to emerge. Of the three class II PI3K isoforms, PI3K C2α and β are widely expressed whereas PI3K C2γ shows a more restricted expression pattern (Kok et al., 2009). The class II PI3Ks are large monomeric enzymes that feature a central Ras-binding and PI3K core domain closely related to the catalytic class I PI3K subunits and further share a carboxy-terminal membrane binding module consisting of PX- and C2-domains (Figure 1-6). The isozymes differ in their amino-terminal extensions which display the largest degree of sequence variability between class II PI3K isoforms. It is likely that the specific localization and activation of class II PI3Ks are determined by these amino-terminal regions (Vanhaesebroeck et al., 2010).

Although the kinase core domains of all PI3Ks are structurally similar, they exhibit key differences in their activation loop sequences, which confer substrate specificity. In the class I enzymes, PI(4,5)P_2 substrate binding depends on two basic boxes that associate with the phosphate groups at the 4- and 5-position of PI(4,5)P_2 (Figure 1-7; (Pirola et al., 2001)). Class II PI3Ks retain only the 4-phosphate coordinating basic residues and thus may not be able to synthesize PI(3,4,5)P_3 but only PI(3)P and PI(3,4)P_2. Finally, the sole class III PI3K hVps34 lacks both basic boxes and consistently produces exclusively PI(3)P. This profile of lipid product specificities has been firmly established for class I and III PI3Ks but is ill-defined for the class II subfamily (Vanhaesebroeck et al., 2010). No evidence of PI(3,4,5)P_3 formation by class II PI3Ks *in vivo* is available, whereas PI(3)P and PI(3,4)P_2 were reported to be

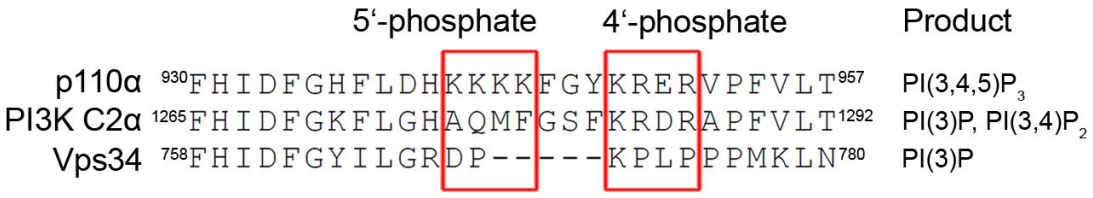

Figure 1-7: Alignment of human class I, II and III PI3K activation loop sequences. The sequence of the substrate binding activation loop displays two basic boxes in class I PI3Ks. Of these, only one is present in class II PI3Ks and none in the class III PI3K hVps34. See main text for details.

in vivo products of class II PI3Ks (Falasca et al., 2007; Leibiger et al., 2010; Yoshioka et al., 2012). However, interpretation of bulk PI(3)P and PI(3,4)P_2 determinations is complicated by the possibility that 4-phosphatases may convert PI(3,4)P_2 into PI(3)P during the process of lipid isolation. Hence, more sophisticated tools for detecting or manipulating these lipids *in situ* are needed to delineate the *in vivo* product(s) of class II PI3Ks.

1.5.2 *PI3K C2α*

The discovery of PI3K C2α traces back to the cloning of a novel PI3K family member that displayed substantial resistance to inhibition by the canonical PI3K inhibitor wortmannin (Domin et al., 1997). The presence of a C2-domain at its carboxy-terminus identified it as a relative of the Drosophila protein PI3K_68D, the founding member of the class II PI3K subfamily (MacDougall et al., 1995). Initial functional analyses implicated PI3K C2α in signaling downstream of the insulin and EGF receptors. Involvement in these pathways appeared to follow distinct mechanisms. Only activated EGF but not insulin receptor complexes recruited PI3K C2α. Furthermore, insulin caused an increase in PI3K C2α lipid kinase activity (Brown et al., 1999; Arcaro et al., 2000). Subsequent investigations proposed insulin-stimulated activation of PI3K C2α to occur at the plasma membrane and to depend on the GTPase TC10, resulting in synthesis of PI(3)P (Falasca et al., 2007). In different cell lines, PI3K C2α was found to produce PI(3,4)P_2 upon insulin stimulation and to contribute to Akt activation (Leibiger et al., 2010). Hence, no clear role of PI3K C2α in RTK signal transduction has emerged, whereas accumulating evidence implicates PI3K C2α in the regulation of membrane traffic.

The enrichment of PI3K C2α in purified CCVs was noted early on (Prior and Clague, 1999; Domin et al., 2000). Soon after, a degenerate clathrin-box motif in the amino-terminal region of PI3K C2α was found to interact with clathrin through its CTD (Gaidarov et al., 2001). Overexpression of ectopic PI3K C2α was found to inhibit CME and intracellular clathrin-dependent trafficking, likely as a consequence of blocking CTD interactions (Gaidarov et al., 2001). No further studies regarding the function of PI3K C2α in CME were reported. Although the C2-PX module is not strictly required for membrane association of the enzyme (Domin et al., 2000), analysis of the PX-domain demonstrated exquisite specificity for binding to PI(4,5)P_2, supporting activity of PI3K C2α at the plasma membrane (Stahelin et al., 2006). Apart from clathrin-

dependent trafficking events, PI3K C2α has been implicated in the exocytosis of secretory granules, both in neurosecretory cells (Meunier et al., 2005; Wen et al., 2008) and in pancreatic β-cells (Dominguez et al., 2011). Notably, PI3K C2α's role in exocytosis appears to involve synthesis of a PI(3)P pool on exocytic vesicles and to be regulated by Ca^{2+}-levels (Wen et al., 2008).

More recently, the physiological role of PI3K C2α at the organismal level has been studied. PI3K C2α hypomorphic mice were found to display reduced growth and increased mortality and to suffer from renal failure as a consequence of altered podocyte morphology and function (Harris et al., 2011). Intriguingly, this phenotype is recapitulated in mice deficient of several endocytic proteins, i.e. dynamin, endophilin, and synaptojanin (Soda and Balkin, 2012). A constitutive global as well as endothelial cell-specific knock-out of the PI3K C2α gene causes embryonic lethality, which could be attributed to defective angiogenesis in these mice (Yoshioka et al., 2012). At the cellular level, this appeared to correlate with defective adherens junction formation and impaired activation of the small GTPases RhoA, Rac1, and Rap1, known stabilizers of VE-cadherin at adherens junctions. A second study reported impaired Rac1 activation downstream of sphingosine-1-phosphate receptors and impaired internalization of these receptors upon PI3K C2α depletion in cultured endothelial cells (Biswas et al., 2013). It still remains unclear by which mechanisms these defects arise and whether they involve alterations in endocytosis, endosomal trafficking, or signal transduction.

1.6 Sorting nexin 9

The sorting nexin (SNX) family currently comprises 33 proteins, all of which contain a characteristic lipid binding PX domain. Mostly, this PX domain associates with PI(3)P. SNXs may contain a variety of additional domains specifying their subcellular role (Cullen, 2008). They serve multiple functions connected to traffic along the endocytic route, especially as cargo sorting adaptors and membrane remodeling factors in the recycling from endosomes (Cullen and Korswagen, 2012). One of the best characterized members of this protein family is SNX9, a protein that does not participate in endosomal sorting but instead regulates CME at the plasma membrane.

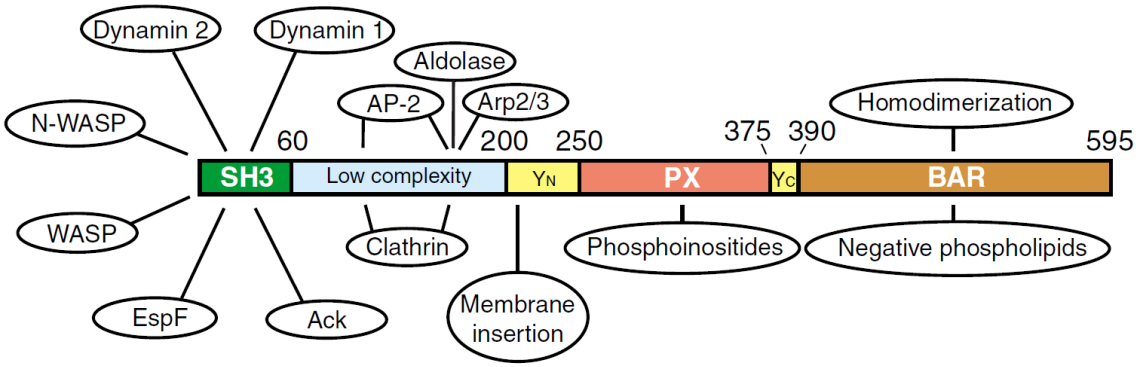

Figure 1-8: Domain structure and interaction partners of SNX9. The amino-terminal ~200 amino acids composed of SH3-domain and unstructured low complexity region engage in interactions with endocytic and actin-regulating proteins. Synaptojanin also interacts with the SH3 domain but is omitted in this scheme. The carboxy-terminal PX-BAR module serves as membrane recognition and bending module and mediates homodimerization. The region designated Y_N is essential for membrane tubulating activity and harbors a potential amphipathic helix. Taken from (Lundmark and Carlsson, 2009).

SNX9 and its close homologs SNX18 and SNX33 share a common domain architecture composed of an amino-terminal SH3-domain, an unstructured linker segment and the carboxy-terminal PX-BAR module (Figure 1-8). Biochemical analyses placed SNX9 in the endocytic protein interaction network, as both clathrin and AP-2 bind the unstructured linker region and dynamin interacts with the SH3-domain (Lundmark and Carlsson, 2003). SNX9 potently enhances dynamin assembly, thereby stimulating its GTPase activity, and is recruited to CCPs at a late stage coinciding with dynamin (Soulet et al., 2005). Furthermore, SNX9 was found to connect to the actin cytoskeleton. Through its SH3-domain, SNX9 binds and simultaneously unlocks N-WASP to stimulate its activity as an Arp2/3 nucleation promoting factor (Yarar et al.,

2007). SNX9's PX-BAR-domain exhibits a potent tubulating activity that may depend on amphipathic helix insertion (Figure 1-8; (Pylypenko et al., 2007)). These findings suggest a role for SNX9 at the juncture of dynamin, actin, and BAR-domain driven membrane remodeling that prepares fission during endocytic vesicle formation (Shin et al., 2008; Lundmark and Carlsson, 2009). This proposal is confirmed by the observation that SNX9 accumulates together with actin and other BAR-domain proteins at the elongated necks of arrested CCPs in dynamin1/2 knock-out cells (Ferguson et al., 2009). An aspect of SNX9 function remaining unclear is the regulation by PIs. Analyses of SNX9's lipid binding specificity by several groups suggest strong but only moderately specific binding to $PI(4,5)P_2$, $PI(3,4)P_2$ or PI(3)P (Lundmark and Carlsson, 2003; Shin et al., 2008; Yarar et al., 2008). This distinguishes SNX9 from the majority of endocytic proteins, which display a clear preference for $PI(4,5)P_2$.

SNX18 and SNX33 represent less well characterized members of the SNX9 subfamily. SNX18 was found to interact and to partially colocalize with the TGN / endosomal clathrin adaptor AP-1 on endosomes (Håberg et al., 2008). Further investigation revealed considerable redundancy of SNX9 and SNX18 concerning interaction partners, localization to CCPs and function in CME and suggested differences in the relative expression levels between cell types (Park et al., 2010). Remarkably, cells depleted of their predominant isoform displayed impaired CME of transferrin that could be fully reconstituted by recombinant expression of the respective other isoform. Thus, SNX9 and SNX18 can reciprocally compensate each other's loss in CME (Park et al., 2010).

1.7 Aims of this study

As detailed in section 1.3, PIs serve as denominators of membrane identity that are crucial for the compartmental specificity of a plethora of cell physiological processes. The maintenance of lipid-defined membrane identity depends on the subcellular localization and activity of the enzymes synthesizing or degrading these lipids. As the endomembrane system of eukaryotic cells is in a state of constant flux and exchange, lipid metabolism must allow for the dynamic interconversion of PI species in between compartments in order to maintain distinct membrane identities.

On the endocytic route, carriers are generated from a PI(4,5)P_2-enriched compartment, the plasma membrane, and subsequently traverse endosomal compartments that are dominated by 3-phosphorylated PIs. Vesicle biogenesis at the plasma membrane requires PI(4,5)P_2 whereas endosomal fusion and degradative sorting from endosomes depend on PI(3)P (see sections 1.4 and 1.3.3, respectively). How precisely is efficient PI conversion on the endocytic route achieved?

The master regulator of endosomal fusion is Rab5 and several PI metabolizing enzymes have been identified as effectors of this small GTPase. Not only does Rab5 recruit the class III PI3K hVps34, it also interacts with PI(3,4)P_2 4- and PI(3,4,5)P_3 5-phosphatases (Ivetac et al., 2005; Shin et al., 2005). This strongly suggests that higher phosphorylated PIs feed into the endosomal PI(3)P pool. In this study, we set out to determine if endocytic vesicle formation is indeed coupled to conversion of PIs toward endosomal membrane identity and to characterize the molecular determinants of such a conversion mechanism.

2 Material and Methods

2.1 Materials

2.1.1 *Chemicals and disposables*

General chemicals were purchased from Carl Roth GmbH, Merck, Sigma-Aldrich, or Invitrogen. For reagents used in specific applications, the supplier is mentioned in the respective methods section. Disposables were obtained from Sarstedt, Greiner, and Whatman.

2.1.2 *Solutions and media*

All solutions and buffers were prepared with ultrapure water (resistance of 18 MΩ, ddH_2O) and pH was adjusted using NaOH or HCl. Buffers for specific protocols are described in the respective methods section.

Table 2-1: Buffers and solutions used for molecular biology experiments.

Molecular biology	
10× TBE	890 mM Tris 20 mM EDTA 890 mM Boric acid
TE buffer	10 mM Tris 2 mM EDTA pH 8.0
LB medium	1.0 % (w/v) yeast extract 0.5 % (w/v) Trypton 0.5 % (w/v) NaCl pH 7.4
Ampicillin stock 500×	50 mg/ml in ddH_2O sterile filtered
Kanamycin stock 200×	10 mg/ml in ddH_2O sterile filtered
2× YT medium	1.0 % (w/v) yeast extract 1.6 % (w/v) Trypton 0.5 % (w/v) NaCl pH 7.4
Ethidium bromide stock ×3000	10 mg/ml in ddH_2O

Table 2-2: Buffers and solutions used for biochemistry experiments.

Biochemistry		
10× TBS	200 mM Tris 1.4 M NaCl pH 7.6	
Lysis buffer A (with Triton X-100)	20 mM Hepes pH 7.4 100 mM KCl 2 mM $MgCl_2$ 1 mM PMSF 0.3% protease inhibitor cocktail (1% Triton X-100)	
6× SDS-PAGE sample buffer	 375 mM Tris 60 % glycerol (v/v) 30 % β-mercaptoethanol (v/v) 18 % SDS (w/v) Bromophenol blue to deep blue color	For 200 ml: 9.07 g 120 ml 60 ml 36 g Do not add H_2O Heat to 55°C pH 6.8
10× SDS running buffer	246 mM Tris 1.92 M Glycine 10 % SDS	
4× SDS stacking gel buffer	0.4 % SDS 0.5 M Tris pH 6,8	
4× SDS separating gel buffer	0.4 % SDS 1.5 M Tris pH 8.8	
Coomassie stain	1 g/l Coomassie G250 10 % Acetic acid 25 % Methanol	
Coomassie destain	10 % Acetic acid 25 % Methanol	
Semi-dry blotting buffer	1x SDS running buffer 20 % Methanol	
Ponceau stain	0,3 % Ponceau S 1% Acetic acid	
Ponceau destain	1 % Acetic acid	
Immunoblot blocking solution	3 % milk powder in 1x TBS	
Immunoblot antibody dilution solution	2 % Bovine serum albumin 0.02 % NaN_3 1x TBS	

Immunoblot stripping buffer	62.5 mM Tris 2% SDS (w/v) pH 6.8 to 10 ml buffer add 78 µl β-mercaptoethanol immediately before use
2× Bradford reagent	140 g/l Coomassie G250 200 ml 85 % H_3PO_4 100 ml Ethanol (filtered)
Mammalian protease inhibitor cocktail	104 mM 4-(2-Aminoethyl)benzenesulfonyl fluoride (AEBSF) 1.5 mM Pepstatine A 1.4 mM E-64 4 mM Bestatine 2 mM Leupeptine 0.08 mM Aprotinine

Table 2-3: Buffers and solutions used for cell biology experiments.

Cell biology	
10× PBS	1.37 M NaCl 27 mM KCl 43 mM Na_2HPO_4 14 mM NaH_2PO_4 pH 7.4 autoclaved
PBS +Mg^{2+}	1× PBS + 10 mM $MgCl_2$
DMEM incl. Glutamax (used for Cos7, HeLa, and Hek293 cells)	Dulbecco's modified eagles medium 4.5 g/l glucose Additives: 10 % fetal calf serum (heat-inactivated) 100 U/ml Penicillin 0.1 mg/ml Streptomycin
DMEM incl. Glutamax (used for mouse embryonic fibroblasts)	Dulbecco's modified eagles medium 4.5 g/l glucose Additives: 10 % bovine calf serum (heat-inactivated) 100 U/ml Penicillin 0.1 mg/ml Streptomycin
Trypsin / EDTA	200 mg/ml Versene (EDTA) 170 000 U trypsin/ml
Live cell imaging solution	1× Hank's balanced salt solution +Ca^{2+} +Mg^{2+} 5% fetal calf serum Non-sterile
Acid wash solution	100 mM Na acetate 100 mM NaCl pH 5.3

PFA fixative	4 % PFA 4 % Sucrose 1× PBS pH 7.4	
IF wash buffer	15.48 mM Na_2HPO_4 4.52 mM NaH_2PO_4 100 mM NaCl 0.3% Triton X-100	For 1l at pH7.4: 77.4 ml 0.2 M Na_2HPO_4 22.6ml 0.2 M NaH_2PO_4
Goat serum dilution buffer	IF wash buffer containing 10 % goat serum	

2.1.3 *DNA Oligonucleotides*

Synthetic DNA oligonucleotides used as primers for polymerase chain reactions (PCRs) were purchased from MWG-Biotech as a lyophilized powder and dissolved in TE buffer to a concentration of 100 µM. Working stocks were diluted to 10 µM in ddH_2O. A complete list of all primers is attached in appendix A.

2.1.4 *Small interfering RNA oligonucleotides*

Synthetic RNA oligonucleotides for RNA interference were obtained from MWG-Biotech as a lyophilized powder and dissolved to a concentration of 100 µM in RNAse-free siMAX buffer supplied by the manufacturer. All small interfering RNA (siRNA) sequences used in this study are listed in the following table and were directed against the human mRNA sequence. Please note that for the depletion of PI3K C2α, siRNA #1 was used in all experiments except where explicitly stated otherwise.

Table 2-4: Sequences of siRNAs used in this study.

Targeted mRNA	siRNA	5' - 3' Sequence	Comment
none	Scrambled siRNA	gtaactgtcggctcgtggt	scrambled µ2 adaptin sequence
PI3K C2α	PI3K C2α#1 "Ambion"	ggatctttttaaacctatt	Used for all experiments in Cos7 including rescue experiments
	PI3K C2α#2 "DhcSP#2"	gcacaaacccaggctattt	Used for Cos7 excluding rescues
	PI3K C2α#3 "MWG"		Used for HeLa cells
Dynamin 2	Dyn2#2	gcaactgaccaaccacatc	
SNX9	SNX9 SP#3	ggacagaacgggccttgaa	Anneals in the 3'-untranslated region of the SNX9 mRNA
SNX18	SNX18	caccgacgagaaagccuggaa	

2.1.5 *Bacterial strains*

For cloning and amplification of plasmid DNA the *E. coli* TOP10 strain (Invitrogen) was used. It features high transformation efficiency and is suited for plasmid propagation.

Recombinant proteins were expressed in the *E. coli* BL21-Codon Plus strain (Stratagene) that is designed for high-level expression of proteins. This strain contains multiple copies of rare tRNA genes that can limit the translation efficiency of heterologous proteins in *E. coli*.

2.1.6 *Eukaryotic cell lines*

For all cell biological experiments, Cos7 cells were used as a model system of mammalian cells that is well amenable to transient genetic manipulations. Cos7 cells were derived from the African green monkey (*Cercopithecus aethiops*) kidney cell line CV-1 by transformation with the Simian vacuolating virus 40 and exhibit a fibroblast-like morphology. For live cell imaging of CCP dynamics, a Cos7 cell line stably expressing eGFP-clathrin light chain (CLC) under control of the CMV promoter was used.

A small subset of experiments was also carried out in HeLa cells that were derived from a cervix carcinoma in 1951. HeLa cells are of human origin, but have undergone extensive genetic alterations (integration of a human papillomavirus genome, multiple copies of chromosomes 6, 8, 12 and 18).

For biochemical experiments requiring large amounts or high concentrations of endogenous or recombinantly expressed proteins, the human embryonic kidney cell line HEK293 was used because of the high protein yield it affords.

2.1.7 *Plasmids*

An overview of the general plasmid backbones used here is provided in Table 2-5. Note that for simple swapping of amino-terminal tags a vector series named “MK” was created in the laboratory. The original pcHA-MK plasmid is a pcDNA3.1(+)-based vector with the sequence between the *Nde*I (within CMV promoter) and *EcoR*V (beginning of polylinker) sites having been exchanged for the corresponding sequence from pcHA2. In all vectors of the MK-series, the sequence encoding the tag is placed between the *Kpn*I and *BamH*I sites, followed by an identical polylinker that allows for

convenient subcloning. Table 2-6 provides an overview of all expression plasmids used in this study.

Table 2-5: Vector backbones used in this study.

Plasmid	Description	Manufacturer
pBluescript II KS (+)	Small vector designed for the initial cloning of cDNAs. T7 promoter for bacterial expression, Ampicillin resistance.	Stratagene
pcDNA3.1 (+)	Designed for expression in mammalian cells, CMV promoter, BGH polyA signal, neomycin/kanamycin resistance.	Invitrogen
pc[tag]MK series	pcDNA3.1(+) based vectors with different tags between *Kpn*I and *BamH*I sites: HA, 6xMyc, eGFP, mCherry. See text for details.	Self-made
pcDNA5/FRT/TO	pcDNA-based vector designed for the generation of stable cell lines using Flp-recombinase mediated insertion of a gene of interest into the FRT-acceptor site engineered into the genome of a host cell line.	Invitrogen
pEGFP-C / N	Vectors for expression of amino- or carboxy-terminally eGFP-tagged proteins, encode red-shifted variant of wt GFP optimized for mammalian codon usage, CMV promoter, SV40 polyA signal, Neomycin/ kanamycin resistance	Clontech
pET-28a (+)	Designed for expression of N-terminally His-tagged fusion proteins in *E. coli*, bacteriophage T7 promoter, IPTG-inducible T7 RNA-polymerase, kanamycin resistance	Novagen (Merck)
pGEX4T-1	Vector for expression of N-terminally GST-tagged proteins in *E. coli*, IPTG-inducible tac promoter, thrombin cleavage site, ampicillin resistance	Pharmacia

Table 2-6: Plasmid DNA constructs used for recombinant protein expression. REN, restriction endonuclease; mRNA, NCBI mRNA accession number; aa, amino acids encoded by the construct; FL, full length; WT, wild type; nts, nucleotides; UTR, untranslated region.

Construct	Vector	REN sites	mRNA	aa	Additional information
pcHA-CAAX	pcHA-MK	*Not*I - *Xho*I	M54968	180-188	Includes Membrane targeting CAAX-box from K-ras
pcmCherry-CAAX	pcmCherry-MK	*Not*I - *Xho*I	M54968	180-188	Includes Membrane targeting CAAX-box from K-ras
HA-INPP4B-CAAX	pcHA-CAAX	*EcoR*V - *Not*I	U96922	FL	WT

Construct	Vector	REN sites	mRNA	aa	Additional information
HA-INPP4B-CAAX C842A	pcHA-CAAX	*EcoR*V - *Not*I	U96922	FL	C842A abolishes phosphatase activity
mCherry-INPP4B-CAAX	pcmCherry-CAAX	*EcoR*V - *Not*I	U96922	FL	WT
mCherry-INPP4B-CAAX C842A	pcmCherry-CAAX	*EcoR*V - *Not*I	U96922	FL	C842A abolishes phosphatase activity
mCherry-MTM1-CAAX	pcmCherry-CAAX	*EcoR*V - *Not*I	U46024	FL	WT
mCherry-PTEN-CAAX	pcmCherry-CAAX	*EcoR*I - *Not*I	U96180	FL	WT
mCherry-INPP5E-CAAX	pcmCherry-CAAX	*EcoR*V - *Not*I	AF187891	FL	WT
RFP-2xPH-TAPP1	pTagRFP	complex	AF286160	188-404	Tandem of TAPP1 PH domains; a gift from the Takenawa laboratory
eGFP-2xFYVE$_{HRS}$	pceGFP-MK	complex	U43895	FYVE domain	Tandem of the FYVE domain of HRS
eGFP-2xPH-PLCδ	pceGFP-MK	complex	U09117	PH domain	Tandem of the PH domain of PLCδ
Btk-PH-eGFP	peGFP-N	*EcoR*I-15 nts UTR-Cds-*BamH*I	X58957	1-177	Single PH domain of Bruton's tyrosine kinase; a gift from M. Wymann
pBS-PI3K C2α WT	pBluescript II KS (+)	*Spe*I - *EcoR*I	Y13367	FL	Assembled construct from cDNA fragments, WT
GFP-PI3K C2α WT	peGFP-C3	*Spe*I - *EcoR*I	Y13367	FL	WT
GFP-PI3K C2α WT siRes#1	peGFP-C3	*Spe*I - *EcoR*I	Y13367	FL	WT bearing 4 silent mutations rendering the mRNA resistant to siRNA#1: agatctattcaaaccgatt
GFP-PI3K C2α WT siRes#2	peGFP-C3	*Spe*I - *EcoR*I	Y13367	FL	WT bearing 4 silent mutations rendering the mRNA resistant to siRNA#2: ggacgaacccgggttattt
GFP-PI3K C2α kinase inactive siRes#1	peGFP-C3	*Spe*I - *EcoR*I	Y13367	FL	Kinase inactive mutant: K1138A, D1157A, D1250A; resistant to siRNA#1 (see above)

Construct	Vector	REN sites	mRNA	aa	Additional information
GFP-PI3K C2α kinase inactive siRes#2	peGFP-C3	*Spe*I - *EcoR*I	Y13367	FL	Kinase inactive mutant: K1138A, D1157A, D1250A; resistant to siRNA#2 (see above)
GFP-PI3K C2α class III mutant siRes#1	peGFP-C3	*Spe*I - *EcoR*I	Y13367	FL	PI(3)P-restricted mutant: ^{1283}KRDR^{1286} to ^{1283}KPLP^{1286} resistant to siRNA#1 (see above)
mRFP-clathrin light chain	pcDNA5/FRT/TO	unknown	unknown	FL	Rat clathrin light chain, designed by Kira Brune
Dynamin2-mCherry	pmCherry-N3	unknown	L31398	FL	Mouse dynamin 2, a gift from O. Daumke
3x-HA-Hip1R	pcDNA3.1	unknown	AB014555	FL	A gift from T.S. Ross
Epsin1-eGFP	pCMV6-AC-GFP	*Sgf*I - *Mlu*I	BC044651	FL	Obtained from Origene (clone RG207099)
GST-SNX9 PX-BAR	pGEX4T-1	*EcoR*I - *Not*I	AF121859	204-595	PX-BAR module of human SNX9
GFP-SNX9 WT	pceGFP-MK	*EcoR*I - *Not*I	AF121859	FL	WT
GFP-SNX9 RYK	pceGFP-MK	*EcoR*I - *Not*I	AF121859	FL	Lipid binding mutant: R286Q, Y287A, K288A
GFP-SNX9 K267N, R327N	pceGFP-MK	*EcoR*I - *Not*I	AF121859	FL	Lipid binding mutant: K267N, R327N
6xMyc-PI3K C2α WT	pc6xMyc-MK	*EcoR*I - *Not*I	Y13367	FL	WT
6xMyc-PI3K C2α kinase inactive	pcDNA5/FRT/TO	*Spe*I - *EcoR*I	Y13367	FL	Kinase inactive mutant: K1138A, D1157A, D1250A; used for radioactive kinase activity assay
6xMyc-PI3K C2α class III mutant	pcDNA5/FRT/TO	*Spe*I - *EcoR*I	Y13367	FL	PI(3)P-restricted mutant: ^{1283}KRDR^{1286} to ^{1283}KPLP^{1286}; used for radioactive kinase activity assay

Construct	Vector	REN sites	mRNA	aa	Additional information
6xMyc-PI3K C2α WT	pcDNA5/FRT/TO	*Spe*I - *EcoR*I	Y13367	FL	WT construct used for generation of a stable HEK293 cell line
His-PI3K C2α aa 2-365	pET-28a (+)	*EcoR*I - *Xho*I	Y13367	2-365	Fragment used for raising and affinity-purifying rabbit antibody to PI3K C2α #58

2.1.8 *Molecular weight standards and loading dye*

Table 2-7: Molecular weight standards.

Marker / buffer	Composition	Manufacturer
6x DNA loading dye	0.03 % Bromophenole blue 0.03 % Xylenecyanol FF 60 % Glycerol 60 mM EDTA	Fermentas
Generuler 1 kb DNA ladder	10, 8, 6, 5, 4, 3.5, 3, 2.5, 2, 1.5, 1, 0.75, 0.5, 0.25 kb DNA fragments	Fermentas
Prestained protein standard	175, 80, 58, 46, 30, 25, 17, 7 kDa protein bands	New England Biolabs
Broad range protein standard	212, 194, 158, 116, 97, 66, 55, 43, 35, 27, 20, 14.3, 6.5, 3.4, 2.3 kDa protein bands	New England Biolabs

2.1.9 *Enzymes*

Restriction endonucleases (RENs), Vent polymerase, and alkaline phosphatase, calf intestinal (CIP) were purchased from New England Biolabs. Alternative RENs were obtained from Fermentas. Phusion DNA polymerase was from Finnzymes, Taq DNA polymerase and T4 DNA ligase were from Fermentas. The Superscript III Reverse Transcriptase was from Invitrogen.

2.1.10 *Molecular biology kits*

Kits for plasmid DNA purification from *E. coli* cultures (“mini / midi”) and kits for DNA purification from agarose gels and PCR reactions were from Macherey-Nagel. The SV Total RNA isolation system was purchased from Promega.

2.1.11 *Antibodies*

All primary antibodies used in this study are listed in

Table 2-8. All fluorescent secondary antibodies were modified with AlexaFluor dyes, were obtained from Molecular Probes (Invitrogen) and were used at a dilution of 1:200. Horse radish peroxidase- (HRP) and alkaline phosphatase-coupled antibodies were obtained from Dianova and were used at a dilution of 1:5000.

Table 2-8: Primary antibodies. IF, immunofluorescence; IB, immunoblot.

Antigen	Host	Clone / catalog #	Source	Dilution IF	Dilution IB
AP180	Rabbit		Synaptic Systems	-	1:2,000
AP-2α (α-adaptin)	Mouse	AP-6	Hybridoma cell line	1:100	-
AP-2α (α-adaptin)	Mouse	AC1M11	Dianova	-	1:200
APPL1	Rabbit		Cell Signaling	1:150	-
β-actin	Mouse	ac-15	Sigma-Aldrich	-	1:10,000
CALM	Rabbit		A gift from E. Ungewickell	1:50	-
Clathrin heavy chain	Mouse	X22	Hybridoma cell line	1:100	-
Clathrin heavy chain	Mouse	TD-1	Hybridoma cell line	-	1:500
Clathrin heavy chain	Rabbit		Abcam	1:200	-
c-myc	Mouse	9E10	Hybridoma cell line	-	1:400
Dynamin	Mouse	Hudy-1	Upstate Biotechnology	1:100	-
Dynamin 1+2	Mouse	41	BD Biosciences	-	1:500
EEA1	Mouse	# 610456	BD Biosciences	1:100	-
Eps15	Rabbit		A gift from P. Di Fiore	1:100	-
Epsin 1	Rabbit		A gift from P. De Camilli	-	1:2,000
FCHo 2	Rabbit		A gift from H. McMahon	1:200	-
HA	Mouse	HA.11	Babco	-	1:1,000
HA	Rabbit		Cayman	1:100	-
Hip1	Rabbit		A gift from E. Wancker	1:100	-
Intersectin	Rabbit	S750	A gift from T. Südhof	1:200	-
PI3K C2α	Rabbit	#58	Raised against aa 2-365 of human PI3K C2α	1:200	1:2,000
$PI(3,4)P_2$	Mouse	Z-P034**b**	Echelon Biosciences	1:150	-
$PI(4,5)P_2$	Mouse	Z-A045	Echelon Biosciences	1:200	-
SNX9	Rabbit		A gift from S. Carlsson	1:250	1:1,000
SNX18	Rabbit	119426	GenTex	-	1:5,000
Synaptophysin	Mouse	7.2	Synaptic Systems	-	1:2,000

2.1.12 *Suppliers*

Abcam	Cambridge, USA
Amaxa	see Lonza
Amersham	GE healthcare, München, Germany
Avanti Polar Lipids	Alabaster, USA
Babco	Covance, Princeton USA
Bandelin	Berlin, Germany
BD Biosciences	Mountain View, USA
BD Transduction	see BD Biosciences
Beckman-Coulter	Krefeld, Germany
Biometra	Göttingen, Germany
Carl Roth GmbH	Karlsruhe, Germany
Cayman	Ann Arbor, USA
Cell Signaling	Danvers, USA
Clontech	see BD Biosciences
Dianova	Hamburg, Germany
Eurogentec S.A.	Liège, Belgium
Eppendorf	Hamburg, Germany
Echelon	Salt Lake City, USA
Fermentas	St. Leon-Rot, Germany
Finnzymes	Espoo, Finland
GeneTex	Irvine, USA
Gibco	see Invitrogen
Hartmann Analytic	Braunschweig, Germany
Herolab	Wiesloch, Germany
Invivogen	San Diego, USA
Invitrogen	Karlsruhe, Germany
Lonza	Cologne, Germany
Macherey-Nagel	Düren, Germany
Merck	Darmstadt, Germany
Millipore	see Merck
Molecular Probes	see Invitrogen
MWG-Biotech	Martinsried, Germany
New England Biolabs	Frankfurt am Main, Germany
Novagen	see Merck
Packard	see Perkin Elmer
Perkin Elmer	Waltham, USA
Pharmacia	Freiburg, Germany
Promega	Münster, Germany
Roche Diagnostics	Mannheim, Germany
Santa Cruz Biotech.	Santa Cruz, USA
Sigma-Aldrich	München, Germany
Stratagene	La Jolla, USA
Synaptic Systems	Göttingen, Germany
Thermo Scientific	Waltham, USA
Upstate Biotechnology	see Millipore
Zeiss	Jena, Germany
Zymed	Vienna, Austria

2.2 Molecular biology methods

2.2.1 *Cloning strategies*

Cloning strategies were devised using the Vector NTI Software 11 from Invitrogen. Primers were designed such that the salt-adjusted melting temperature, calculated using the Promega online tool

http://www.promega.com/techserv/tools/biomath/calc11.htm,

lies between 50°C and 60°C and that, if possible, the last two nucleotides at both ends are a G or C. The complete plasmid was then constructed *in silico* to exclude conceptual errors, such as frame shifts or restriction site incompatibilities.

2.2.2 *Polymerase chain reaction and site-directed mutagenesis*

The polymerase chain reaction (PCR) allows the exponential amplification of a specific DNA sequence from a given template (Saiki et al., 1988). In a repeated cycle of template DNA denaturation, annealing of specific oligonucleotides for priming of DNA synthesis and elongation of DNA strands, the newly synthesized DNA serves as template in the following cycles and thus leads to an exponential DNA amplification.

PCRs were used for amplification of protein coding sequences from cDNA or plasmid DNA for subsequent cloning into expression vectors and for screening of *E. coli* colonies after transformation of ligation reactions (colony-PCR). Standard PCRs were performed in a volume of 50 µl containing 1× polymerase reaction buffer, 200 µM of each dNTP, 10 µM of each primer, 10 ng of plasmid DNA or 1 µl of cDNA and 1 unit of Phusion polymerase or 2 units of Vent polymerase. The following program was then run in a thermocycler:

	Phusion polymerase		Vent polymerase	
Initial Denaturation	98°C	30 s	95°C	1 min
Denaturation	98°C	5 s	95°C	30 s
Primer annealing	50-65°C	20 s	50-65°C	30 s
Elongation	72°C	15 s/kb	72°C	1 min/kb
Final elongation	72°C	7 min	72°C	5 min
	4°C	∞	4°C	∞

Steps 2 to 4 were repeated in 30 cycles. The annealing temperature (step 3) depends on the primers used and was generally chosen to be equal to the salt-adjusted melting temperature of the primers.

For the generation of mutations, two alternative strategies employing mutagenic PCR primers were used. In most cases, a mutagenic reverse and forward primer annealing to the region containing the targeted nucleotides were used in combination with a forward and a reverse primer that anneal to the start and end of the cDNA of interest, respectively, so that two individual amplificates would result, a 5'- and a 3'-fragment. The mutagenic primers were designed such that the 5'- and 3'-fragments would share an overlapping sequence (that contains the mutated nucleotides) and that this overlap has a salt-adjusted melting temperature of at least 60°C. The 5'- and 3'-fragments were then fused together by PCR, using equimolar amounts of both fragments, the non-mutagenic outer forward and reverse primers used to generate these fragments in the first place, and Phusion or Vent DNA polymerase. In a Fusion PCR reaction, the first five cycles were conducted with an annealing temperature about 8°C below the melting temperature of the overlap in order to increase the probability of successful fusion events. For the remaining 25 cycles, the annealing temperature was increased to about 2°C below the melting temperature of the overlap in order to increase specificity during the exponential amplification stage of the PCR. Initial mutagenic PCRs and the Fusion PCR were always carried out in quick succession and UV-exposure of 5'- and 3'-fragments was minimalized or, in difficult cases, avoided entirely.

In situations where a Fusion PCR strategy seemed difficult because of large 5'- and 3'-fragments, a pair of complementary mutagenic forward and reverse primers was designed and used in a vector PCR with Phusion polymerase on 100 ng of wild type plasmid. The resulting product, a mixture of wild type template plasmids and mutated, complete but nicked plasmids, was then digested with 1 µl *Dpn*I overnight at 37°C to degrade all methylated template DNA and transformed into competent *E. coli*.

Colony-PCRs serve to identify clones that have successfully integrated the DNA insert into the desired vector backbone and generally use a pair of primers that is specific for the insert and the target vector. Reactions were performed in a volume of 20 µl containing 1× Taq polymerase reaction buffer, 200 µM of each dNTP, 10 µM of each primer and 0.625 units of Taq polymerase. After completion of the reaction mixture, a

pipette tip with a picked colony was left standing in the solution for about 2 min and removed. The following thermocycler program was then run:

Initial Denaturation	95°C	1 min
Denaturation	95°C	30 s
Primer annealing	50-65°C	30 s
Elongation	72°C	1 min per kb
Final elongation	72°C	5 min
	4°C	∞

Steps 2 to 4 were repeated in 30 cycles.

2.2.3 *Preparative and analytical agarose gel electrophoresis*

Agarose was dissolved in 1× TBE buffer to a concentration of 0.7 % to 1.5 % (w/v) by heating. The gel was cast and covered with 1× TBE buffer, DNA samples in 1× DNA loading dye were applied and separated at 90-110 V for 20 to 45 min. The gel was stained in a water bath containing 3 µg/ml ethidium bromide (EtBr) for at least 15 min and DNA was visualized with UV light. In case DNA was destined for further preparative use, UV-exposure was reduced to an absolute minimum.

2.2.4 *Purification of DNA from agarose gels and PCRs*

For purification of DNA from agarose gels and restriction digests of PCR products the respective kits from Machery-Nagel were used according to the manufacturer's instructions. The DNA band of interest was excised from an agarose gel and dissolved in binding buffer, whereas binding buffer was directly added to restriction digests. The DNA was then reversibly bound to a silica membrane and washed with non-aqueous washing buffer. Pure DNA was eluted using 30 µl of TE-buffer.

2.2.5 *Restriction digests*

Restriction digests were performed in a total volume of 20 µl to 50 µl using enzymes from New England Biolabs (NEB) with the supplied buffer and BSA solution or the Fermentas FastDigest enzymes. 1 µg (restriction analysis) or 2 µg to 3 µg (preparative restriction digests) of vector DNA were incubated with approximately 10

units of restriction enzyme per µg DNA for 1 to 2 hours at 37°C (NEB) or 0.5 µl of FastDigest enzyme per µg DNA for 30 to 60 min at 37°C. Following preparative restriction digests of vector DNA, DNA was separated on agarose gels and purified.

For restriction digests of PCR products, 20 units of each restriction enzyme, the appropriate buffer and BSA were added to the purified DNA in 30 µl TE buffer and incubated for 1 to 2 hours at 37°C.

2.2.6 *Dephosphorylation of vector DNA*

Linearized vector DNA was dephosphorylated by adding 10 units of CIP directly to the completed restriction digest reaction and incubating 5 min at 37°C. CIP hydrolyzes the 5'-phosphates from linear DNA molecules, thereby preventing spontaneous recircularization of linearized vectors and reducing the number of false positive colonies after transformation of ligation reactions.

2.2.7 *Ligation of DNA fragments into linearized vectors*

The concentration of the DNA fragment (insert) and the linearized vector were compared on an agarose gel. Assuming a linear increase of ethidium bromide fluorescence with the size of the DNA molecule, the insert was used in a 3- to 6-fold molar excess over vector DNA. Ligation reactions were performed in a volume of 10 µl containing 1× ligase buffer and 1 unit of T4 DNA ligase. Reactions were incubated at 16°C overnight or at 4°C for three days and 5 µl of a ligation reaction were transformed into chemically competent *E. coli*.

2.2.8 *Preparation of chemically competent* E. coli

For preparation of chemically competent bacteria, a 50 ml LB culture of the *E. coli* strain of interest was started from a fresh plate or from a glycerol stock validated to give highly competent bacteria. This culture was grown at 37°C and 250 rpm until the optical density at 600 nm (OD_{600}) reached 0.4. Bacteria were harvested in sterile centrifuge tubes by centrifuging for 10 min at 4000 rpm and 4°C. The pellet was resuspended in 10 ml ice-cold and sterile 0.1 M $CaCl_2$ solution and incubated on ice for at least 15 to 30 min. Bacteria were then sedimented for 10 min at 4000 rpm and 4°C and the pellet was resuspended in 2 ml 0.1 M $CaCl_2$ solution. Glycerol was added to a

final concentration of 10 % and 50 µl aliquots were prepared, snap-frozen in liquid nitrogen and stored at -80°C.

2.2.9 *Transformation of chemically competent* E. coli

Chemically competent *E. coli* of the TOP10 strain were transformed following a heat shock protocol. 50 µl of $CaCl_2$ chemically competent cells were thawed on ice, DNA was added (5 µl of ligation reactions, 5 ng of plasmid DNA) and cells were left on ice for 30 min. The heat shock was carried out by incubating 50 s at 42°C followed by 1 to 2 min on ice. 600 µl of LB medium without antibiotics were added. *E. coli* to be selected on kanamycin containing plates were allowed to recover 45 min at 37°C, whereas in the case of selection on ampicillin containing medium cells were plated directly. Before spreading, the bacteria were pelleted by briefly accelerating to maximal speed in a microcentrifuge, resuspended in about 150 µl of LB medium and then transferred to a selective LB agar plate (for bacteria transformed with plasmid DNA, only 30 µl of the bacteria in 600 µl LB were plated).

2.2.10 *Overnight cultures of* E. coli

Clones found to be positive by colony-PCR screening (or colonies resulting from the transformation of plasmid DNA) or cells from a glycerol stock were picked with a sterile pipette tip and grown overnight at 37°C shaking at 200 rpm in 5 ml (for "mini-prep") or 100 ml (for "midi-prep") LB-medium containing the appropriate antibiotic.

2.2.11 *Preparation of cDNA libraries*

To obtain template DNA for the cloning of various protein coding sequences, complementary DNA (cDNA) libraries from HeLa cells and from rat brain were prepared. Total RNA was extracted with the SV total RNA isolation system from Promega and cDNAs were synthesized from messenger RNAs (mRNAs) using the Superscript III Reverse Transcriptase (RT) from Invitrogen.

The isolation of RNAs critically depends on RNase-free materials and reagents. Therefore, gloves and RNase-free disposables and solutions were used at all times. HeLa cells were washed with 1× PBS (PBS), trypsinized and counted. Cells were pelleted by spinning 5 min at 1300× g. 1.25×10^6 HeLa cells were resuspended in 175

µl of RNA lysis buffer (RLA) and 350 µl of RNA dilution buffer were added. Similarly, 170 mg of rat brain from 3 months old rats stored at -80°C were homogenized in 100 µl RLA with a small tissue homogenizer and 400 µl RLA were added. Cells lysis was achieved by heating to 70°C for 3 min in a heating block. The RLA contains β-mercaptoethanol and guanidine thiocyanate (GTC) that both contribute to inactivating RNAses released from the disrupted cells. Further, cellular mRNAs are generally incorporated in nucleoprotein complexes; GTC and SDS in the RLA denature nucleoprotein complexes and thus release mRNAs into the solution. Next, cellular debris was removed by centrifugation for 10 min at 13,000 rpm at room temperature. The supernatant was transferred to a new tube and 200 µl of 96 % ethanol were added to precipitate the RNA. The solution was loaded onto a silica membrane spin column and washed once with RNA wash solution. 50 µl of Yellow Core Buffer containing DNase I were added and incubated 15 min at room temperature to destroy remaining genomic DNA contaminations. After washing twice with RNA wash solution, total cellular RNA was eluted with 100 µl nuclease-free water and the RNA concentration was determined (see below).

RNAs were immediately used for RT-PCR. RT synthesizes a complementary DNA strand on an RNA template (first-strand synthesis) that then represents the coding DNA sequence and can be used for PCR amplification of coding sequences for cloning. 11 µl of purified total RNA were combined with 1 µl of dNTPs (Superscript III RT kit) and 1 µl of either random hexamer primers (Gibco, diluted 1:20) or oligodT primers (Roche Diagnostics, at 80 µM). This mixture was incubated for 5 min at 65°C to denature the RNA template and chilled on ice for 1 minute to allow primer annealing. Then, 4 µl of 5× RT buffer and 1 µl each of 0.1 M DTT, RNAsin and Superscript III RT were added (all included in the Superscript III RT kit). Reverse transcription was performed by incubating 5 min at 25°C and 45 min at 50°C. The resulting cDNAs were stored at -20°C.

2.2.12 *Purification of plasmid DNA from* E. coli *cultures*

Small scale plasmid DNA preparations from 5 ml of *E. coli* overnight cultures (mini-prep) were carried out using the Nucleospin Plasmid kit from Macherey-Nagel according to the manufacturer's instructions. Following alkaline lysis of the cells, precipitated genomic DNA and protein are removed by centrifugation. The plasmid

DNA is then bound to a silica membrane and washed to remove contaminants. DNA was eluted in 35 µl of TE buffer.

For larger amounts and a higher purity, plasmid DNA was purified from 100 ml *E. coli* overnight cultures using the Nuclebond Midi kit from Macherey-Nagel according to the manufacturer's instructions. With this system, plasmid DNA is first purified on a silica membrane of higher DNA binding capacity and then precipitated using isopropanol. The precipitate is washed with ethanol and finally resuspended to the desired concentration in TE buffer.

2.2.13 *UV spectroscopy for determining nucleic acid concentrations*

The concentration of DNA and RNA preparations was determined using a photometer. 2 -5 µl DNA were diluted in a total of 100 µl ddH_2O and 80 µl were transferred to a UV-transmitting plastic cuvette. The extinction at 260 nm (E_{260nm}) was measured and the concentration was calculated according to Lambert-Beer's law, assuming an extinction coefficient ε_{dsDNA} of 50 ml/µg × cm (d: lightpath in the solution = 1 cm)

$$c = \frac{E_{260nm}}{d \cdot \varepsilon_{dsDNA}} \cdot dilution = \frac{E_{260nm}}{1cm \cdot 50 \frac{ml}{\mu g \cdot cm}} \cdot 50$$

The quality of the DNA preparation was judged satisfactory if the coefficient of extinction at 260 nm (absorption maximum of dsDNA) over 280 nm (strong protein absorption) was between 1.8 and 2.1.

The concentration of RNA preparations was determined identically, assuming an extinction coefficient ε_{RNA} of 40 ml/µg × cm.

2.2.14 *Sequencing*

Sequencing of plasmid DNA was carried out at MWG Biotech according to the dideoxy nucleotide method by Saenger. 2 µg of DNA were sent by express mail at RT. Sequencing results were analyzed with the Vector NTI 11 software.

2.3 Biochemical methods

2.3.1 *Expression of recombinant proteins in* E. coli

Overnight cultures of the *E. coli* BL21 strain transformed with pET-28a or pGEX4T-1 expression constructs were diluted 1:20 to 500 ml 2x YT medium containing the appropriate antibiotic and grown to an OD_{600} of 0.7 to 0.8. At this point, cultures enter the log phase and rapidly proliferate. Expression of recombinant proteins was then induced by adding isopropyl thiogalactoside (IPTG) to a concentration of 0.5 mM. Induced cultures were incubated for 3 hours at 30°C shaking at 200 rpm. Alternatively, expression was carried out at 16°C overnight.

Bacteria were harvested by centrifugation at 4000× g for 20 min, the supernatant was decanted and the pellet resuspended in PBS. Four aliquots were again pelleted by spinning 10 min at 4000× g, the supernatant was aspirated and the pellets stored at -20°C.

2.3.2 *Purification of GST- and His_6-fusion proteins expressed in* E. coli

In order to obtain purified recombinant proteins for in vitro experiments, Glutathione S-Transferase- (GST, a 27 kDa protein) or 6× Histidine-tagged (His_6) proteins are bound to an affinity gel. Using the so-called batch protocol, GST can be bound to glutathione immobilized on beads, whereas His_6-tags bind to Nickel ions (Ni^{2+}) that in turn are linked to agarose beads via the chelator nitrilotriacetic acid (Ni-NTA beads).

E. coli BL 21 pellets were thawed on ice, resuspended in 20 ml of ice-cold PBS and 125 units benzonase (a DNase), a spatula tip of lysozyme (a bacterial cell wall degrading enzyme from chicken egg white) and PMSF to 1 mM were added. After incubating on ice for 15 min, cells were sonicated one minute on ice (50 % duty cycle, 70 % power), Triton X-100 was added to a concentration of 1 % and the mixture was sonicated again (s.a.). The mixture was incubated 15 min on ice and then centrifuged for 15 min at 35,000× g to pellet the debris of the lysed cells. Supernatants containing the expressed recombinant protein were then added to the appropriate binding resin and incubated rotating on 4°C for 1.5 hours. For GST-fusion proteins, 400 µl resuspended GST-bind resin from Novagen pre-washed in 30 ml PBS were used; for His_6-tagged proteins, 300 µl resuspended His Ni-NTA agarose from Sigma pre-washed in 30 ml

PBS containing 10 mM imidazole were used. Beads were generally sedimented by centrifuging 2 min at 3000× g (JS 5.3 rotor in Avanti J-26 XP). To reduce unspecific binding to the Ni-NTA agarose, 10 mM imidazole was added during binding and washing. Beads were washed 3 times in PBS for 10 min at 4°C (+10 mM imidazole for His_6-tag purification). GST fusion proteins were then resuspended in 1 ml PBS, the protein concentration was determined by Bradford assay and proteins were stored at 4°C. His_6-tagged proteins were washed briefly in 30 ml PBS with 20 mM imidazole, sedimented and resuspended in 1 ml PBS. After transferring to a microcentrifuge tube, His_6-tagged proteins were eluted in 300 to 500 µl of 300 mM imidazole in PBS for 30 min rotating at 4°C. The beads were pelleted by spinning 5 min at 13,000 rpm and the supernatant was ultracentrifuged for 30 min at 100,000× g in an Optima TXL using the TLA 100.2 rotor. The protein concentration was determined by Bradford assay or measuring absorption at 280 nm and the protein was stored at 4°C.

2.3.3 *Purification of denatured protein from inclusion bodies*

For the purification of large amounts of natively unfolded protein fragments, the protein of interest was expressed in *E. coli* BL21 at 22°C overnight (2 l of culture for His-PI3K C2α amino acids 2 – 365). Cell pellets from 1 l of culture were resuspended in 25 ml resuspension buffer (20 mM Tris pH 8.0, 500 mM NaCl) and cells were lysed using 500 units benzonase (20 µl of 25 U/µl working stock) and a big tip-of-a-spatula of lysozyme in the presence of 1 mM PMSF on ice for 15 min. Lysis was completed by sonicating 2 times for 2 min (50 % duty cycle, 70 % power, flat plate, no tip). Debris was removed by centrifuging at 9,000× g for 15 min at 4°C and the pellet was washed four times by resuspending vigorously in 20 ml washing buffer (20 mM Tris pH 8.0, 500 mM NaCl, 0.05% Triton X-100, 0.05% Chaps) and sedimenting as described above. After the last wash, the pellet was resuspended in 30 ml denaturing buffer (8 M urea, 20 mM Tris pH 8.0, 500 mM NaCl). Undissolved inclusion bodies were removed by ultra-centrifugation for 30 min at 125,000× g and 4°C in a Ti70 rotor. Protein concentration was determined by measuring absorption at 280 nm and the predicted extinction coefficient of the protein of interest (obtained from ProtParam at expasy.org). The cleared inclusion body solution was filtered through a 0.45 µm membrane, imidazole was added to 10 mM and protein was bound to a 1 ml HisTrap FF column (GE Healthcare) equilibrated in column wash buffer (6 M urea, 20 mM Tris pH 8.0, 500 mM NaCl, 10 mM imidazole; degased) using an Äkta prime at a flow rate of 0.5 - 1

ml/min (~1 hour). The column was washed with column wash buffer at 1 ml/min until absolutely no more protein was detected in the eluate, followed by washing with about 15 ml of intermediate wash buffer (4 M urea, 20 mM Tris pH 8.0, 500 mM NaCl, 10 mM imidazole; degased) to prevent precipitation of urea. Bound protein was eluted with elution buffer (4 M urea, 300 mM imidazole, 20 mM Tris pH 8.0, 500 mM NaCl; degased) in 1 ml fractions, with total protein eluting within 7-12 ml (or 13-17 ml, depending on the volume of the tubing system). The eluate was concentrated to 1 ml using a Millipore centrifugal filter device and dialyzed against 20 mM Tris pH 8.0, 150 mM NaCl, 10 mM imidazole in 1l for 1h.

2.3.4 *Affinity purification of polyclonal antibodies from serum*

Polyclonal antibodies against amino acids 2 – 365 of human PI3K C2α (purification of the antigen see 2.3.3) were raised in rabbits at Eurogentec S.A.. Specific antibodies were affinity purified from serum using the same protein fragment employed for immunization crosslinked to sepharose. 0.4 g of CNBr-activated sepharose 4B (GE Healthcare) were washed three times with 50 ml 1 mM HCl, sedimenting the beads for 5 min at 600 rpm, and washed once with buffer B (8M urea, 0.1 M NaH_2PO_4, pH 8.0). 4 mg of protein antigen were diluted into a total volume of 10 ml buffer B, the washed sepharose beads were resuspended in this solution, transferred to a 15 ml falcon, and filled up to 15 ml with buffer B. Cross-linking was allowed to proceed gently rotating at 4°C overnight. On the second day, the beads were pelleted, washed three times with buffer B and once with 1M ethanolamine. Residual CNBr-groups were blocked by gently rotating 2 h at room temperature in 10 ml 1M ethanolamine. Beads were then washed three times alternatingly with a) 0.1 M sodium acetate, 500 mM NaCl pH 4.0 and b) 0.1 M sodium tetraborate, 500 mM NaCl pH 8.0, followed by three washes with PBS. For preparation of the column, the outlet was closed, filled with 10 ml PBS and a porous filter disc was pushed to the bottom using a glass pipette. The beads were resuspended in PBS from the column, transferred to the column, and allowed to settle for 30 min. For pre-elution of the column, 10 ml elution buffer (2 M glycine / HCl pH 2.2) with 1 ml freshly added 1,4-dioxan were added immediately after letting the PBS drain and allowed to flow straight through. The column was washed with PBS until pH was back to 7.4. The serum input material was cleared of cells and fat by centrifuging 10 ml serum for 30 min at 4,000 rpm and 4°C. A fat film accumulates at the top while remaining cells form a pellet. The PBS was allowed to drain from the column, the outlet

was firmly closed with a cap, and the cleared serum was added to the beads. The top of the column was sealed using the lid and parafilm and incubated slowly rotating at 4°C overnight. The next day, the beads were left to settle on ice and the serum was allowed to flow through. The column was then gently filled to the top with PBS (this defines the washing volume for the following steps), rinsing beads to the bottom, and a porous filter disc was placed on top of the beads, leaving 1-2 mm above the gel bed. PBS was drained and the column was washed with 0.1 M sodium tetraborate, 500 mM NaCl, 0.1 % Tween-20 followed by at least three washes with PBS. For elution, ten 1.5 ml tubes containing 200 µl 1M Tris / HCl pH 8.8 and elution buffer containing 10 % fresh 1,4-dioxan were prepared. PBS was allowed to drain from the column and outlet was closed before adding 1 ml elution buffer, letting the first fraction of precisely one column volume drain and again closing the outlet. This was incubated for one minute. The second fraction was collected and subsequently, 750 µl PBS were added for each fraction, completely collecting them before adding the next 750 µl PBS. pH in the second fraction was tested and, if necessary, neutralized with 1M Tris pH 8.8. The elution procedure was repeated as described above for a second time and absorption at 280 nm was measured in all fractions. All fractions containing significant amounts of protein were pooled, dialyzed against PBS, concentrated, and NaN_3 was added to 0.02 % for storage at 4°C. For storage at -20°C, glycerol was added to 50 %.

2.3.5 *Protein determination (Bradford assay)*

For determining the protein concentration of cell extracts and purified protein solutions, samples were diluted 1:50 to 1:1,000 in 500 µl PBS and 500 µl 2× Bradford reagent were added. The mixture was then incubated 5 min at room temperature and OD_{595} was determined with a photometer blanked against 1× Bradford reagent and buffer. Only extinction values between 0.1 and 0.5 were considered reliable. The protein concentration was calculated from a standard curve covering the range of 1 µg to 10 µg BSA.

2.3.6 *Preparation of protein extracts from eukaryotic cells*

Total protein extracts from eukaryotic cells were prepared using lysis buffer A with 1 % Triton X-100 (LBA). This non-ionic detergent disrupts membranes and solubilizes integral and membrane associated proteins. Cos7, HeLa, or HEK293 cells grown on plastic dishes were gently washed with PBS and buffer was aspirated

completely. Dishes were transferred to ice, LBA was added and cells were harvested using a cell scraper. Confluent 6-wells were harvested in a total volume of 50 to 100 µl LBA. Lysis was completed by incubating 30 min on ice. Lysates were clarified by spinning at 13,000 rpm and 4°C in a tabletop microcentrifuge. If extracts were to be used for further experiments, e.g. association studies or activity determinations, aggregated protein was removed by ultracentrifugation at 65,000 rpm and 4°C in TLA-110 or TLA-100.2 rotors.

2.3.7 *SDS polyacrylamide gel electrophoresis (SDS-PAGE)*

Sodium dodecysulfate (SDS) polyacrylamide gel elctrophoresis (PAGE) is a method for separating proteins based on their molecular mass. SDS (sodiumdodecylsulfate, $H_3C\text{-}(CH_2)_{11}\text{-}SO_4^{2-}$ complexed with Na^+) is a ionic detergent that disrupts the non-covalent interactions stabilizing the protein's secondary and tertiary structure. It associates with the protein in a ratio of about 1 SDS molecule per 2 amino acids and thereby i) completely masks the protein's native charge with its triply negatively charged head group and ii) generates a constant protein mass to charge ratio. Therefore, proteins are separated depending on their molecular weight only.

The polyacrylamide gel is formed by radical polymerization of an acrylamide / N, N'-methylenebisacrylamide (AA/BA) mixture. The decay of the radical initiator ammonium peroxodisulfate (APS) is catalyzed by tetraethylenediamine (TEMED), producing $SO_4^{-\cdot}$ radicals that then attack the carbon-carbon double bond in acrylamide molecules and initiate the formation of a chain. N, N'-methylenebisacrylamide serves as a linker of polyacrylamide chains and thus generates a gel-like network.

SDS-PAGEs were carried out according to Laemmli (Laemmli, 1970), using Tris-glycine based buffers and a 3 % stacking and 8 % to 12 % separating gel (Table 2-9). In the pH 6.8 stacking gel, glycine molecules are only partly ionized and migrate slowly. Together with Cl^- ions at the front, glycine leads to a modulation of electric field intensity (stronger at the rear, weaker at the front) over the protein stack and thus allows isotachophoresis: all protein molecules of one species assemble at the same position in the protein stack, finally resulting in sharp protein bands. The effect of glycine as the slow terminating ion is lost upon entry into the pH 8.8 separating gel and proteins are separated according to their mass.

Table 2-9: SDS-polyacrylamide gels.

	12 %	10 %	8 %	3 %
ddH_20	2.5 ml	3 ml	3.5 ml	1.25 ml
4x buffer	1.875 ml	1.875 ml	1.875 ml	0.625 ml
AA/BA mixture	3 ml	2.5 ml	2 ml	0.33 ml
TEMED	7.5 µl	7.5 µl	7.5 µl	3.75 µl
APS	75 µl	75 µl	75 µl	37.5 µl

SDS-PAGEs were run at 12 to 15 mA per gel. After electrophoresis, gels were either processed for immunoblotting or proteins were visualized by staining with Coomassie. Coomassie stain was heated to about 60°C and the gel was stained for 25 min. Background staining was removed by repeatedly washing with Coomassie destain. The sensitivity of detection by Coomassie was limited to about 100 ng of protein.

2.3.8 *Immunoblotting*

Immunoblotting or "Western Blotting" is a highly sensitive method for detecting specific proteins after separation by SDS-PAGE. The proteins, still associated with SDS and thus negatively charged, are transferred from the gel onto a nitrocellulose membrane in an electrical field.

The transferred protein was reversibly stained with Ponceau stain for 5 min at room temperature to check for correct transfer and the amount of protein loaded onto the gel. After washing once in 1× TBS (TBS), the highly protein-adsorptive membrane was blocked against unspecific antibody binding using 3 % milk powder in TBS for one hour at room temperature. A specific primary antibody diluted 1:200 to 1:10,000 in antibody dilution solution was then incubated on the membrane for 2 hours at room temperature or, preferably, overnight at 4°C. The antibody was recycled and the membrane was washed 3 times for 10 min at room temperature in TBS. Secondary HRP-coupled antibodies that specifically recognize immunoglobulins of the species the first antibody was raised in were used to detect the protein of interest. The secondary antibody was incubated on the membrane diluted 1:5,000 in 3 % milk powder in TBS for one hour at room temperature. Unspecific secondary antibody binding was reduced by washing 3 times for 10 min at room temperature in TBS. Signal was detected by adding enhanced chemiluminescence reagent (ECL reagent, Amersham Biosciences) to the membrane and exposing to an x-ray film. The ECL reagent serves as a substrate for HRP that catalyzes a luminescent reaction of luminol with hydrogen peroxide.

2.3.9 *Preparation of clathrin-coated vesicles from calf brain*

Preparation of CCVs was carried out essentially as described (Campbell et al., 1984). 4 calf brains were repeatedly washed in a 4 l beaker with ice-cooled tap water in a cold room until water remained relatively clean. White matter and large vessels were removed and brains were cut into ~2.5 cm cubes and placed in a blender with 400 ml Buffer A (100 mM Mes pH 6.5, 1 mM EGTA, 0.5 mM $MgCl_2$, 0.02 % NaN_3, 0.5 mM DTT). 10 ml of 50 ml PMSF (50 mM in EtOH) were added and brains were homogenized for 1 minute at low speed and then blended at maximal speed for another two min. The homogenate was centrifuged 45 min at 10,000 rpm (17,700× g) in a JA-10 rotor at 4°C. Supernatants were carefully collected and distributed on 2 JLA-16.250 tubes. 60 ml Buffer A were added to each pellet and pellets were vigorously resuspended, distributed on 4 JLA-16.250 tubes and centrifuged for 45' at 14,200 rpm and 4°C in JLA-16.250 (30,000× g). Supernatants were carefully transferred into a chilled 1 l beaker with a 10 ml glass pipette (cytosol and microsomal fraction w/o mitochondria, lysosomes, or peroxisomes). The cleared supernatant was loaded into Ti-45 tubes and centrifuged for 1 hour at 44,000 rpm (150,000× g) and 4°C to pellet all light membranes (supernatant: cytosol). Supernatants were discarded and membrane pellets were resuspended in a total of 2 × 20 ml Buffer A + 200 µl 50 mM PMSF. Pellets were homogenized using a teflon homogenizer (5-10 strokes, 900 rpm). Resuspended pellets were pooled a in glass bottle and filled up to 50 ml with Buffer A + 250 µl 50 mM PMSF. To this, 50 ml of 12.5 % Ficoll / 12.5 % sucrose were added and mixed well. The solution has now the same density as the homogenous CCVs which upon centrifugation will float whereas heavier membranes will pellet. This mixture was distributed on four Type Ti-70 tubes (25 ml each) and centrifuged for 25 min at 30,000 rpm (90,600× g) and 4°C. Supernatants were collected in a pre-cooled, graduated 100 ml cylinder and equal volumes were distributed to six Ti-45 tubes, filled to the top with buffer A and centrifuged for 1 hour at 44,000 rpm (150,000× g) and 4°C. Supernatants were discarded and pellets were resuspended in a total of 10 ml buffer A and homogenized as described above to obtain the CCV fraction. From 4 calf brains, about 50 mg of CCVs can be obtained.

For stripping of CCVs, to 1 ml of CCV preparation 500 µl buffer B (2.4 M Tris-HCl pH 7.4, 3 mM EGTA. 0.04 % NaN_3, 1 mM DTT) and 30 µl 50 mM PMSF (in EtOH) were added and mixed well. This was incubated at room temperature overnight. The following morning, the stripped CCVs were transferred into a TLA-110 tube and

1.5 ml ddH_2O were added to reduce Tris concentration to 0.4 M. Membranes and protein aggregates were quantitatively removed by centrifuging 30 min at 68,000 rpm in TLA-110 at 20°C and then increasing the speed to 100,000 rpm for ten more minutes.

2.3.10 In vitro *lipid kinase activity assay*

The kinase activity of immunoprecipitated 6xMyc-PI3K C2α WT, kinase inactive, or class III mutant was analyzed by *in vitro* kinase activity assays using γ-^{32}P-ATP (Wieffer et al., 2012).

A confluent 10 cm dish of HEK293 cells transiently expressing 6xMyc-PI3K C2α for about 20 h was washed gently with 10 ml PBS and all liquid was aspirated thoroughly. Cells were harvested in 500 µl IP Buffer (20 mM Hepes, 100 mM KCl, 2 mM $MgCl_2$, 1% CHAPS, 1mM PMSF, 0.3% protease inhibitor cocktail) and transferred to a microcentrifuge tube. Cells were incubated on ice for 30 min, debris was removed by centrifuging for 10 min at 13,000 rpm and 4 °C and the supernatant was ultracentrifuged in a TLA110 rotor for 15 min at 65,000 rpm. For immunoprecipitation (IP), 40 µl of protein A/G agarose bead slurry (pre-washed with PBS, sedimentation at 3500 rpm for 1 min) were incubated with about 15 µg of mouse-anti-c-myc antibody in 500 µl PBS for 1h at room temperature and washed. HEK cell extract was added and incubated at 4°C for 1 to 2 h. Beads were washed using 0.5 ml IP buffer without detergent two times for 5-10 min on a rotating wheel at 4°C and once on / off. After the final wash, all buffer was removed using a Hamilton syringe.

Beads were resuspended in 200 µl kinase buffer (5 mM Hepes/KOH pH 7.2, 25 mM KCl, 2.5 mM MgOAc, 150 mM KGlu, 10 µM $CaCl_2$, 0.2% CHAPS) and 25 µl (= 1/8 IP) were aliquoted to each kinase assay tube. Remaining IP sample was used for immunoblot determination of the relative amount of enzyme present in experiments comparing mutants of PI3K C2α.

100 µg of synthetic dried phosphatidylinositol, PI(4)P, or PI(4,5)P_2 lipid films in glass vials were resuspended in 200 µl kinase buffer and sonicated for 1 min, followed by incubation for at least 30 min at RT. The required volume of resuspended lipid (200 µM final lipid concentration) was transferred to a microcentrifuge tube, kinase buffer was added to 25 µl total volume per reaction, and ATP was added to 200 µM. In the isotope laboratory, 10 µCi γ^{32}-P-ATP per reaction were added and 25 µl of lipid / ATP-mix were dispensed on each 25 µl IP sample and immediately incubated for 10 min at 37°C (staggered by 30s for each sample). Reactions were stopped by adding 500 µl

[methanol : H_2O : HCl (32%) at 10:10:1 v/v], again staggered by 30 s per sample. Samples were mixed vigorously for 2 min. The acidic milieu is required to keep phosphate groups of inositol lipids protonated and to render them sufficiently soluble in chloroform. 500 µl chloroform were added, samples were mixed vigorously for 1 min and centrifuged 5 min at 1200× g to properly separate phases. The aqueous supernatant was collected into a new tube, the chloroform extraction was repeated and the chloroform phase was collected and pooled with the first extraction step. Half of the samples was now transferred to a new tube and the chloroform phases were cleaned by adding 500 µl of [methanol : H_2O : HCl (32%) at 10:10:1 v/v], mixing for 1 min and centrifuging as described above. The aqueous supernatant was discarded and lipids were dried completely in a SpeedVac at room temperature. The extracted lipids were then separated in a thin layer chromatography (TLC) and detected using storage phosphor screens (section 2.3.11).

2.3.11 *Thin layer chromatography of lipids and storage phosphor detection*

TLC plates (HPTLC F254, Merck) were equilibrated for 30 min in 1 % potassium oxalate in MeOH : H_2O (2:3 v/v) with 2 mM EDTA to remove Calcium and dried for 15 to 30 min at 130°C. Dried lipids were dissolved in 12 µl chloroform and spotted onto the TLC plate in 1.5 µl steps. The TLC plate was then placed into a glass chamber filled with 64 ml $CHCl_3$, 30 ml acetone, 24 ml methanol, 30 ml acetic acid and 13 ml ddH_2O and tightly sealed to allow saturation of the atmosphere with solvent. The TLC was run for 3 hours and then dried at room temperature. Radioactivity was detected using a storage phosphor system (storage phosphor screens and Cyclone Phosphorimager from Packard), exposing the storage phosphor screen overnight or up to 3 days at -80°C.

2.3.12 *PIP beads pull down assay*

Agarose PIP Beads (Echelon Biosciences) containing 10 nanomoles of bound $PI(4,5)P_2$ or $PI(3,4)P_2$ per ml of beads were used to pull down proteins from rat brain extract. Rat brain extract was prepared from 2.5 g frozen rat brain homogenized in homogenization buffer (4 mM HEPES pH 7.4, 320 mM sucrose, 1mM PMSF, 0.3 % protease inhibitor cocktail) using 13 strokes of a glass-teflon-homogenizer at 900 rpm. The homogenate was centrifuged at 900× g for 10 min at 4° C. To the supernatant PIP

pulldown buffer (20 mM HEPES pH 7.4, 50 mM NaCl, 0.25 % NP-40) was added to 1× concentration and incubated on ice for 30 min followed by centrifugation at 43,500× g at 4° C. The supernatant was centrifuged again at 265,000× g for 15 min at 4° C to remove aggregated proteins. 6-8 mg of protein were added to 100 µl of 1:1 washed agarose-bead slurry and incubated at 4° C for 1.5 hours on a rotating wheel. Beads were pelleted, washed 3 times with PIP pulldown buffer and bound proteins were eluted two times in 30 µl of 1× Laemmli sample buffer. 30 µl of the pooled eluate were then loaded onto an 8% acrylamide gel for SDS-PAGE followed by immunoblotting.

2.3.13 *Liposome binding: flotation assay*

Liposome preparation. A total of 600-800 µg of lipids were dissolved in a mixture of $CHCl_3$:MetOH:1N HCl (2:1:0.01) to the desired concentration, combined in a glass vial and dried under pressurized N_2 followed by vacuum for 30 min. Liposomes were rehydrated in 300 µl HEPES buffer [50 mM HEPES pH 7.4, 100 mM KCl (140 mM KCl for experiments with GFP-SNX9 WT or K267N, R327N; 200 mM KCl for experiments with GST-SNX9 PX-BAR)] for one hour at room temperature under frequent vortexing. After the addition of 1.7 ml H_2O the liposomes were centrifuged in a TLA110 rotor at 20,000 rpm at 4° C for one hour. The resulting pellet was resuspended in HEPES buffer to a final lipid concentration of 3 mg/ml. Liposome mixtures were extruded 14 times through an 800 nm polycarbonate membrane (Whatman) using a manually operated extruder (LiposoFast, Avestin, Inc.). The final concentration of lipid species in mol% were: 50 % phosphatidylcholine, 20 % cholesterol, 19 % phosphatidylethanolamine, 1% Rhodamine-phosphatidylethanolamine, 5 % phosphatidylserine, and 5 % PIs.

Flotation assay. 450 µg liposomes in HEPES buffer were combined with either 2 µg of purified GST-SNX9 PX-BAR protein or with 30 µg of HEK293 cell extract containing overexpressed HA-SNX9 PX-BAR or GFP-SNX9 full length protein and incubated for 15 min at 4° C on a rotating wheel. The mixture was then adjusted to 30 % sucrose by adding 75 % sucrose in HEPES buffer and transferred to a TLS-55 centrifuge tube. This was overlaid with 200 µl of 25% sucrose in HEPES buffer followed by 50 µl of HEPES buffer. Liposomes were floated by centrifuging one hour at 55,000 rpm (~240,000× g) in a TLS 55 swing out rotor (Beckman Coulter). The fractions were harvested using a blunt ended needle attached to a calibrated syringe by removing the bottom layer first (~250 µl total volume), followed by the middle layer

(200 µl) and in the end the top layer containing the liposomes and any bound protein. Top and bottom fractions were separated on 8 % acrylamide gels and stained with Coomassie for GST-SNX9 PX-BAR and immunoblotted for HA-SNX9 PX-BAR or GFP-SNX9 full length.

2.4 Cell biological methods

2.4.1 *Mammalian cell culture*

Cos7, HeLa, and HEK293 cells were cultured in a humidified incubator at 37°C and 5 % CO_2. As general culture medium, Dulbecco's Modified Eagles Medium (DMEM + Glutamax, purchased from Lonza) with 4.5 g/l glucose, 10 % heat-inactivated fetal calf serum (FCS), and 50 units/ml penicillin and 50 µg/ml streptomycin was used. Cells were passaged every 2 to 4 days and seeded to a new culture dish at a dilution of 1:3 to 1:20. For detaching, cells were washed with PBS and trypsinized with one volume of trypsin-EDTA (1 ml for a 10 cm dish, Gibco) for 5 min at 37°C and resuspended in 10 volumes of culture medium with FCS to inactivate the trypsin. Freshly thawed cells were passaged at least once before use in an experiment. Cells were abandoned beyond passage 30 to 35.

Mouse embryonic fibroblasts (MEFs) were handled similarly, but were cultured in DMEM containing 10 % bovine calf serum instead of fetal calf serum and generally kept at densities below confluence. Importantly, PI3K C2α$^{-/-}$ MEFs could not be used for more than a few passages for analysis of PI3K C2α knock out related phenotypes because compensatory mechanism appeared to increasingly take effect with time in culture.

2.4.2 *Transfection of plasmid DNA*

HeLa, Cos7, and HEK293 cells were seeded to a density of ~ 50 % one day prior to transfection in order to achieve ~ 90 % confluency for transfection. Plasmid DNA was transfected using lipofectamine 2000 (Invitrogen) according to the manufacturer's instructions, for a 6-well using 3.2 µg plasmid DNA with 4 µl lipofectamine 2000. Cells were used for experiments between 20 to 48 h post-transfection. For microscopy, coverslips were coated with matrigel (BD Biosciences; 50 µl matrigel per 12-well for at least one hour at 37°C) and cells were split to coverslips 2 h after removal of the transfection reagent. For overnight starvation, cells were allowed another 2 h to attach after seeding and were then washed with PBS and changed to serum-free medium.

For transfection of MEFs with plasmid DNA, the Amaxa nucleofector electroporation system was used. For two 6-wells, 3×10^6 cells were resuspended in 100 µl electroporation buffer (25 mM Hepes pH 7.6, 10 mM K_2HPO_4 / KH_2PO_4 pH 7.6,

2 mM $MgCl_2$, 120 mM KCl), 10 µg of plasmid DNA were added and electroporation was performed using the Amaxa program "T-20". Cells were immediately resuspended in 500 µl culture medium and distributed to two 6-wells. Note that cell viability and transfection efficiency varied immensely with the plasmid DNA used. Whereas eGFP-transfected MEFs were confluent the next day and up to ~75 % of cells were expressing eGFP, eGFP-PI3K C2α-transfected cells were only ~30 % confluent the next day and displayed dramatically lower transfection efficiency. Further, expression levels were mostly low so that detection of eGFP by antibody staining was necessary to identify transfected cells.

2.4.3 *Small interfering RNA treatments and rescue experiments*

Cos7 or HeLa cells seeded on day 0 were transfected with siRNAs using oligofectamine (Invitrogen) according to the manufacturer's instructions (for one 6-well: 2 µl 100 µM siRNA with 4 µl oligofectamine in a final volume of 1 ml OptiMEM; after 4 h addition of recovery DMEM containing 1.5× FCS and antibiotics) on day 1, expanded on day 2, transfected a second time on day 3, seeded onto matrigel coated coverslips for the experiment on day 4, and used for the experiment on day 5. Cos7 cells were seeded to be 60 – 70 % confluent and HeLa cells to be about 80 % confluent for siRNA transfections. Cell viability varied between siRNAs. For expression of recombinant proteins in knockdown cells, siRNA transfection complexes were removed from the cells after 4 h on day 3 instead of leaving the transfection on overnight. Plasmids were then transfected using lipofectamine 2000 (Invitrogen) according to the manufacturer's instructions on day 4. In the case of INPP4B-CAAX constructs, cells were sequentially transfected first with siRNAs and then with plasmid (2 h recovery period after each transfection) both on day 3 to allow for a total expression time of 40 h.

For simultaneous depletion of two proteins, referred to as 'double knock down', the described protocol was applied identically using 2 µl of a 100 µM stock of each siRNA per 6-well, effectively doubling the amount of siRNA present without changing the amount of oligofectamine. Knock down efficiency was validated using immunoblotting of cell extracts for every siRNA used and for all combinations of double knock downs.

2.4.4 *Generation of stable cell lines using the Flp / FRT system*

For the generation of a HEK293 cell line with stable inducible expression of 6xMyc-PI3K C2α, the Flp / FRT system was used. A HEK293 acceptor cell line bearing a Flip recombinase acceptor site at a safe harbor locus and stably expressing the Tet operon repressor protein (TetR) was co-transfected with a Flip recombinase expression plasmid and the pcDNA5/FRT/TO-6xMyc-PI3K C2α plasmid, which features an expression cassette flanked by Flip recombinase recognition sites. Upon integration of this cassette into the safe harbor locus of the acceptor cell line, the inserted protein lies under control of a TetR-regulated CMV promoter. Further, only integration of the cassette at the pre-designed site in the genome allows expression of the contained hygromycin resistance gene. For a 10 cm dish, 16 µg pOG44 (Flip recombinase) and 2 µg of the plasmid of interest were transfected into the acceptor cell line using lipofectamine 2000. Cells were split to two 15 cm dishes and selection with 100 µg/ml hygromycin (HygroGold, Invivogen) and 10 µg/ml blasticidin (blasticidin hydrochloride, Invivogen) was commenced 24 h post-transfection. After about 3 weeks, individual colonies were picked and analyzed for recombinant protein expression upon induction with doxycycline.

2.4.5 *Immunofluorescence*

Cells adhering on coverslips were immediately fixed with paraformaldehyde (PFA, 500 µl of 4 % PFA with 4 % sucrose in PBS pH 7.4 for a 12-well) for 10 to 45 min at room temperature or with 100 % methanol (500 µl pre-cooled to -20°C) for 10 min at -20°C. The method of fixation was dependent on the proteins of interest and the PFA-sensitivity of epitopes to be used for the immunostaining. If necessary, a combination of both methods (3 min PFA + 7 min methanol) was used. Fixed cells were washed twice with PBS and were then blocked against unspecific antibody binding with 10 % goat serum and permeabilized using 0.3 % Triton X-100 for intracellular immunostainings by incubating 30 min at room temperature with goat serum dilution buffer (GSDB).

Primary antibodies were diluted 1:50 to 1:1,000 in GSDB and 40 µl were spotted onto parafilm in a humid chamber. Coverslips were placed upside down on the spotted antibody solution spots and incubated for one hour at room temperature. After washing 3 times for 5 min with IF wash buffer, secondary goat α-mouse or α-rabbit antibodies coupled to Alexa 488, 568 or 647 were applied at a dilution of 1:200 as

described above and incubated 1 hour at room temperature. Coverslips were washed 3 times for 10 min in IF wash buffer, dipped into ddH_2O to remove salt and mounted onto microscopy slides using 16 µl Immumount mounting solution (Thermo Electron) supplemented with 1 µg/ml DAPI.

For lipid antibody stainings, Cos7 cells were fixed in 2 % PFA at room temperature for 20 min and permeabilized with saponin (30 min at room temperature in 0.5 % saponin, 1 % bovine serum albumine (BSA) in PBS). Cells were labeled with lipid-specific antibodies (see Table 2-8) diluted in 1 % BSA in PBS for 2 h at room temperature. After washing three times for 5 min with PBS, cells were incubated with appropriate fluorescent secondary antibodies for 1 h and washed three times for 10 min with PBS.

2.4.6 *Transferrin and EGF uptake assays*

Cos7 or HeLa cells treated with siRNAs or transfected with mCherry-PI-phosphatase-CAAX constructs were seeded on matrigel (BD Biosciences) coated coverslips. On the day of the experiment, cells were serum-starved for 3 h (Cos7) or 1.5 h (HeLa) and used for either transferrin uptake, transferrin receptor surface labeling, or EGF uptake (Cos7 only). For transferrin uptake, cells were incubated with 25 µg/ml transferrin-Alexa568 or transferrin-Alexa647 (Molecular Probes, Invitrogen) for 10 min at 37°C. After two washes with ice-cold PBS cells were acid washed at pH 5.3 (0.2 M sodium acetate, 200 mM NaCl) on ice for two min to remove surface-bound transferrin, washed 2 times with ice-cold PBS and fixed with 4 % PFA for 45 min at room temperature. For transferrin surface labeling, cells were incubated with 25 µg/ml fluorescently-labeled transferrin at 4°C for 45 min to block endocytosis and to label transferrin receptors on the cell surface. Cells were washed 3 times with ice-cold PBS on ice for one min and fixed with 4 % PFA for 45 min at room temperature. For EGF-uptake, Cos7 cells were incubated with 100 ng/ml EGF-Alexa647 (Molecular Probes, Invitrogen) for 10 min at 37°C and further processed as described for transferrin above.

2.4.7 *Fluorescence microscopy*

Fluorescence microscopy is a technique that uses the phenomenon of fluorescence to specifically detect biomolecules in fixed or live cells. A fluorophore is excited with light of a specific wavelength and relaxes into the electronic ground state, emitting light of a defined, but longer wavelength. Generally, two different kinds of

fluorophores are available: Fluorescent dyes coupled to antibodies that can be used to specifically label either endogenous or overexpressed proteins and genetically encoded fluorescent proteins that allow monitoring overexpressed proteins both in fixed and live cells. Depending on experimental requirements, different microscopic techniques were used.

Epifluorescence microscopy. For the quantitative analysis of fluorescence intensities on a per cell basis, e.g. for the analysis of ligand internalization experiments, epifluorescence widefield microscopy was used. Since no measures are taken to enhance resolution in z, epifluorescence detection samples a large volume of the cell, thereby achieving a good excitation to emission ratio, and is hence ideally suited for the quantitative assessment of total labeling intensity. The epifluorescence setups used were from Zeiss [Zeiss Axiovert 200M with DG4 excitation unit and Coolsnap HQ2 EM-CCD camera (Roper Scientific) operated by Slidebook software (Intelligent Imaging)] or Nikon (Nikon Eclipse Ti, equipped with Andor sCMOS camera, Okolab incubator for live imaging and Nikon PerfectFocus autofocus system).

Spinning disc confocal microscopy. Experiments that required the resolution of subcellular structures were routinely analyzed by spinning disc confocal microscopy [Ultra View ERS Rapid Confocal Imager (Perkin Elmer) equipped with an EM-CCD-camera (Hamamatsu), photokinesis unit for photobleaching experiments, and connected to a Zeiss Axiovert 200M microscope]. Confocal spinning-disc microscopy uses two rotating pinhole discs to acquire confocal images without point-by-point scanning of the specimen. This greatly reduces acquisition time and photobleaching of fluorophores. Thus, spinning disc microscopes are ideally suited for live cell imaging. The software used for operating the microscope was Volocity (Improvision, Perkin Elmer).

Fluorescence recovery after photobleaching (FRAP). FRAP experiments address the mobility of fluorescent proteins within a cell and provide a measure of the stability and lifetime of structures labeled by the protein of interest. For measuring FRAP, a defined region of interest is bleached and the recovery of fluorescence in this region, as a consequence of molecules exchanging with the unbleached regions of the cell, is monitored. FRAP was performed using the photokinesis unit of the spinning disk confocal microscope described above. One to three regions of interest in the peripheral, flat part of an eGFP-clathrin light chain (CLC) expressing Cos7 cell were selected. A timelapse series at 0.5 Hz was recorded with 10 frames before and 60 frames after bleaching. For quantification, the sum eGFP-CLC fluorescence intensity at CCPs was

quantified over time and normalized to the mean sum intensity during the pre-bleaching period.

Total internal reflection fluorescence (TIRF) microscopy. For the selective visualization of structures and processes at the basal plasma membrane of adherent cells TIRF microscopy was used (Axelrod, 1981). This technique employs objectives that allow the excitation laser beam to be directed onto the coverslip at a variable angle. When this angle is set to the critical angle of total internal reflection, the incident light is entirely reflected at the phase boundary of glass (coverslip) and aqueous medium (sample). However, in this process an evanescent wave is generated that propagates in parallel to the phase boundary and exponentially decays in intensity with the distance from the phase boundary. This results in the selective illumination of fluorophores within about 200 nm of the phase boundary which in a cellular context means that only the plasma membrane and its immediate cytoplasmic environment will be imaged. TIRF imaging was performed using a Zeiss Axiovert 200M microscope equipped with an incubation chamber (EMBL workshop, Heidelberg), a 100x TIRF objective and a dual-colour TIRF setup from Visitron Systems using Slidebook imaging software (3i Inc.) or a Nikon Eclipse Ti, equipped with Andor sCMOS camera, Okolab incubator for live imaging, Nikon PerfectFocus autofocus system, 60x TIRF-objective, a custom-built solid state laser setup, operated by open source ImageJ-based Micromanager software (Edelstein et al., 2010). For analysis of CCP dynamics, timelapse series of 3 min with a frame rate of 0.5 Hz were recorded. CCP lifetimes were assessed by arbitrarily selecting 50 or 25 CCPs per cell in the center frame of the timelapse series and determining the frame of appearance and disappearance. In case CCPs already existed in the first frame or persisted until the last frame, these frames were counted. For the analysis of recruitment time courses of proteins to CCPs, only CCPs were used that both appeared and disappeared within the timelapse series. From these fluorescence intensities over time were quantified and aligned on the time axis by the last frame of GFP-PI3K C2α presence (t = 0, fission). Fluorescence intensities for all time points in relation to t = 0 were averaged over all CCPs in the analysis and renormalized to the resulting peak value. For analysis of the degree of membrane association of PI-binding protein domains, TIRF and epifluorescence images of the same cell were acquired and the TIRF fluorescence intensity was normalized to the epifluorescence signal in order to achieve intrinsic correction for expression level variations between cells.

2.4.8 *SD-dSTORM superresolution microscopy*

SD-*d*STORM superresolution microscopy was performed as previously described (Lampe et al., 2012). Briefly, *d*STORM (direct stochastic optical reconstruction microscopy) uses commercially available organic dyes coupled to antibodies that are switched into a prolonged OFF state by strong illumination (643nm) and reducing agents (Heilemann et al., 2008). The short, stochastic ON states are imaged over time (few minutes) and the spatiotemporally separated single molecules are localized with a precision of 20 to 30 nm using open source software rapi*d*STORM (Wolter et al., 2010). SD-*d*STORM is a novel variant of *d*STORM that combines the advantages of spectral demixing with the buffer compatible blinking properties of red emitting carbocyanine dyes. SD-*d*STORM uses an emission splitter and custom-written software to separate the overlapping emissions of 2 dyes (i.e. Alexa 647 and Alexa 700) coupled to antibodies, offering aberration free and nearly cross-talk free reconstruction multi-color *d*STORM.

2.4.9 *Image analysis and quantification*

Qualitative and quantitative image analysis were performed using Volocity software for spinning disc confocal images and Slidebook or ImageJ (Schneider et al., 2012) for epifluorescence and TIRF microscopy data. Quantitative data were processed using Microsoft Excel and figures arranged using Adobe Photoshop.

3 Results

3.1 $PI(3,4)P_2$ is a regulator of clathrin-mediated endocytosis

The formation of CCVs from the plasma membrane depends on the presence of $PI(4,5)P_2$ whereas the subsequent endosomal stages of the endocytic pathway depend on 3-phosphorylated PIs. It remains unclear how the conversion of PI identity from $PI(4,5)P_2$-positive endocytic intermediates to PI(3)P-containing endosomes is achieved. In addition to the PI3K hVps34 several $PI(3,4)P_2$ 4- and $PI(3,4,5)P_3$ 5-phosphatases have been identified as effectors of the GTPase Rab5 (Shin et al., 2005), the master regulator of endosome biogenesis (Zeigerer et al., 2012). Thus, endosomal PI(3)P may originate in part from hydrolysis of higher phosphorylated PIs. Given the strict dependence of $PI(3,4,5)P_3$ formation on growth factor signaling (Wymann and Schneiter, 2008; Vanhaesebroeck et al., 2010) and the prevalence of 4-phosphorylated PIs at the plasma membrane (Hammond et al., 2012), we hypothesized that $PI(3,4)P_2$ might serve as an intermediate plasma membrane PI species en route to endosomal compartments.

3.1.1 *$PI(3,4)P_2$ is present at clathrin-coated pits*

Visualization and localization of PIs has been made amenable by the development of lipid-binding domain-based sensors (Di Paolo and De Camilli, 2006; Lemmon, 2008) and the generation of antibodies specifically recognizing select PI headgroups. In order to analyze the subcellular distribution of $PI(3,4)P_2$ we made use of a specific anti-$PI(3,4)P_2$ antibody (Bae et al., 2010). The predominant plasma membrane labeling displayed several larger membrane structures in the cell periphery but mostly localized to diffraction-limited puncta that were found all over the plasma membrane. Interestingly, these puncta partially colocalized with plasmalemmal CCPs as revealed by co-labeling for clathrin heavy chain (Figure 3-1a). This is further illustrated by a fluorescence intensity line profile showing a subset of clathrin-coated structures to closely overlap with the $PI(3,4)P_2$ labeling (Figure 3-1a). Confirming the specificity of the antibody, $PI(3,4)P_2$-antibody labeled structures were positive for the $PI(3,4)P_2$-sensing tandem PH-domain of TAPP1 (Dowler et al., 2000; Oikawa et al., 2008) to a

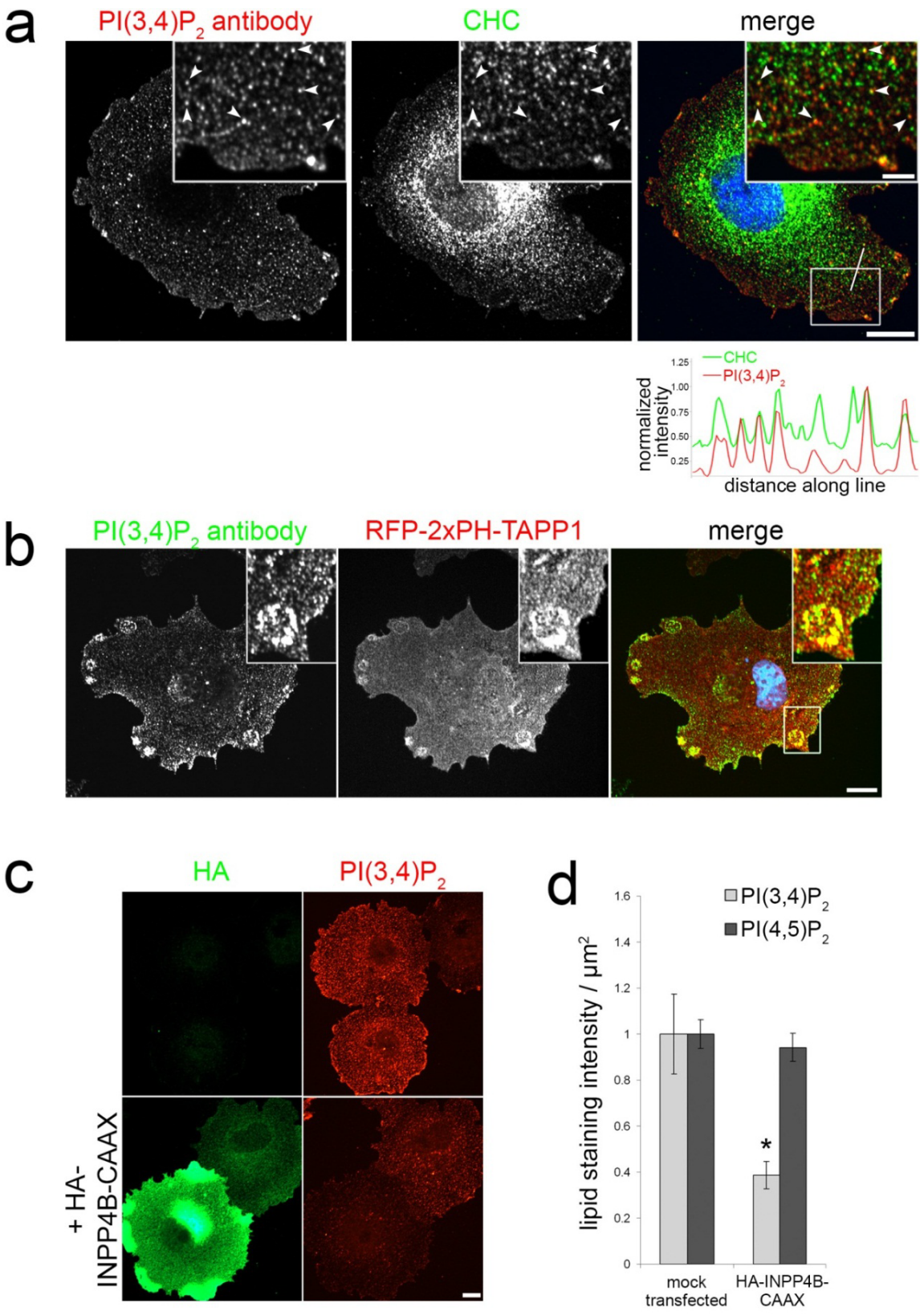

Figure 3-1: $PI(3,4)P_2$ is present at clathrin-coated pits. a) Partial colocalization of $PI(3,4)P_2$ with CCPs. Confocal images of Cos7 cells stained for $PI(3,4)P_2$ and clathrin heavy chain (CHC). Arrowheads, structures immunopositive for $PI(3,4)P_2$ and clathrin. Scale bar, 10 µm (inset: 2 µm). **b)** The $PI(3,4)P_2$-sensing PH domain of TAPP1 colocalizes with immunostained $PI(3,4)P_2$. Confocal images of Cos7 cells

expressing the tandem PH-domain of TAPP1 immunostained for $PI(3,4)P_2$. Note the considerable similarity of staining patterns and spatial overlap between both $PI(3,4)P_2$ markers. Scale bar, 10 µm. **c,d)** Selective depletion of $PI(3,4)P_2$ by the $PI(3,4)P_2$-specific phosphatase INPP4B (INPP4B-CAAX). **c,** Cos7 cells transfected with HA-INPP4B-CAAX were immunostained for $PI(3,4)P_2$ and the HA-epitope. Note the decrease in $PI(3,4)P_2$ labeling in HA-INPP4B-CAAX-expressing cells that correlates with the expression level of the HA-INPP4B-CAAX. Scale bar, 10 µm. **d,** Levels of $PI(3,4)P_2$ or $PI(4,5)P_2$ were quantified by immunostaining for $PI(3,4)P_2$ or $PI(4,5)P_2$ (mean ± s.e.m.; n = 5 independent experiments; * $p < 0.05$, t-test).

large extent, both in small punctate structures and larger membrane structures reminiscent of circular dorsal ruffles seen in migratory cells (Figure 3-1b; (Oikawa et al., 2008)).

To further verify labeling specificity we analyzed cells overexpressing the $PI(3,4)P_2$-specific 4-phosphatase, type II inositol 3,4-bisphosphate 4-phosphatase (Gewinner et al., 2009) that was modified with a carboxy-terminal prenylation signal derived from K-ras (Malecz et al., 2000) to achieve constitutive plasma membrane targeting (INPP4B-CAAX). As expected, overexpression of INPP4B-CAAX resulted in a significant depletion of antibody-decorated $PI(3,4)P_2$ whereas the cellular levels of $PI(4,5)P_2$ measured by specific antibodies (van den Bogaart et al., 2011) remained unchanged (Figure 3-1c,d). These data indicate that the levels and distribution of $PI(3,4)P_2$ are faithfully reported by anti-$PI(3,4)P_2$ antibodies or by the 2xPH-TAPP1 sensor and, further, that overexpression of INPP4B-CAAX results in the depletion of plasma membrane $PI(3,4)P_2$.

3.1.2 *A tool-kit for the selective depletion of plasma membrane PIs*

The effect of INPP4B-CAAX overexpression on plasma membrane PI levels was assessed in more detail by quantitative determination of the membrane enrichment of specific PI-binding domain-based sensors using ratiometric TIRF / epifluorescence imaging. To derive a quantitative measure of membrane association of a PI-binding domain from a population of cells expressing the sensor at varying levels, we compared the ratio of TIRF intensity over epifluorescence intensity on a single cell basis. Only the $PI(3,4)P_2$-specific sensor 2xPH-TAPP1, but not sensors for other PIs such as PI(3)P, $PI(4,5)P_2$, or $PI(3,4,5)P_3$ showed a decrease in TIRF / epifluorescence ratio and, hence, membrane association in INPP4B-CAAX expressing cells (Figure 3-2a). This

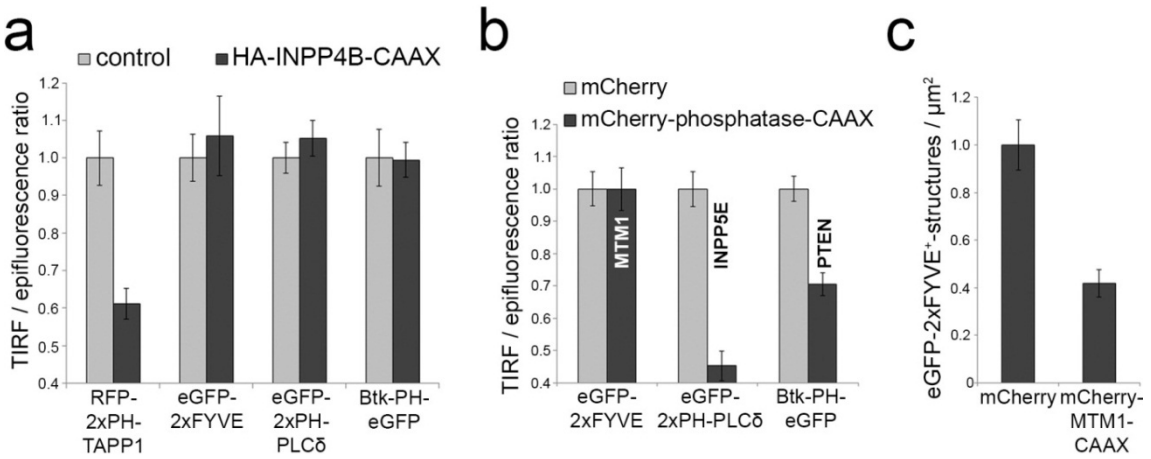

Figure 3-2: Membrane-anchored PI-phosphatases are tools for the selective depletion of plasma membrane PI species. a) Expression of INPP4B-CAAX decreases the plasma membrane association of the PI(3,4)P_2-sensing TAPP1-PH domain but not of other PI-binding domains as determined by ratiometric TIRF / epifluorescence imaging (mean ± s.e.m. of n = 19-25 cells per condition). eGFP-2xFYVE, a sensor for PI(3)P; eGFP-2xPH-PLCδ, a sensor for PI(4,5)P_2; Btk-PH-eGFP, a sensor for PI(3,4,5)P_3. **b,c)** Expression of PI-phosphatase-CAAX chimeras causes selective PI depletion. **b**, ratiometric TIRF/ epifluorescent imaging of the PI(4,5)P_2-sensor eGFP-2xPH-PLCδ in INPP5E-CAAX-expressing cells (i.e. depletion of PI(4,5)P_2) or of the PI(3,4,5)P_3 sensor eGFP-PH-Btk in PTEN-CAAX (i.e. to deplete PI(3,4,5)P_3) expressing cells (basal conditions) reveals loss of the corresponding PI from the plasma membrane. The weak plasma membrane association of the PI(3)P-sensing FYVE-domain is unaffected by expression of membrane-targeted MTM1 (mean ± s.e.m. of n = 19-30 cells per condition). **c**, Expression of MTM1-CAAX causes a decrease in the number of punctuate structures labeled by the PI(3)P-sensor eGFP-2xFYVE, indicative of a depletion of endosomal PI(3)P (mean ± s.e.m. of n = 20-30 cells per condition).

demonstrates that INPP4B-CAAX can be used to selectively deplete PI(3,4)P_2 at the plasma membrane.

In order to expand the possibilities of manipulating plasma membrane PIs we created additional PI-phosphatase-CAAX constructs. Expression of membrane-anchored versions of the PI(4,5)P_2-5-phosphatase INPP5E (Varnai et al., 2006) and the PI(3,4,5)P_3-3-phosphatase PTEN reduced plasma membrane association of the corresponding PI sensor (Figure 3-2b). Further, expression of the PI(3)P-specific phosphatase, MTM1-CAAX (Fili et al., 2006), reduced the number of PI(3)P-positive endosomes labeled by eGFP-2xFYVE while the TIRF / epifluorescence ratio was unchanged (Figure 3-2b,c). This suggests absence of a PI(3)P-pool at the plasma membrane, a conclusion supported by the observation that the TIRF / epifluorescence signal for soluble eGFP is almost identical to that produced by 2xFYVE (0.92 +/- 0.03

of the 2xFYVE signal; n = 3). The set of membrane-anchored phosphatases presented here may serve as a toolkit for the selective depletion of PIs at the plasma membrane.

3.1.3 *PI(3,4)P_2 regulates clathrin-mediated endocytosis*

Given the apparent presence of PI(3,4)P_2 at CCPs we asked whether this lipid might be of functional importance for CME itself. To this end, we analyzed the endocytosis of transferrin, a canonical clathrin-dependent endocytic ligand, and determined the ratio of internalized over surface-bound transferrin. This provides a direct measure for the efficiency of CME irrespective of transferrin receptor surface

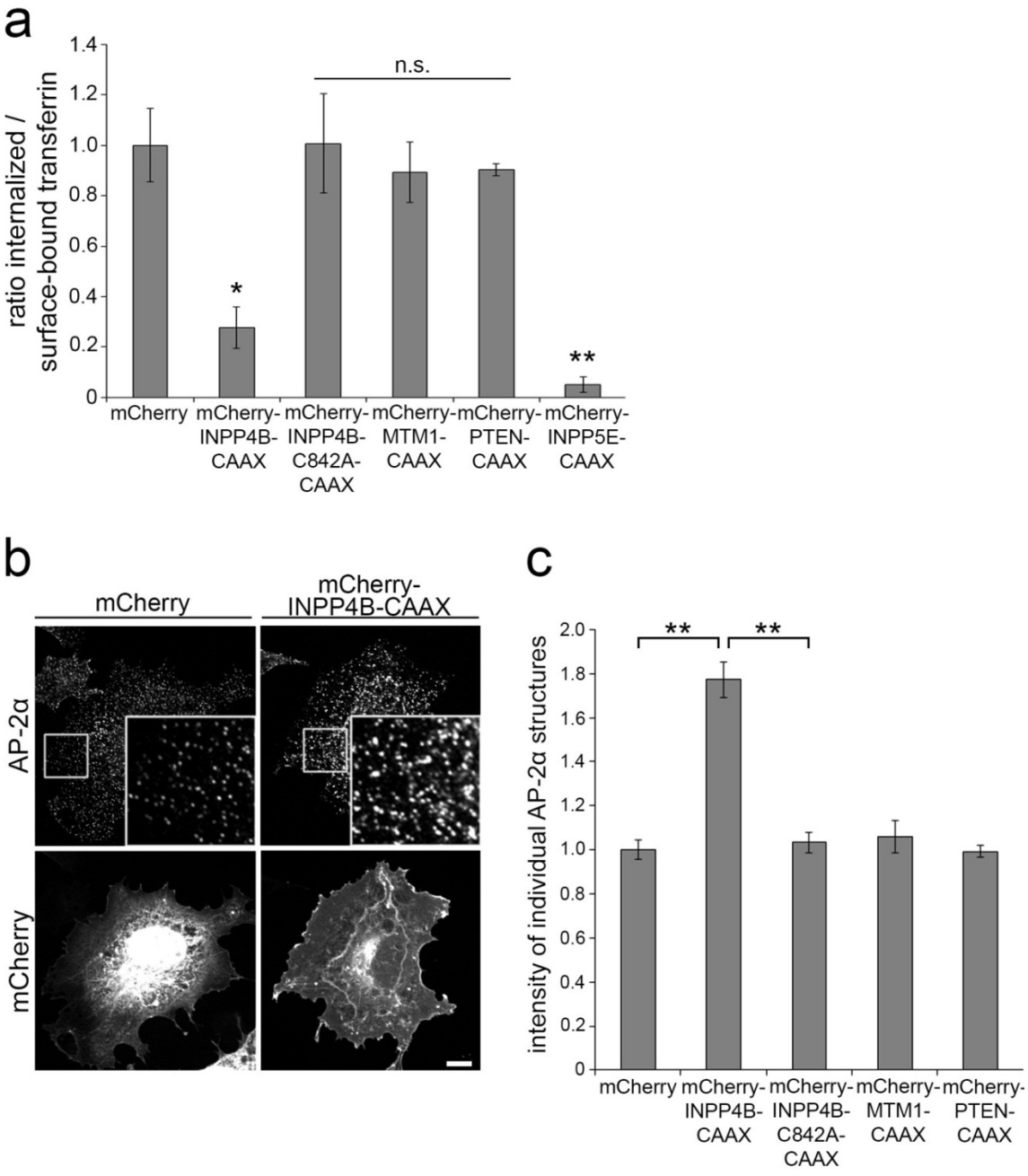

Figure 3-3: PI(3,4)P_2 regulates clathrin-mediated endocytosis. a) Selective depletion of plasma membrane PI(3,4)P_2 impairs CME of transferrin. Expression of membrane-targeted inactive INPP4B (C842A), of the PI(3)P phosphatase MTM1, or of the PI(3,4,5)P_3 phosphatase PTEN do not affect CME. INPP5E-mediated depletion of PI(4,5)P_2 known to block CME was used as a control. Bar diagrams represent ratio of internalized (10 min, 37°C) to surface transferrin (45 min, 4°C) (mean ± s.e.m.; n = 3 independent experiments, for INPP4B (C842A) n = 2; * $p < 0.05$, ** $p < 0.01$, t-test). **b,c)** Accumulation of AP-2-positive CCPs in PI(3,4)P_2-depleted cells. Confocal images of Cos7 cells expressing mCherry or mCherry-INPP4B-CAAX stained for endogenous AP-2α. **b,** Scale bar, 10 µm. **c,** Mean intensity of endocytic AP-2α-containing CCPs (mean ± s.e.m.; n = 3 independent experiments; ** $p < 0.01$, t-test).

levels, as these may be affected by alterations in internalization or endosomal trafficking of the receptor. Indeed, depletion of cellular PI(3,4)P_2 by INPP4B-CAAX impaired clathrin-dependent endocytosis of transferrin and led to increased transferrin receptor surface levels, similar to depletion of PI(4,5)P_2 by INPP5E-CAAX, a lipid required for CCP nucleation (Figure 3-3a). Overexpression of membrane targeted catalytically inactive INPP4B (C842A, (Gewinner et al., 2009)), the PI(3)P-phosphatase MTM1, or the PI(3,4,5)P_3-phosphatase PTEN did not affect CME of transferrin (Figure 3-3a). These surprising effects of PI(3,4)P_2 depletion indicate a hitherto unknown regulatory role for PI(3,4)P_2 in CME.

To understand the mechanistic basis for this effect we analyzed the distribution and dynamics of key endocytic proteins. PI(3,4)P_2 depletion by INPP4B caused the accumulation of AP-2α-positive CCPs on the plasma membrane, a phenotype similar to that seen in dynamin 1/2-knockout (KO) cells due to a late block in CME (Ferguson et al., 2009). No such effects were observed for catalytically inactive INPP4B (C842A), MTM1, or PTEN (Figure 3-3b,c). This defect corresponded to drastically attenuated dynamics of CCPs as monitored by TIRF live imaging of stably eGFP-clathrin light chain expressing Cos7 cells. Upon depletion of PI(3,4)P_2, CCPs displayed increased lifetimes and a tendency to cluster in close proximity to each other, although infrequent endocytic events could still be observed (Figure 3-4, central left panel). CCP dynamics in cells undergoing PI(3)P- or PI(3,4,5)P_3-depletion were unaltered, whereas depletion of PI(4,5)P_2 caused the expected (Zoncu et al., 2007) and distinctly different phenotype of loss of CCPs from the plasma membrane (Figure 3-4, lower right panel). These data identify PI(3,4)P_2 as a novel regulator of CME that is possibly involved in a late stage in the pathway. This regulatory role is clearly distinct from the PI(4,5)P_2-controlled initiation of CCP assembly (Loerke et al., 2009).

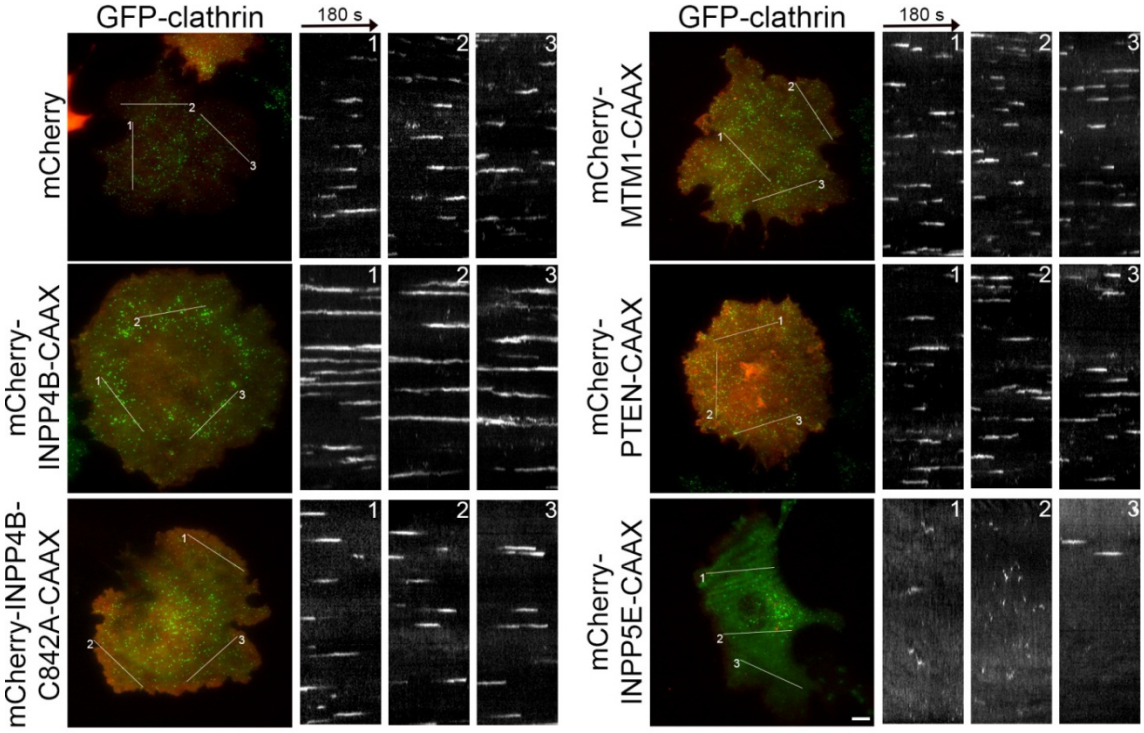

Figure 3-4: CCPs depend on PI(3,4)P_2 or PI(4,5)P_2 at different stages of maturation. Analysis of CCP dynamics by TIRF imaging of eGFP-clathrin in mCherry-PI-phosphatase-CAAX expressing cells. Depletion of PI(3,4)P_2 by INPP4B-CAAX causes an accumulation of long-lived CCPs (left central panel) whereas depletion of PI(4,5)P_2 by INPP5E-CAAX (bottom right) prevents the formation of CCPs. Expression of catalytically inactive INPP4B-CAAX (C842A) or depletion of PI(3)P by MTM1-CAAX or of PI(3,4,5)P_3 by PTEN-CAAX did not affect CCP dynamics. Shown are 3 representative kymographs of eGFP-clathrin fluorescence over 180 s along the lines depicted in the left panel. Scale bar, 10 µm.

3.2 PI3K C2α controls maturation of clathrin-coated pits

The unexpected identification of $PI(3,4)P_2$ as a modulator of CME raised the question for the origin of this lipid. $PI(3,4)P_2$ can be generated downstream of growth factor activation by the sequential activity of wortmannin-sensitive class I PI3Ks and 5-phosphatases such as SHIP2 that subsequently hydrolyze $PI(3,4,5)P_3$ (Bunney and Katan, 2010). Consistent with this we found that growth factor-induced increase of $PI(3,4,5)P_3$ was abrogated by pre-incubating cells with wortmannin (Figure 3-5a). Surprisingly, class I PI3K inhibition had only a moderate effect on the basal level of $PI(3,4)P_2$ (Figure 3-5b). These data argue for the existence of a class I PI3K-independent pool of $PI(3,4)P_2$ and are consistent with CME being a constitutive process in most cell types that can occur independently of growth factor activation. An alternative, less well characterized pathway for $PI(3,4)P_2$ production is the class II PI3K-mediated phosphorylation of PI(4)P (Rameh and Cantley, 1999), a PI species abundant at the Golgi complex and at the plasma membrane (Hammond et al., 2012). The contribution of class II PI3Ks to cellular $PI(3,4)P_2$ synthesis is so far unknown. Previous work has identified the class II enzyme PI3K C2α as a direct

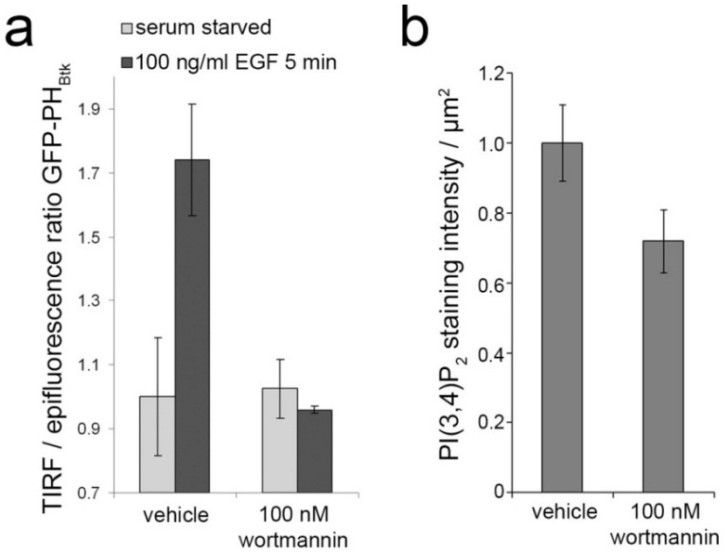

Figure 3-5: A class I PI3K-independent pool of $PI(3,4)P_2$. a) Wortmannin (WM) abrogates the agonist-induced increase of $PI(3,4,5)P_3$. Membrane association of eGFP-PH_{Btk}, a $PI(3,4,5)P_3$ sensor, was determined by ratiometric TIRF / epifluorescent imaging of Cos7 cells serum-starved and pre-treated with vehicle or 100 nM WM before stimulation with 100 ng/ml epidermal growth factor (EGF) where indicated [mean ± s.e.m. of n = 3 (vehicle) or n = 2 experiments]. **b)** Treatment with WM has a limited effect on the $PI(3,4)P_2$ level. Antibody staining of Cos7 cells treated with vehicle or 100 nM WM in serum-free medium for 30 min (mean ± s.e.m.; n = 4 experiments).

interactor of clathrin and a potential regulator of clathrin-dependent membrane trafficking (Gaidarov et al., 2001). Furthermore, PI3K C2α's $PI(3,4)P_2$-synthesizing activity is stimulated by clathrin (Gaidarov et al., 2001) but largely refractory to inhibition by wortmannin (Domin et al., 1997; Patel and Watson, 2005). Quantitative proteomics showed PI3K C2α to be enriched in clathrin-coated vesicles (CCVs) with about 10 copies per vesicle (Borner et al., 2012). Based on these observations, we hypothesized that PI3K C2α may be responsible for the synthesis of a $PI(3,4)P_2$ pool dedicated to CME. Accordingly, perturbation of PI3K C2α function should cause endocytic defects phenocopying those observed upon depletion of $PI(3,4)P_2$.

3.2.1 *PI3K C2α regulates clathrin-mediated endocytosis*

In agreement with previous data (Gaidarov et al., 2001) we found endogenous PI3K C2α to colocalize with clathrin in endocytic CCPs (Figure 3-6a) and confirmed its enrichment in purified CCVs (Figure 3-6b). RNAi-mediated depletion of clathrin caused a complete dispersal of overexpressed PI3K C2α to the cytosol, indicating that membrane targeting of PI3K C2α requires clathrin (Figure 3-6c). To analyze the function of PI3K C2α we assessed the effects of its small interfering RNA (siRNA)-mediated depletion in Cos7 cells. Efficient silencing of PI3K C2α expression was achieved using two independent siRNAs 1 and 2 (Figure 3-7a). PI3K C2α-depleted cells were impaired in CME as evidenced by reduced transferrin uptake and increased transferrin-receptor surface levels (228 +/- 23% of mock control; rescue: 111 +/- 12% of mock; s.e.m., n = 5 independent experiments). This effect was specific, as re-expression of siRNA-resistant eGFP PI3K C2α fully restored internalization of transferrin (Figure 3-7b). Remarkably, depletion of PI3K C2α caused a phenotype highly similar to the effects seen upon depletion of $PI(3,4)P_2$ (see Figure 3-3a).

Corroborating our data, defective transferrin-CME was also observed in mouse embryonic fibroblasts (MEFs) derived from PI3K C2α KO mice (in collaboration with Dr. Emilio Hirsch, Molecular Biotechnology Center, Torino, Italy), a phenotype rescued by re-expression of wild-type but not a catalytically inactive (Gaidarov et al., 2005) mutant PI3K C2α (Figure 3-7c). The internalization of epidermal growth factor (EGF) was also reduced, albeit to a lesser extent (Figure 3-7d). Of note, in order to obtain a sufficient signal the assay was performed using 100 ng/ml EGF-Alexa647, a concentration at which the internalization of EGF is known not to strictly depend on clathrin (Goh et al., 2010).

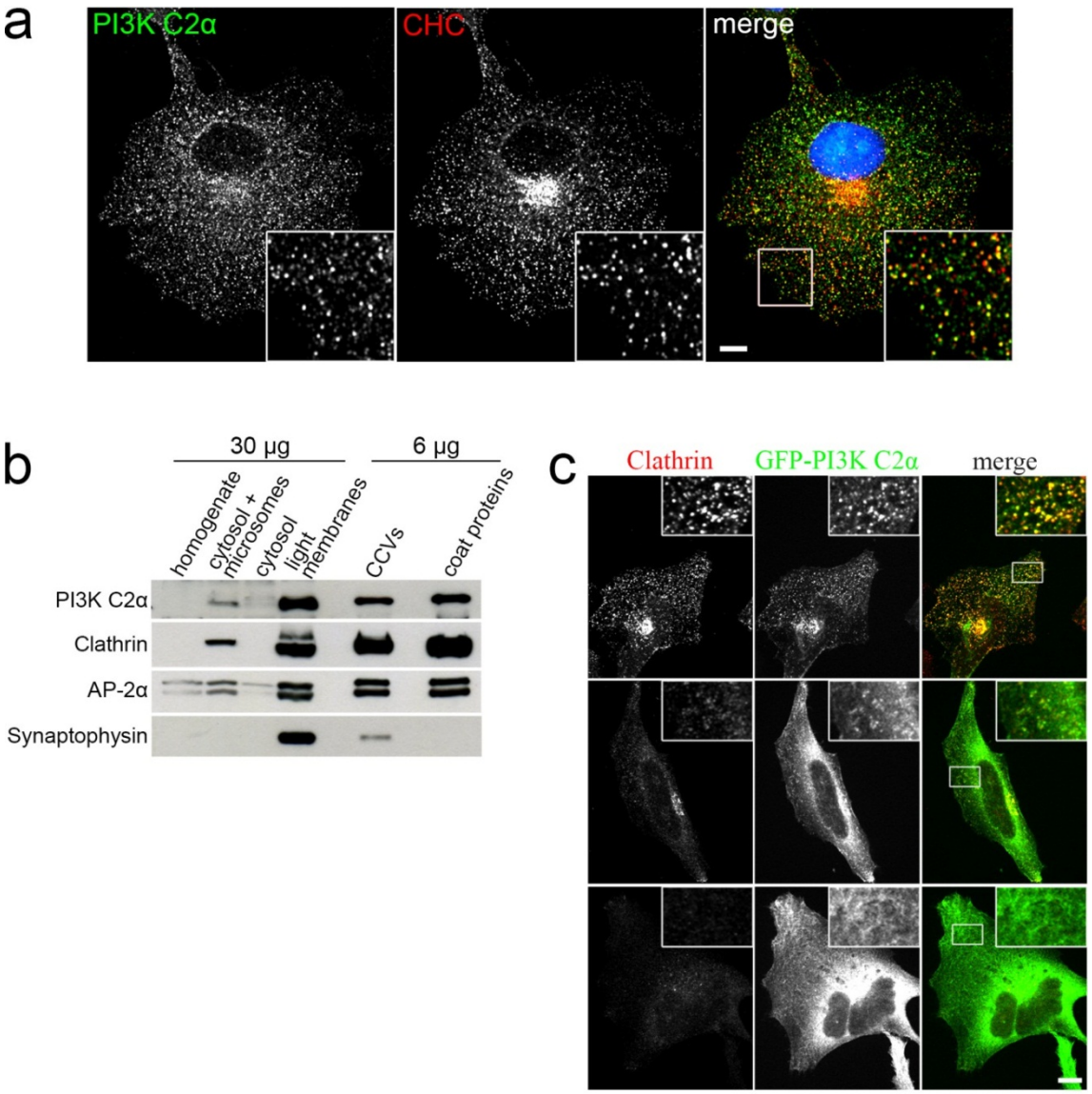

Figure 3-6: PI3K C2α localizes to clathrin-coated structures. a) Confocal images of Cos7 cells stained for endogenous PI3K C2α and clathrin heavy chain (CHC). Scale bar, 10 µm. **b)** PI3K C2α is enriched in purified CCVs. CCVs were purified from calf brain and analyzed by immunoblotting. PI3K C2α is highly enriched in the coat of CCVs to an extent similar to that of clathrin and AP-2α. Note that only a fifth of the protein amount of CCVs and coat proteins was loaded in comparison to the fractions from earlier steps in the purification process. **c)** Localization of PI3K C2α depends on clathrin. HeLa cells expressing eGFP-PI3K C2α were transfected with clathrin heavy chain (CHC) siRNA. Loss of CHC causes dispersion of eGFP-PI3K C2α: in cells expressing residual amounts of CHC a low level punctuate signal for eGFP-PI3K C2α remains (middle panel), whereas complete loss of CHC results in full dispersion of eGFP-PI3K C2α to the cytosol (bottom panel). Scale bar, 10 µm.

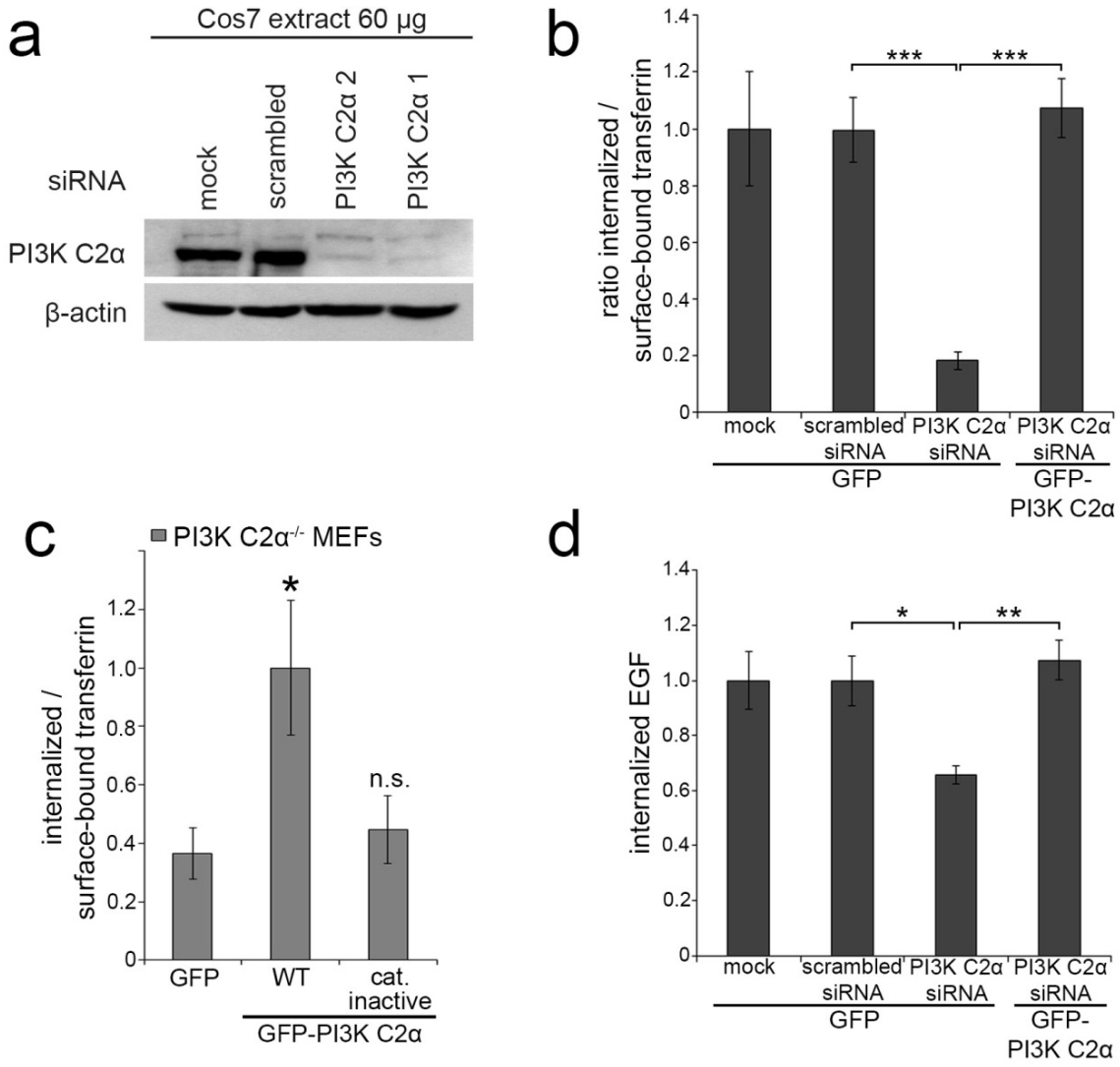

Figure 3-7: Depletion of PI3K C2α inhibits endocytosis of transferrin and EGF. a) Efficient RNAi-mediated depletion of PI3K C2α in Cos7 cells. Immunoblot analysis of extracts from Cos7 cells treated with two different siRNAs targeting PI3K C2α. Detection of β-actin shows equal loading in all lanes. **b)** PI3K C2α depletion impairs CME of transferrin. Cos7 cells depleted of PI3K C2α expressing eGFP or siRNA-resistant eGFP-PI3K C2α WT were assayed for CME of transferrin. Bar diagrams represent the ratio of internalized (10 min, 37°C) to surface transferrin (45 min, 4°C) (mean ± s.e.m.; n = 5 independent experiments; *** $p < 0.001$, t-test). **c)** Mouse embryonic fibroblasts (MEFs) derived from PI3K C2α$^{-/-}$ mice expressing either eGFP, siRNA-resistant eGFP-PI3K C2α WT, or a catalytically inactive siRNA-resistant eGFP-PI3K C2α were assayed for CME of transferrin as in b (mean ± s.e.m.; n = 4 (GFP, WT) or n = 3 (catalytically inactive) independent experiments; * $p < 0.05$, t-test). **d)** PI3K C2α depletion impairs the internalization of EGF. Cos7 cells depleted of PI3K C2α and expressing either eGFP or siRNA-resistant eGFP-PI3K C2α WT were assayed for internalization of EGF at 100 ng/ml for 10 min at 37°C (mean ± s.e.m.; n = 4 independent experiments; * $p < 0.05$, ** $p < 0.01$, t-test).

3.2.2 *Depletion of PI3K C2α impairs clathrin-coated pit dynamics*

To mechanistically dissect the nature of this endocytic defect we analyzed the dynamics of plasmalemmal CCPs in cells depleted of PI3K C2α by TIRF microscopy. Cells lacking PI3K C2α showed increased lifetimes of CCPs, again displaying a striking resemblance to CCPs in cells where $PI(3,4)P_2$ was depleted (see Figure 3-4). The percentage of CCPs appearing and endocytosing within 60 s was reduced almost three-fold while the percentage of CCPs persisting for 3 min or more was increased more than four-fold (Figure 3-8a,b). This quantitative analysis was performed using stably eGFP-clathrin light chain expressing Cos7 cells. For unknown reasons, fusion proteins of PI3K C2α with mRFP or mCherry do not express well, thus precluding rescue experiments in this setting. Hence, transient mRFP-clathrin light chain expression was used for a qualitative analysis of CCP dynamics in spite of the considerably poorer signal-to-noise ratio this construct affords. Our analysis demonstrated that attenuated CCP dynamics can be rescued by re-expression of siRNA-resistant eGFP-PI3K C2α (Figure 3-8c). Whilst nucleation and growth of pits were unaltered in absence of PI3K C2α they frequently failed to mature to a fission-competent state. Instead, CCPs appeared to grow beyond the size at which they would normally undergo fission in control cells and occasionally could be seen to split into two or three closely neighbored CCPs (Figure 3-8d). This agrees well with the observation of CCPs clustering in close proximity, documented by a decreased average nearest neighbor distance of CCPs in cells depleted of PI3K C2α (Figure 3-8e; compare Figure 3-4, merged image in the center left panel, for a highly similar phenotype upon $PI(3,4)P_2$ depletion). Data obtained by TIRF analysis of CCP dynamics were confirmed by fluorescence recovery after photo-bleaching experiments (Figure 3-9a,b). The increased lifetimes of clathrin-coated structures resulted in a significant delay of fluorescence recovery in PI3K C2α-depleted cells.

3.2.3 *PI3K C2α regulates a late maturation stage of clathrin-coated pits*

The above data suggest that PI3K C2α regulates maturation of CCPs, either prior to or in conjunction with dynamin-mediated fission of endocytic pits. To distinguish between these possibilities we examined cells depleted of PI3K C2α ultrastructurally (in collaboration with Dr. Dmytro Puchkov, Leibniz Institute for Molecular Pharmacology). Quantitative morphometric analysis revealed an increased number of U-shaped CCPs, a stage preceding constriction and dynamin-mediated fission, whereas the frequencies of

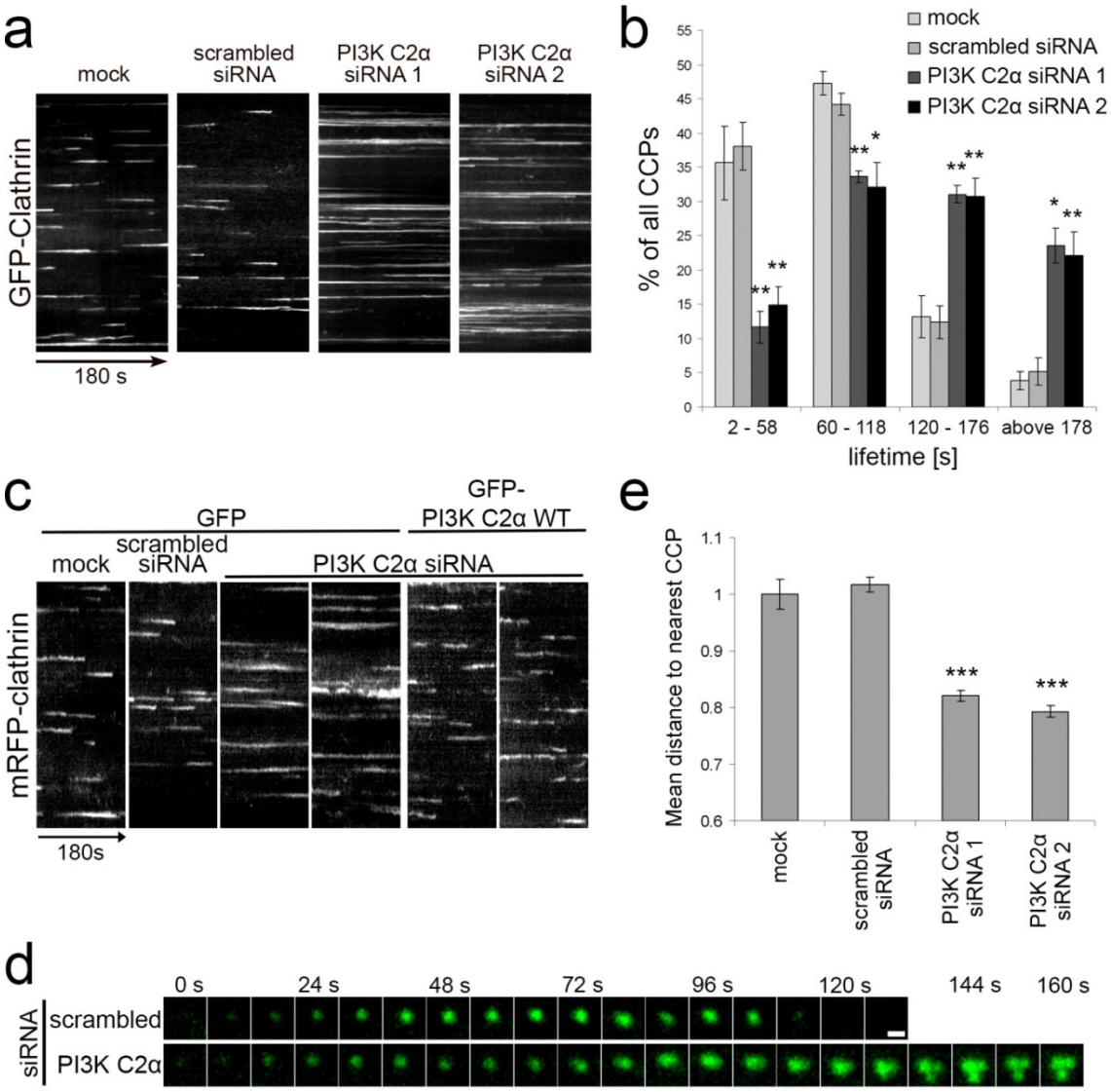

Figure 3-8: Depletion of PI3K C2α attenuates the dynamics of clathrin-coated pits. a,b) PI3K C2α depletion impairs CCP dynamics analysed by TIRF imaging of eGFP-clathrin expressing Cos7 cells depleted of PI3K C2α by two different siRNAs. **a**, Kymographs show increased CCP-lifetimes in cells depleted of PI3K C2α. **b**, Lifetime distribution of CCPs binned in categories of 60 s. Data represent mean ± s.e.m. (n = 3 independent experiments with > 1,000 CCPs per condition; * $p < 0.05$, ** $p < 0.01$, t-test for scrambled vs. PI3K C2α siRNA-treated cells). **c)** Re-expression of siRNA-resistant GFP-PI3K C2α WT rescues the impairment of CCP dynamics in PI3K C2α depleted Cos7 cells as observed by TIRF imaging of mRFP-clathrin light chain, shown in representative kymographs. **d)** Maturation defect of CCPs in absence of PI3K C2α. Representative examples of CCPs in eGFP-clathrin light chain expressing control or PI3K C2α-depleted Cos7 cells imaged by TIRF microscopy. Scale bar, 0.5 µm. **e)** Decreased distances between CCPs in cells depleted of PI3K C2α. The mean distance to the nearest neighboring CCP was determined from TIRF images of eGFP-clathrin light chain expressing control or PI3K C2α-depleted Cos7 cells (mean ± s.d.; n = 3 independent experiments; *** $p < 0.0001$, t-test).

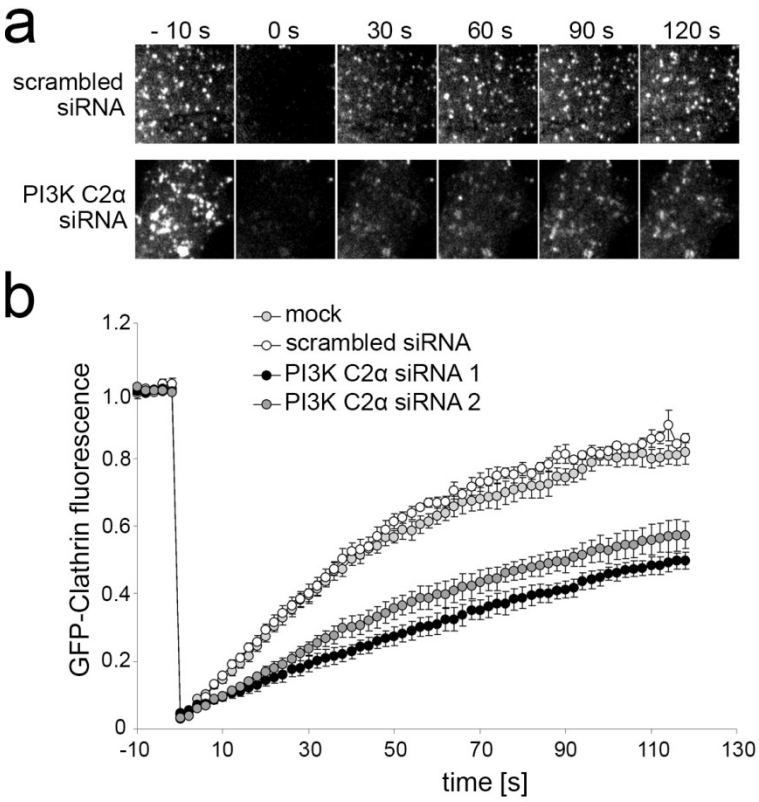

Figure 3-9: Delayed fluorescence recovery of clathrin-coated structures in PI3K C2α-depleted cells. a,b) Fluorescence recovery after photobleaching (FRAP) analysis of CCP dynamics in control or PI3K C2α-depleted Cos7 cells expressing eGFP-clathrin light chain. **a**, representative frames of a FRAP experiment showing the regions of interest before bleaching (-10 s), directly after bleaching (0 s), and during a 120 s recovery phase. Note that after 60 s fluorescence in the control cell has largely recovered whereas recovery is delayed in the PI3K C2α-depleted cell. **b**, Quantification of eGFP-clathrin fluorescence recovery over a period of 120 s after photobleaching (mean ± s.e.m.; n = 3 independent experiments).

early shallow CCPs, Ω-shaped constricted CCPs, or of free CCVs were unaltered (Figure 3-10a,b). Further, we analyzed dynamics of endocytic protein recruitment to CCPs in order to precisely define the stage during which PI3K C2α is present. Dual color TIRF imaging revealed PI3K C2α recruitment to lag behind clathrin but to clearly precede the final burst of dynamin2 recruitment (Figure 3-10c,d). Half-maximal recruitment of PI3K C2α to CCPs was delayed by about 12 s as compared to clathrin and occurred about 20 s before dynamin2.

Taken together, these findings argue for a role of PI3K C2α in CCP maturation upstream of dynamin. PI3K C2α appears to facilitate the transition from invaginated to Ω-shaped constricted CCPs, a step that involves extensive membrane remodeling in order to prepare a lipid template that will allow assembly of the dynamin helix.

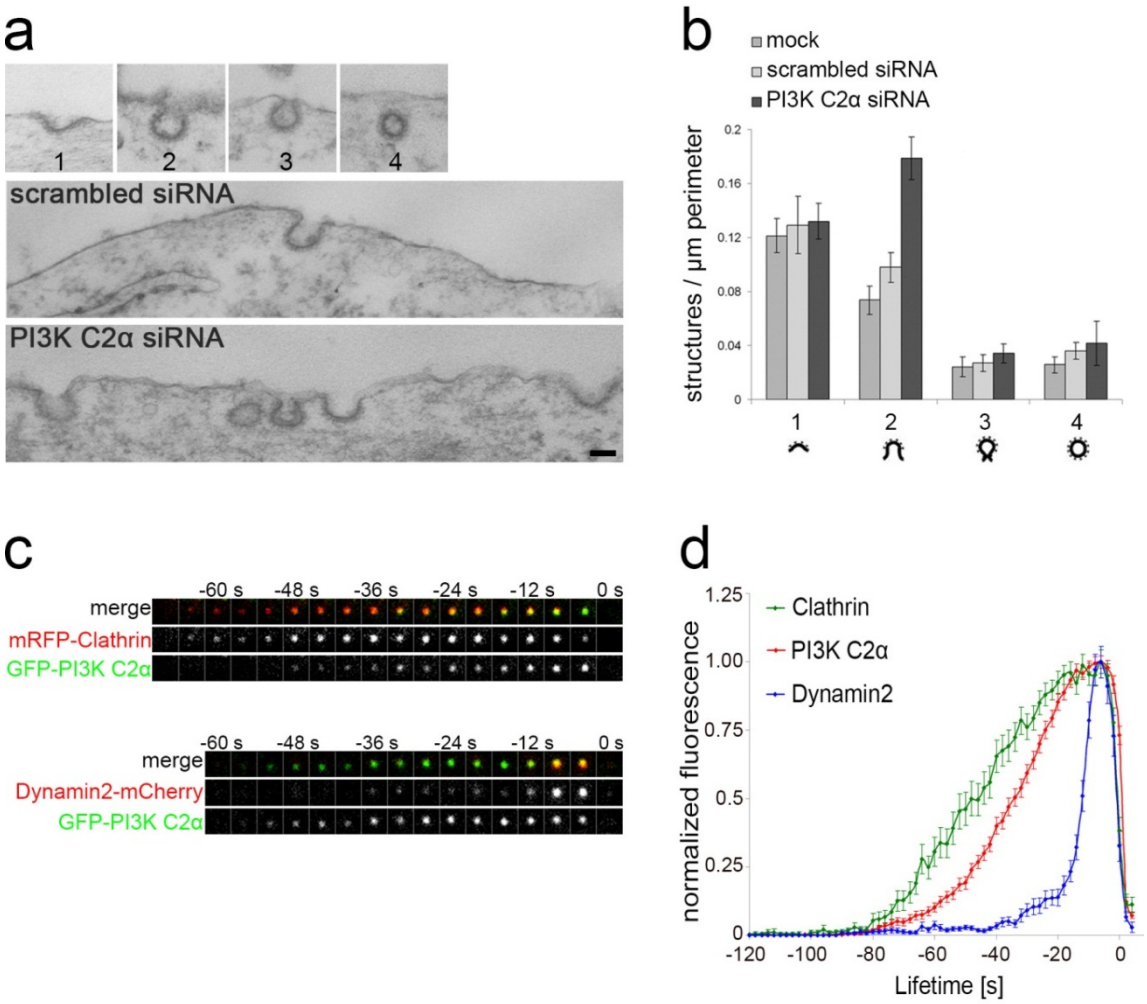

Figure 3-10: A role for PI3K C2α in late clathrin-coated pit maturation. a,b) Ultrastructural analysis of clathrin-coated structures in control or PI3K C2α-depleted cells. Morphological groups were shallow (stage 1), non-constricted U-shaped (stage 2), constricted Ω-shaped pits (stage 3), or structures containing complete clathrin coats (stage 4). **a**, representative images from controls (top and middle) or a PI3K C2α-depleted cell illustrating accumulation and clustering of U-shaped pits (bottom). Scale bar, 100 nm. **b**, Bar diagram detailing the relative abundance of different clathrin-coated structures in control or PI3K C2α-depleted cells [mean ± s.e.m.; n = 10 (mock, scrambled siRNA) or n = 11 (PI3K C2α siRNA) cell perimeters]. **c,d)** Timing of recruitment of PI3K C2α to CCPs analyzed by TIRF microscopy. **c**, Snapshots of eGFP-PI3K C2α and mRFP-clathrin light chain or dynamin2-mCherry at single CCPs (fission at t = 0). **d**, Mean time course of relative fluorescence intensity at CCPs. Data represent mean ± s.e.m. (n = 3 independent experiments with a total of N CCPs: N = 148 for PI3K C2α, N = 58 for clathrin, N = 85 for dynamin2).

3.3 PI(3,4)P_2 is the major product of PI3K C2α at CCPs

The above results unambiguously identified PI3K C2α as a regulator of CME. Still, it remained unclear how the enzyme exerts control over this process. As PI3K C2α in addition to its kinase domain features a largely unexplored amino-terminal region with potential for a scaffolding function, we sought to determine whether enzymatic activity was necessary for CME and if so, to identify the specific reaction product.

3.3.1 *The kinase activity of PI3K C2α is required for CME*

To explore whether the function of PI3K C2α in CME requires its kinase activity we tested the ability of a catalytically inactive mutant PI3K C2α bearing mutations in both the ATP-binding and the catalytic sites ((Gaidarov et al., 2005); see also Figure 3-14b) to rescue defective CME. We capitalized on the observation that endocytic proteins such as AP-2 accumulate at CCPs following depletion of PI(3,4)P_2 (Figure 3-3b,c) or depletion of endogenous PI3K C2α (Figure 3-11a,b). AP-2 accumulation was rescued by re-expression of siRNA-resistant wild-type (WT) PI3K C2α whereas the

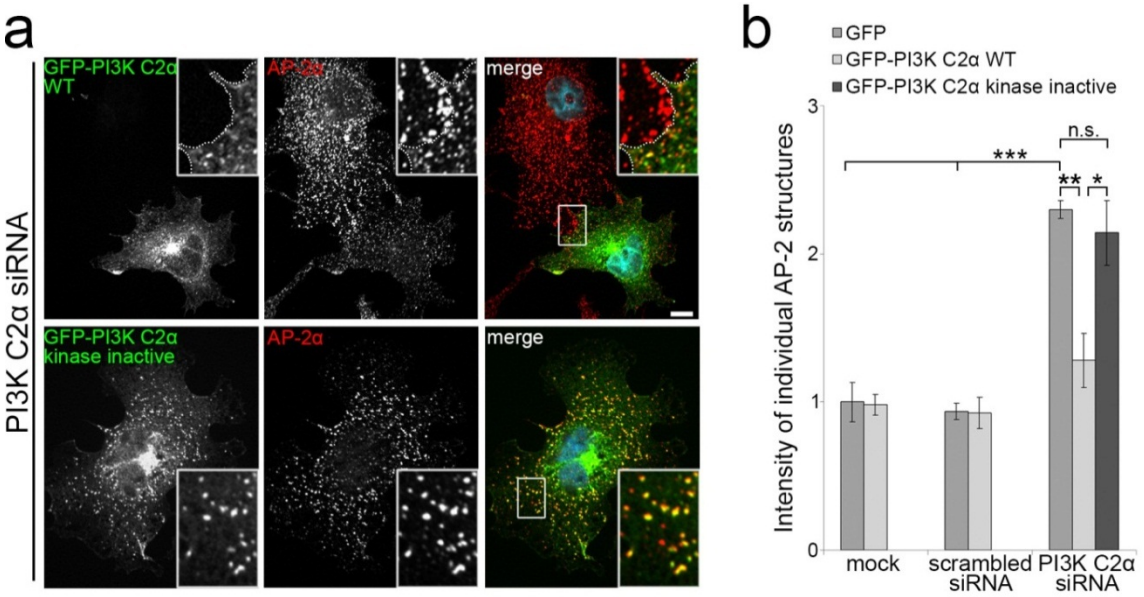

Figure 3-11: A kinase-inactive mutant fails to rescue CME in PI3K C2α-depleted cells. Analysis of AP-2α structures in PI3K C2α-depleted Cos7 cells expressing siRNA-resistant wild-type (WT; see inset in upper panel) or kinase inactive eGFP-PI3K C2α. **a)** Confocal images of the distribution of AP-2α. The dotted line in the inset demarcates the border between the PI3K C2α-depleted and the rescued cell. Scale bar, 10 µm. **b)** Mean intensity of endocytic AP-2α-containing CCPs. Data represent mean ± s.e.m. (n = 3 independent experiments; * $p < 0.05$, ** $p < 0.01$, *** $p < 0.001$, t-test).

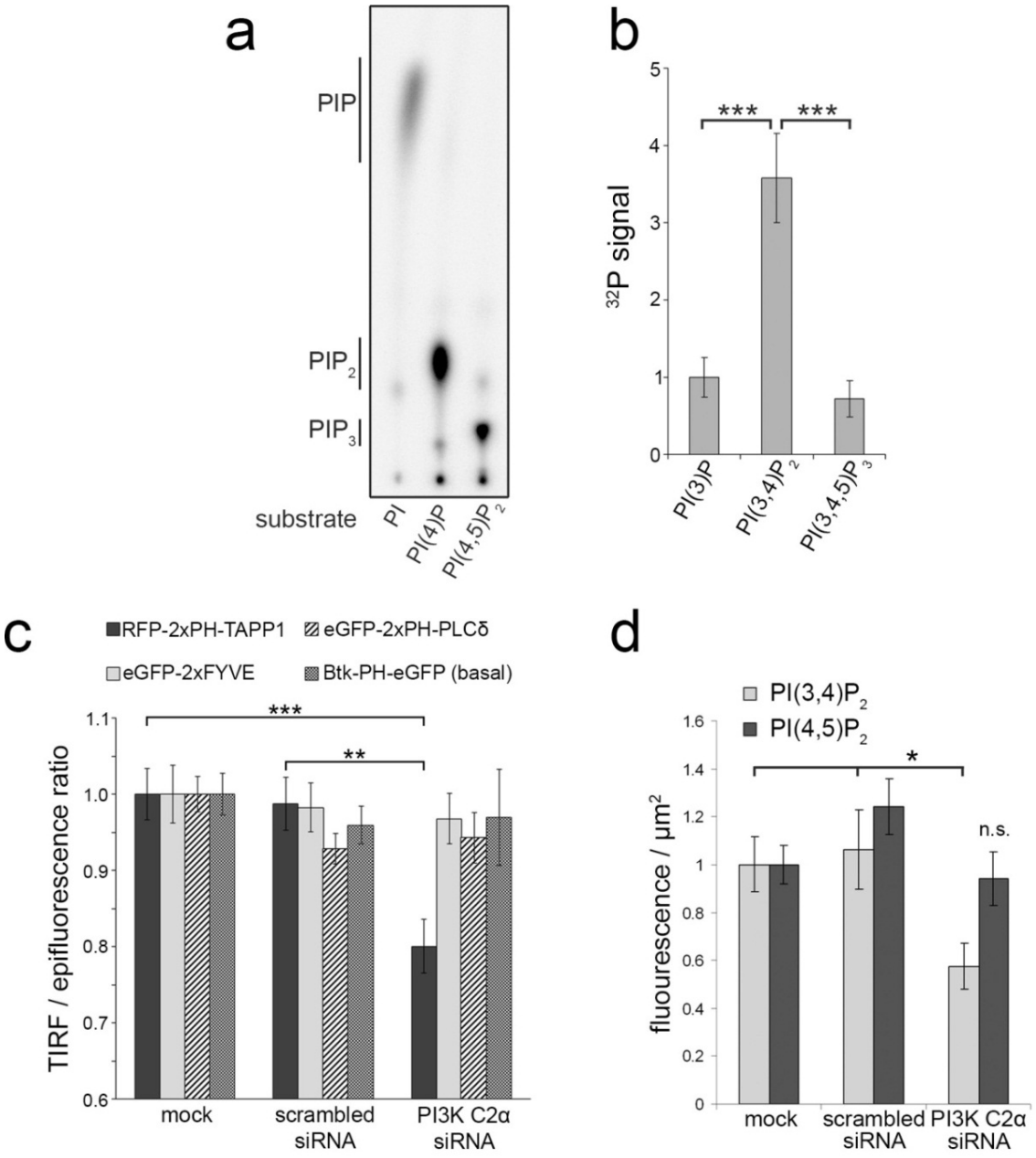

Figure 3-12: PI3K C2α synthesizes PI(3,4)P_2 *in vitro* and *in vivo*. a,b) PI3K C2α preferentially synthesizes PI(3,4)P_2 *in vitro*. Enzymatic activity of immunoprecipitated 6xMyc-PI3K C2α was assayed using γ-^{32}P-ATP and different PI substrates. **a**, Storage phosphor screen detection of extracted lipids separated by thin layer chromatography (positions of PIP, PIP_2, and PIP_3 as determined by standards). **b**, Quantification of n = 9 experiments as in a. Data represent mean ± s.e.m. normalized to the level of PI(3)P synthesis (*** $p < 0.001$, t-test). No PI3K activity was detectable in absence of induction of PI3K C2α expression. **c,d)** Selective PI(3,4)P_2 reduction in PI3K C2α-depleted cells. **c**, Loss of plasma membrane association of the PI(3,4)P_2-sensor 2xTAPP1-PH but not of probes for other PI-species determined by ratiometric TIRF/ epifluorescent imaging [mean ± s.e.m.; n (independent experiments) = 9 (2xTAPP1-PH), n = 7 (2xFYVE, a sensor for PI(3)P), n = 4 (PH-PLCδ, a sensor for PI(4,5)P_2, and PH-Btk, a sensor for PI(3,4,5)P_3); ** $p < 0.01$, *** $p < 0.001$, t-test). **d**, Levels of PI(3,4)P_2 or PI(4,5)P_2 quantified by specific antibodies (mean ± s.e.m.; n = 6 independent experiments; * $p < 0.05$, t-test).

catalytically inactive mutant failed to rescue this defect although it properly localized to CCPs (Figure 3-11a,b). Hence, the function of PI3K C2α in CME requires its PI3K activity.

3.3.2 *The lipid product of PI3K C2α*

Previous studies have yielded conflicting data regarding the predominant lipid product of PI3K C2α, reporting either preferential synthesis of $PI(3,4)P_2$ or PI(3)P (Falasca et al., 2007; Leibiger et al., 2010), and under certain *in vitro* conditions also $PI(3,4,5)P_3$ (Gaidarov et al., 2001). To address this question we directly assayed the activity of native PI3K C2α immunoprecipitated from stably transfected HEK293 cells towards distinct PI substrates. PI3K C2α preferentially produced $PI(3,4)P_2$ as compared to either PI(3)P or $PI(3,4,5)P_3$ (Figure 3-12a,b), in agreement with

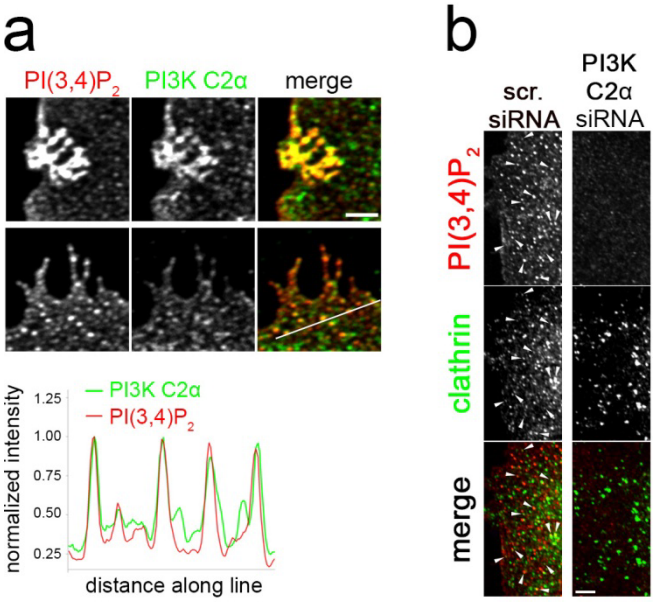

Figure 3-13: Analysis of $PI(3,4)P_2$ immunostaining in relation to PI3K C2α. a) Endogenous PI3K C2α colocalizes with $PI(3,4)P_2$-containing plasma membrane sites. Cos7 cells were immunostained for PI3K C2α and $PI(3,4)P_2$ and imaged by confocal microscopy. Images depict peripheral regions of a cell, illustrating colocalization in ruffle-like structures (upper panel) and small CCP-like puncta (lower panel). For the lower panel, an intensity profile along the line drawn in the merged image is shown. Note the closely matching intensity peaks. Scale bar, 4 µm. **b)** $PI(3,4)P_2$ labeling is lost from CCPs upon depletion of PI3K C2α. Cos7 cells treated with scrambled or PI3K C2α siRNA were immunolabeled for $PI(3,4)P_2$ and clathrin heavy chain. Arrowheads, structures immunopositive for $PI(3,4)P_2$ and clathrin. Scale bar, 4 µm.

(Leibiger et al., 2010). If PI3K C2α were to contribute to PI(3,4)P_2 formation *in vivo*, knockdown of PI3K C2α should result in reduced PI(3,4)P_2 levels. The levels of various PIs were quantitatively assessed by ratiometric TIRF / epifluorescence microscopy-based analysis of the enrichment of specific PI-binding domain-based sensors at the plasma membrane. This analysis revealed a selective reduction of PI(3,4)P_2 in PI3K C2α-knockdown cells, whereas the levels of PI(3)P, PI(4,5)P_2, or PI(3,4,5)P_3 remained unchanged (Figure 3-12c). A decrease of PI(3,4)P_2 but not of PI(4,5)P_2 staining intensity was also detectable with PI-specific antibodies (Figure 3-12d). Consistent with these results, PI(3,4)P_2 displayed a significant degree of colocalization with the plasma membrane pool of PI3K C2α in large ruffle-like structures and in small diffraction-limited puncta (Figure 3-13a). Conversely, we failed to detect PI(3,4)P_2 at CCPs in PI3K C2α-depleted cells (Figure 3-13b). These results are consistent with the preferential production of PI(3,4)P_2 by PI3K C2α *in vitro* and support the hypothesis that PI3K C2α contributes to PI(3,4)P_2 formation at CCPs *in vivo*.

3.3.3 *PI(3,4)P_2 synthesis by PI3K C2α is required for CME*

To further differentiate between PI(3,4)P_2 and PI(3)P as PI3K C2α's possible *in vivo* products and to address the question of the lipid product of PI3K C2α at CCPs we capitalized on the fact that the specificity of PI3Ks is encoded within the activation loop that binds the lipid substrate (Pirola et al., 2001). The activation loop is conserved in all human PI3Ks but displays systematic differences between the three classes of PI3Ks. The PI(3,4,5)P_3-producing class I PI3Ks contain two basic boxes in their activation loop that coordinate the phosphates of their substrate PI(4,5)P_2. None of these basic boxes is present in the sole class III PI3K hVps34, an enzyme that exclusively produces PI(3)P (Figure 3-14a). Consistent with its ability to synthesize PI(3,4)P_2, PI3K C2α retains the basic residues required to coordinate the 4-phosphate group but lacks those coordinating the 5-phosphate. To distinguish between PI3K C2α-mediated formation of PI(3,4)P_2 or PI(3)P at CCPs we constructed a mutant version of the enzyme, in which the 4-phosphate coordinating box was exchanged with the corresponding sequence from hVps34 (Figure 3-14a). This class III-like mutant PI3K C2α selectively synthesized PI(3)P with WT-PI3K C2α activity, but failed to produce PI(3,4)P_2 (Figure 3-14b,c). When tested for its ability to reconstitute defective CME in PI3K C2α-depleted cells the class III-like mutant of PI3K C2α was unable to rescue endocytosis of transferrin (Figure 3-14d) and the accumulation of endocytic proteins at CCPs (Figure 3-14e). It thus appears

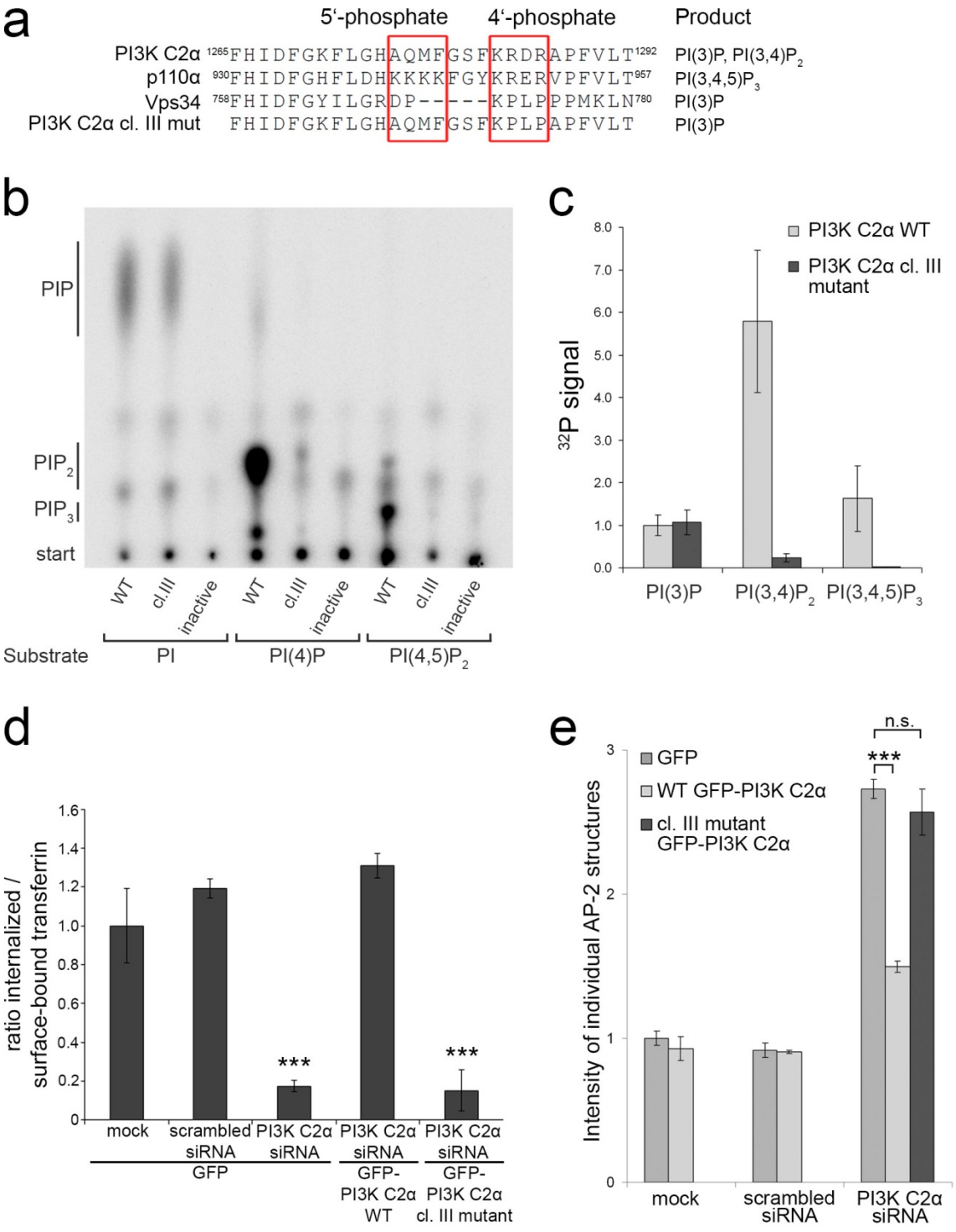

Figure 3-14: A PI(3)P-restricted mutant of PI3K C2α fails to reconstitute CME in PI3K C2α-depleted cells. a) Alignment of human PI3K substrate-binding loop sequences. Two basic clusters coordinate the 4- and 5-phosphate groups of PIs. In the class III-like mutant (cl.III mut) of PI3K C2α, the 4-phosphate binding residues are replaced with those from hVps34. **b, c)** Catalytic activities of wild-type (WT), catalytically inactive (CI) or class III-like mutant (cl.III) PI3K C2α towards different substrates. The class III-like mutant (cl.III) PI3K C2α has selectively lost the ability to produce $PI(3,4)P_2$, but does still produce PI(3)P. **b**, Storage phosphor screen detection of *in vitro* kinase activity assay with immunoprecipitated kinase (positions of PIP, PIP_2 and PIP_3 as determined by standards). **c**, Quantification

of n = 3 experiments as in b (mean ± s.e.m.). **d,e)** Requirement for PI3K C2α-mediated $PI(3,4)P_2$ synthesis in CME. **d**, Impaired internalization of transferrin in PI3K C2α-deficient cells is rescued by WT but not class III-like mutant eGFP-PI3K C2α. Ratio of internalized (10 min, 37°C) to surface transferrin (45 min, 4°C) (mean ± s.e.m.; n = 3 independent experiments; *** $p < 0.001$, t-test vs. scrambled siRNA). **e**, Mean intensity of endocytic AP-2α-containing CCPs in PI3K C2α-deficient Cos7 expressing WT or class III-like mutant PI3K C2α (mean ± s.e.m.; n = 3 independent experiments; *** $p < 0.001$, t-test).

that CME specifically requires PI3K C2α-mediated production of $PI(3,4)P_2$ but not of PI(3)P.

To challenge this hypothesis by an independent approach we made use of recently developed cell-permeable PI-derivatives (Laketa et al., 2009; Subramanian et al., 2010) that allow the bulk supply of exogenous PI(3)P or $PI(3,4)P_2$. In these compounds, the charged phosphates are masked with acetoxymethylester (AM) groups, rendering the molecule largely unpolar and therefore membrane-permeable. Inside the cell, endogenous esterases cleave off the AM groups within minutes and release the PI molecule. Addition of cell-permeable $PI(3,4)P_2$ /AM partially rescued the endocytic protein accumulation at CCPs in PI3K C2α-depleted cells whereas PI(3)P /AM

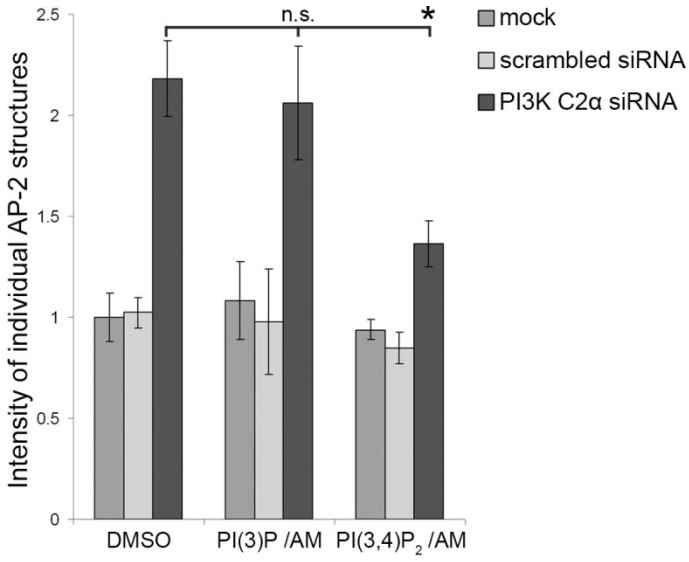

Figure 3-15: Supply of exogenous $PI(3,4)P_2$, but not PI(3)P, reconstitutes CCP dynamics in PI3K C2α-depleted cells. Lipid reconstitution experiments using cell-permeant PI derivatives. Cos7 cells depleted of PI3K C2α were treated with vehicle, 200 µM PI(3)P/ acetoxymethylester (AM) or 200 µM $PI(3,4)P_2$/ AM and stained for AP-2α. The mean intensity of endocytic AP-2α-containing pits as determined from confocal images was strongly increased in PI3K C2α-depleted cells and could be partially reconstituted by treatment with $PI(3,4)P_2$/ AM, but not with PI(3)P/ AM (mean ± s.e.m.; n = 3 ($PI(3,4)P_2$) or n = 2 (PI(3)P) independent experiments; * $p < 0.05$, t-test).

was inactive (Figure 3-15). Comparable results were obtained with a second, independently synthesized batch of $PI(3,4)P_2$ /AM. To confirm the functionality of PI(3)P /AM under the conditions used here, we analyzed its effect on the endosomal compartment. On Rab5-positive endosomes, the APPL1- and EEA1-positive subcompartments are reciprocally regulated by PI(3)P. Upon depletion of PI(3)P, the APPL1-compartment expands whereas the EEA1-compartment is diminished (Zoncu et al., 2009). In agreement with these data, exogenous supply of PI(3)P using the AM compound caused a decrease in APPL1 and an increase in EEA1 staining (Figure 3-16). Although these effects occurred sequentially, this indicates that PI(3)P /AM stimulated early endosome fusion as described (Subramanian et al., 2010).

Collectively, these data indicate that PI3K C2α is required for local synthesis of $PI(3,4)P_2$ at endocytic CCPs.

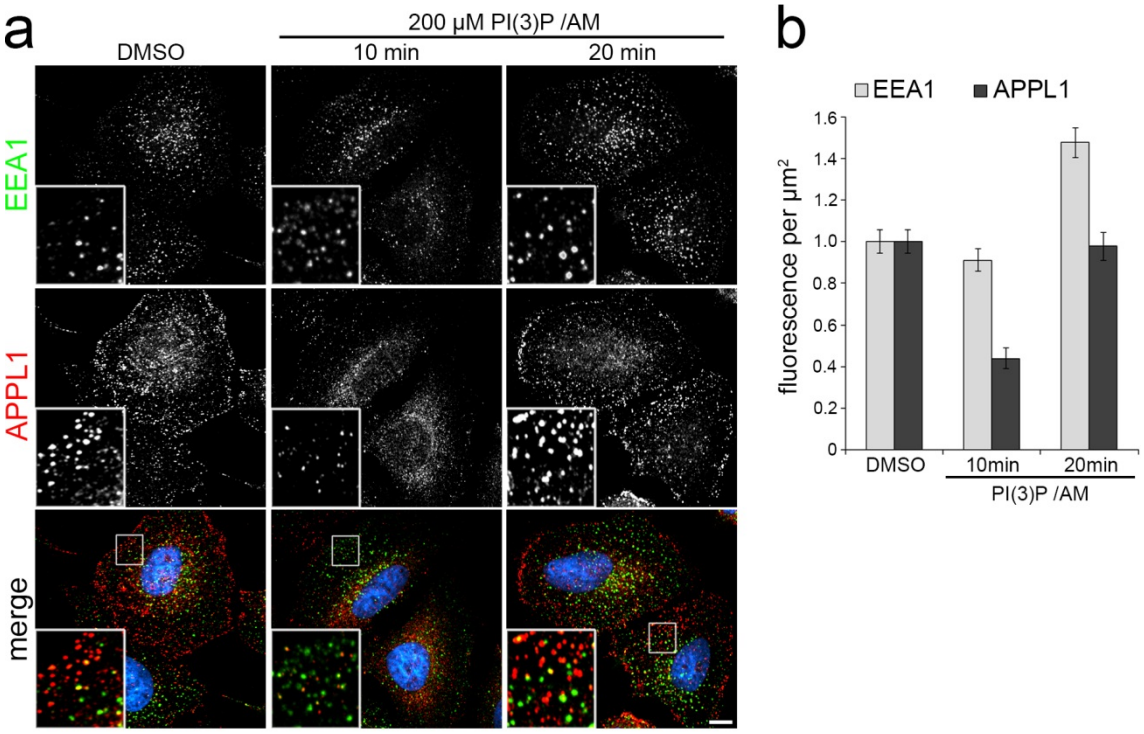

Figure 3-16: PI(3)P /AM treatment affects the endosomal compartment. Cos7 cells were treated with 200 µM PI(3)P /AM for 10 min or 20 min and stained for the endosomal marker proteins APPL1 and EEA1. **a**, Representative confocal micrographs. Scale bar, 10 µm. **b**, Quantitative analysis of total EEA1- and APPL1-intensity per cell area (mean ± s.e.m.; n = 60 images from 2 independent experiments).

3.4 SNX9 is an effector of PI(3,4)P_2 at clathrin-coated pits

According to the data presented above, absence of PI3K C2α or depletion of its lipid product PI(3,4)P_2 causes a kinetic delay in the maturation of CCPs. How this lipid regulates the late steps of CCV formation remains elusive. Conceptually, the local increase of a distinct lipid species can affect the biophysical properties of the membrane or can alter the activity of membrane-associated proteins. The vast majority of cellular processes regulated by PIs depend on the recruitment of effector proteins through local enrichment of a distinct PI species (see section 1.3). It thus appeared likely that the CME machinery comprises one or several PI(3,4)P_2 effector proteins that participate in shaping nascent CCVs in preparation of the final scission reaction. We applied both subcellular localization analysis and biochemical lipid association studies in order to identify and subsequently characterize PI(3,4)P_2 effectors in CME.

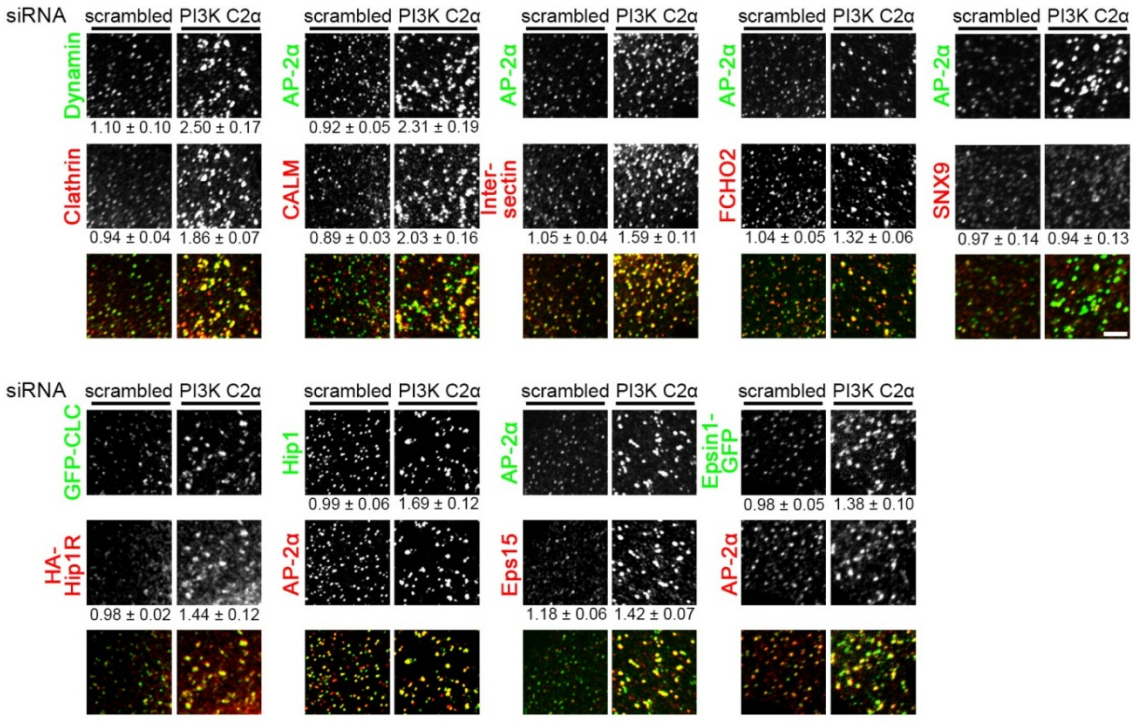

Figure 3-17: SNX9 is the only protein tested not accumulating at CCPs in absence of PI3K C2α. Subcellular distribution of endocytic proteins in Cos7 cells treated with scrambled or PI3K C2α siRNA analyzed by immunostaining and confocal microscopy. For clarity, defined plasmalemmal regions of the imaged cells are shown. The mean intensity of individual structures was quantified and normalized to mock treated cells (not shown) and is denoted below the respective images (mean ± s.e.m.; n = 15 images except for [epsin1-GFP, scrambled siRNA n = 12] and [dynamin, PI3K C2α siRNA n = 14]). Note the accumulation of endocytic proteins except SNX9 in PI3K C2α-depleted cells. Scale bar, 4 µm.

3.4.1 *SNX9 is a putative PI(3,4)P_2 effector protein*

To identify putative effectors of PI(3,4)P_2 at CCPs we took advantage of the observed accumulation of AP-2 in PI3K C2α-deficient cells (see Figure 3-11) and systematically assessed the enrichment of other endocytic proteins at CCPs upon PI3K C2α depletion (Figure 3-17). Proteins acting during both early (i.e. FCHo2, Eps15, intersectin, CALM) and late stages (i.e. HIP1R, dynamin2) of CCP formation accumulated at CCPs in a manner highly similar to AP-2. The only endocytic protein tested that failed to enrich at CCPs in PI3K C2α-depleted cells was sorting nexin 9 (SNX9) (Figure 3-17).

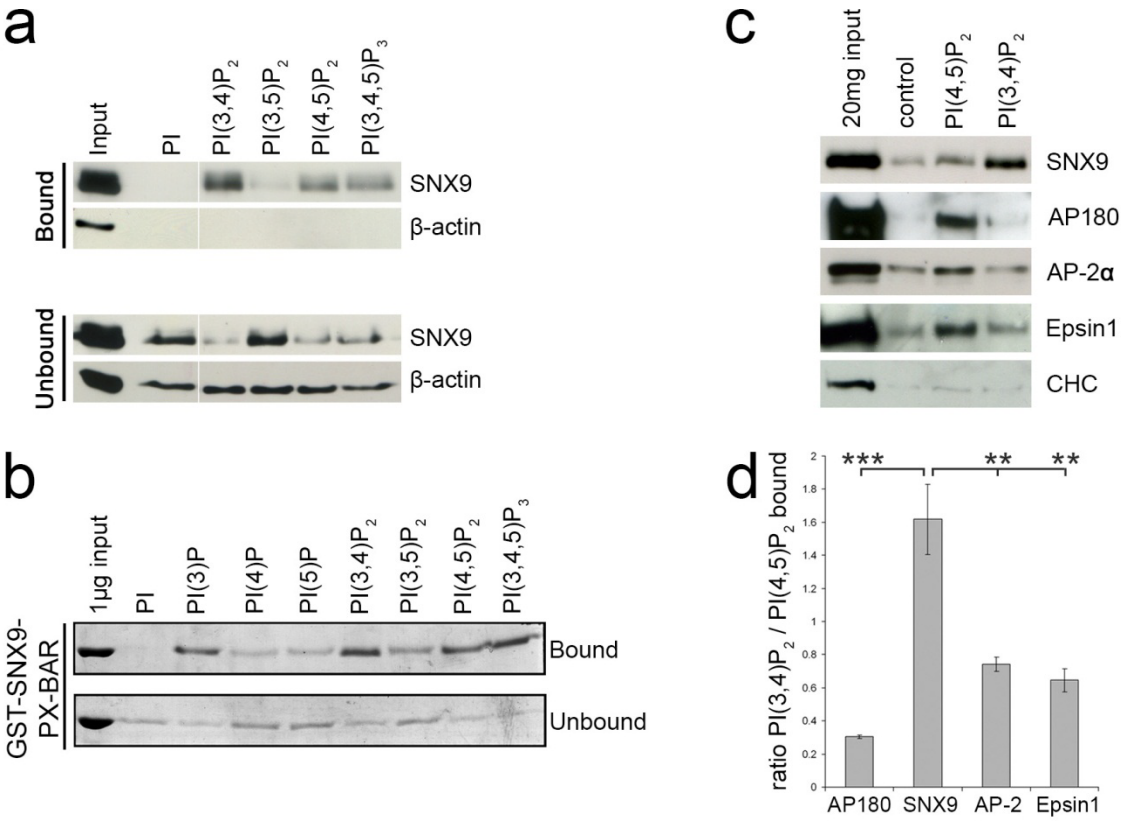

Figure 3-18: Analysis of SNX9 lipid binding specificity. a) Binding of endogenous SNX9 from HEK293 cells to liposomes containing 5 mol% of the indicated PI in flotation assays. Input, 10 µg protein for bound (top) or 30 µg (bottom) for unbound fractions. Data are representative of three independent experiments. **b)** Binding of the GST-tagged PX-BAR domain (amino acids 204 to 595) of SNX9 to liposomes containing 5 mol% of the indicated PI in flotation assays. 50% of the top and 15% of the bottom fractions were analysed by coomassie staining. **c,d)** Association of SNX9 affinity-isolated from rat brain extracts with PI(3,4)P_2-containing beads. Endocytic proteins AP180, AP-2α, or epsin1 preferentially associate with PI(4,5)P_2-beads. Clathrin served as a negative control. **d**, Densitometric quantification of data shown in c (mean ± s.e.m.; n = 3 independent experiments; ** $p < 0.01$, *** $p < 0.001$, t-test).

As SNX9 harbors a PX- domain postulated to confer specific lipid binding (Lundmark and Carlsson, 2003), we analyzed the ability of SNX9 to associate with liposomal membranes containing select PIs by flotation experiments. Endogenous SNX9 from cytosolic HEK293 cell extracts (Figure 3-18a) or the purified PX-BAR module (Figure 3-18b) was found to preferentially bind to PI 3-phosphates including PI(3,4)P_2, PI(3)P, and PI(3,4,5)P_3; however, both proteins also associated with PI(4,5)P_2, in agreement with earlier reports (Lundmark and Carlsson, 2003; Shin et al., 2008; Yarar et al., 2008). In order to directly compare PI association of SNX9 with that of other endocytic proteins, we used rat brain extract as a source of concentrated endocytic proteins in affinity purification experiments employing PI-coated agarose beads. Interestingly, the lipid-binding behavior of SNX9 differed from that of other endocytic proteins such as AP180, epsin 1, or AP-2. Only SNX9 preferred association with PI(3,4)P_2 over PI(4,5)P_2, whereas other endocytic proteins showed preferential PI(4,5)P_2 binding (Figure 3-18c,d). These experiments identify SNX9 as a putative PI(3,4)P_2 effector in CME.

3.4.2 *SNX9 recruitment to late-stage CCPs depends on PI3K C2α and PI(3,4)P_2*

To better understand the function of SNX9 in CME we analyzed its subcellular distribution and localization at CCPs in cells depleted of PI3K C2α or PI(3,4)P_2. In addition to its PX-BAR module SNX9 contains clathrin- and AP-2-binding motifs as well as an amino-terminal SH3 domain that associates with and regulates dynamin (Soulet et al., 2005). We capitalized on the observation that loss of dynamins results in the accumulation of SNX9 assemblies on actin-stabilized elongated necks of arrested CCPs (Ferguson et al., 2009). These late-stage endocytic intermediates were used to analyze the dependence of SNX9 recruitment on PI3K C2α by depleting cells of dynamin2 alone or dynamin2 and PI3K C2α simultaneously (double knockdown, Figure 3-19a). The dramatic enrichment of endogenous SNX9 at AP-2-coated endocytic intermediates in cells depleted of dynamin2, i.e. CCPs arrested at a late stage of CME, was confirmed. Strikingly, double knockdown of PI3K C2α and dynamin2 completely prevented SNX9 accumulation at arrested CCPs (Figure 3-19b,c), whereas other endocytic proteins such as AP-2 and intersectin accumulated irrespective of the presence of PI3K C2α (Figure 3-19b,d).

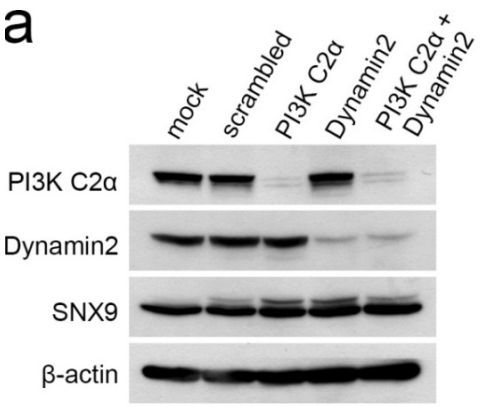
a
mock
scrambled
PI3K C2α
Dynamin2
PI3K C2α + Dynamin2
PI3K C2α
Dynamin2
SNX9
β-actin

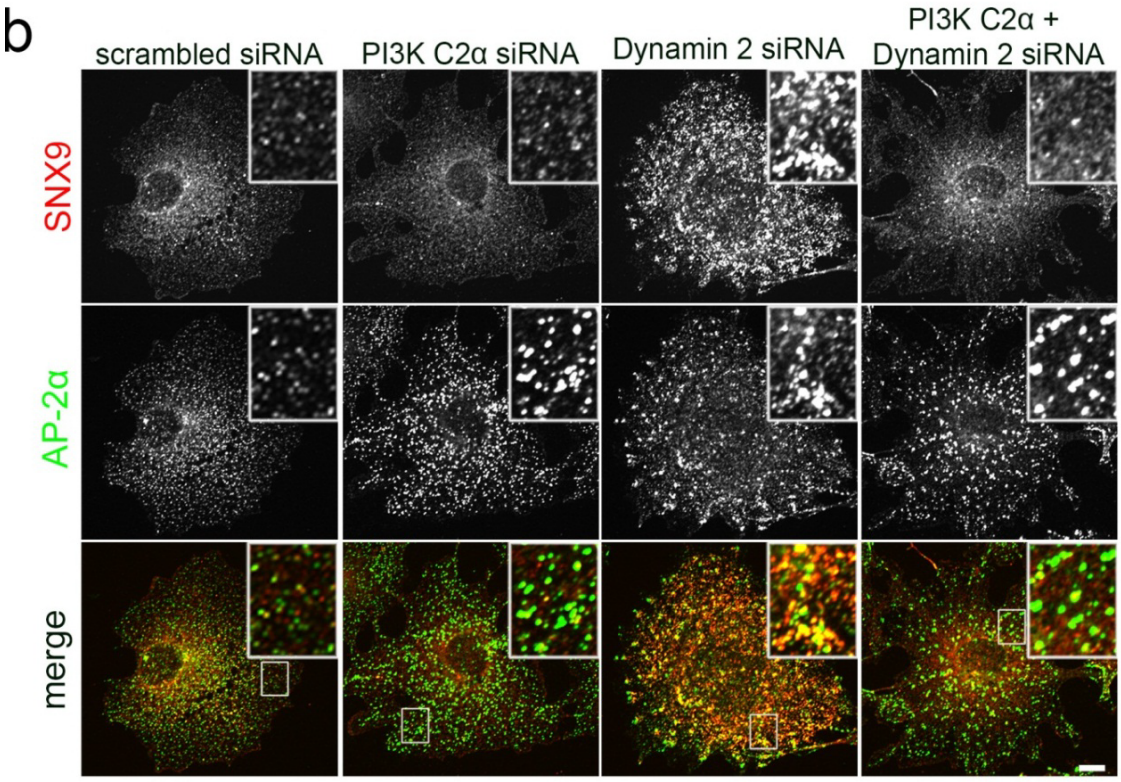
b
scrambled siRNA
PI3K C2α siRNA
Dynamin 2 siRNA
PI3K C2α + Dynamin 2 siRNA
SNX9
AP-2α
merge

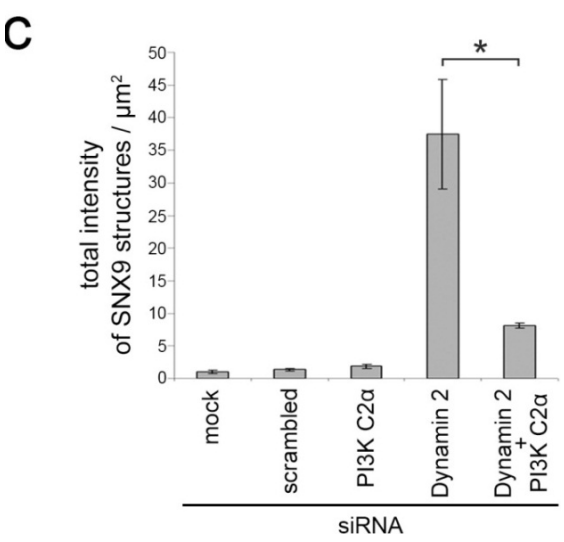
c
total intensity of SNX9 structures / µm²
*
mock
scrambled
PI3K C2α
Dynamin 2
Dynamin 2 + PI3K C2α
siRNA

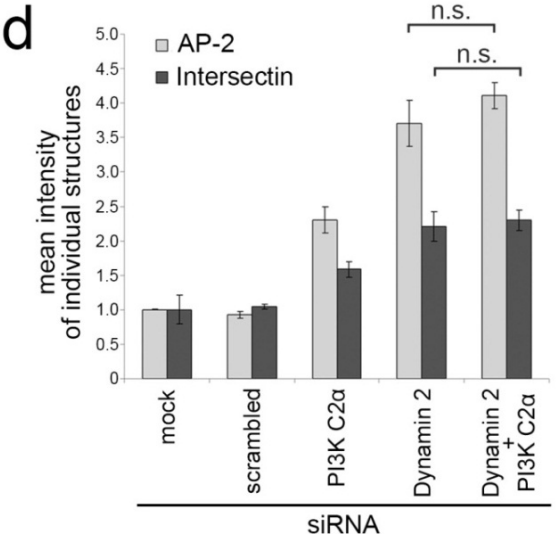
d
AP-2
Intersectin
mean intensity of individual structures
n.s.
n.s.
mock
scrambled
PI3K C2α
Dynamin 2
Dynamin 2 + PI3K C2α
siRNA

Figure 3-19: Recruitment of SNX9 to late-stage CCPs depends on PI3K C2α. a) Efficient co-silencing of PI3K C2α and dynamin2 in Cos7 cells. Immunoblot analysis of extracts from Cos7 cells depleted of PI3K C2α, dynamin2 or both proteins using RNA interference. Detection of β-actin demonstrates equal loading in all lanes. **b,c)** PI3K C2α is required for accumulation of SNX9 at endocytic intermediates. Confocal images of Cos7 cells depleted of PI3K C2α, dynamin2, or both, stained for AP-2α and SNX9. **b**, Scale bar, 10 μm. **c**, Quantitative analysis of SNX9 levels at endocytic intermediates as shown in d (mean ± s.e.m.; n = 3 independent experiments; * $p < 0.05$, t-test). **d)** Accumulation of AP-2 and intersectin at arrested CCPs is independent of PI3K C2α. Quantification of the mean intensity of individual AP-2α- or intersectin-positive structures in Cos7 cells depleted of PI3K C2α, dynamin2, or both proteins measured by confocal imaging (mean ± s.e.m.; n = 3 independent experiments, t-test).

Loss of SNX9 from arrested CCPs in dynamin2-deficient cells upon depletion of PI3K C2α may reflect either the selective failure of SNX9 to localize to these structures or a general impairment of the formation of constricted and elongated necks on which SNX9 assembles. To differentiate between these possibilities, we analyzed the behavior of a second protein shown to decorate the elongated necks of CCPs in dynamin-deficient cells, the p34 subunit of the Arp2/3 complex. Importantly, presence of Arp2/3 was shown to be required for the formation and stabilization of elongated necks, making this protein an easily accessible marker for the existence of such structures (Ferguson et al., 2009). Behavior of Arp2/3 paralleled that of SNX9 as it strongly accumulated at CCPs in dynamin2-depleted cells but was absent from CCPs in dynamin2 / PI3K C2α doubly deficient cells (Figure 3-20). This argues for a general failure of the accumulating endocytic intermediates to form constricted and elongated necks. Furthermore, simultaneous depletion of SNX9 and dynamin2 also caused a marked, though somewhat less pronounced reduction of Arp2/3 localization to CCPs.

It thus appears that recruitment of SNX9 during late-stages of CME depends on PI3K C2α and that in absence of either PI3K C2α or SNX9, no elongated necks are formed from stalled endocytic intermediates in spite of dynamin2 deficiency. We further tested this hypothesis by examining the effects of selective $PI(3,4)P_2$ depletion on SNX9 recruitment to arrested CCPs. Depletion of $PI(3,4)P_2$ by INPP4B-CAAX displaced SNX9 from endocytic structures in dynamin2-knockdown cells (Figure 3-21a,b), whereas AP-2 enrichment was unaffected (Figure 3-21c). This further strengthens the link between PI3K C2α-mediated $PI(3,4)P_2$ synthesis and recruitment of SNX9 to late-stage CCPs.

3.4.3 *SNX9 is required for clathrin-mediated endocytosis*

If SNX9 was an effector of PI3K C2α and PI(3,4)P_2 at CCPs, then perturbation of SNX9 function would be expected to phenocopy PI(3,4)P_2 depletion and to inhibit CME. Previous work has indeed shown that depletion of SNX9 interferes with CME in HeLa cells (Soulet et al., 2005) and we confirmed this (Figure 3-22). In other cell lines (i.e. Cos7) SNX9 may be functionally redundant with its paralog SNX18, as both proteins were demonstrated to compensate for loss of the other with respect to the internalization of transferrin (Park et al., 2010). Consistently, pilot experiments failed to detect an endocytic defect in Cos7 cells when only SNX9 was depleted. However, concomitant depletion of SNX9 and SNX18 in Cos7 cells (Figure 3-23a) inhibited the

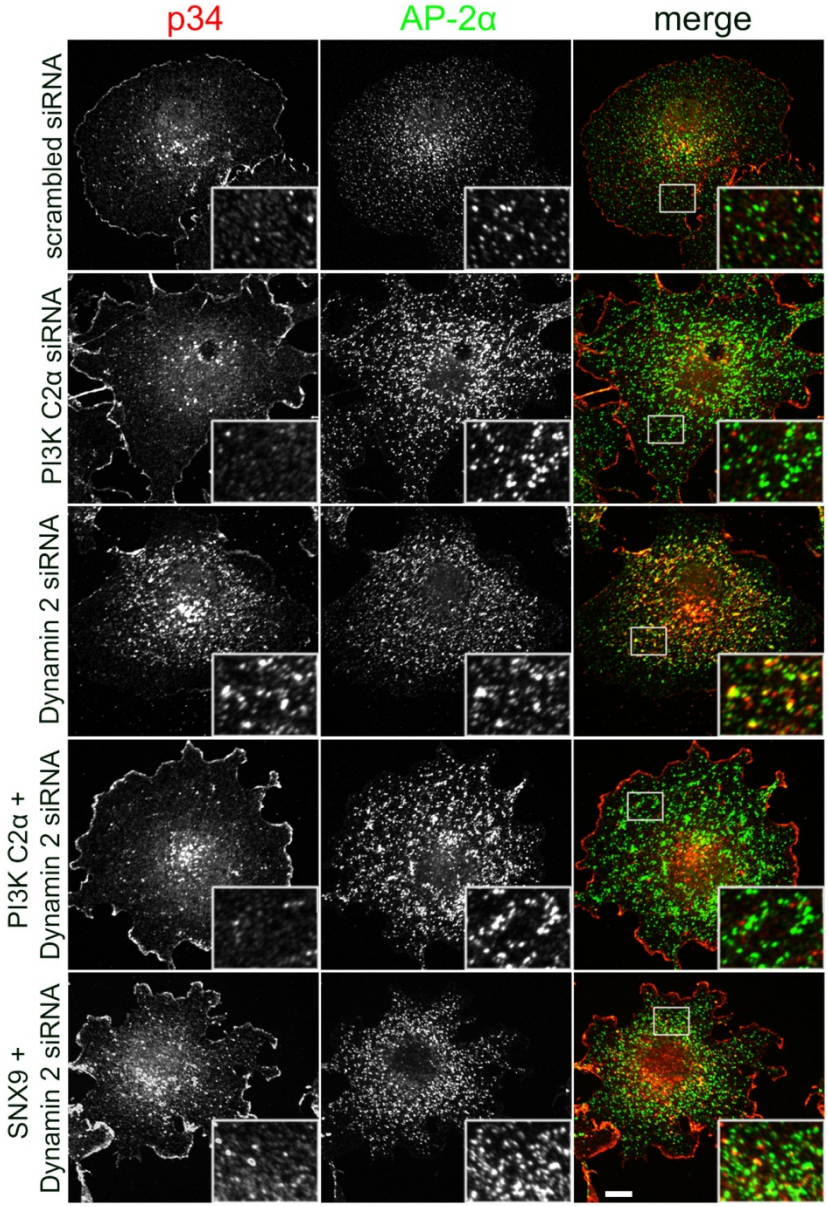

Figure 3-20: Accumulation of the Arp2/3 complex at endocytic vesicle necks upon depletion of dynamin2 depends on PI3K C2α and SNX9. Cos7 cells were depleted of dynamin2 either alone or in combination with PI3K C2α or SNX9 using specific siRNAs. Cells were immunostained for AP-2α and the Arp2/3 complex subunit p34. Co-silencing of PI3K C2α with dynamin2 leads to a complete loss of p34 from AP-2α-containing endocytic structures arrested at the fission stage. Note that also absence of SNX9 causes loss of p34 from AP-2α-containing endocytic structures. Scale bar, 10 µm.

endocytosis of transferrin (Figure 3-23c) and interfered with CCP dynamics evidenced by AP-2 accumulation (Figure 3-23d), similar to the effects seen upon depletion of PI(3,4)P_2 or PI3K C2α. Interestingly, neither SNX9 nor SNX18 depletion alone was sufficient to impair the internalization of transferrin, and the defect upon SNX9 and SNX18 double knockdown was completely rescued by re-expression of only SNX9. This strongly supports a redundant but in itself essential function of SNX9 and SNX18 during CME.

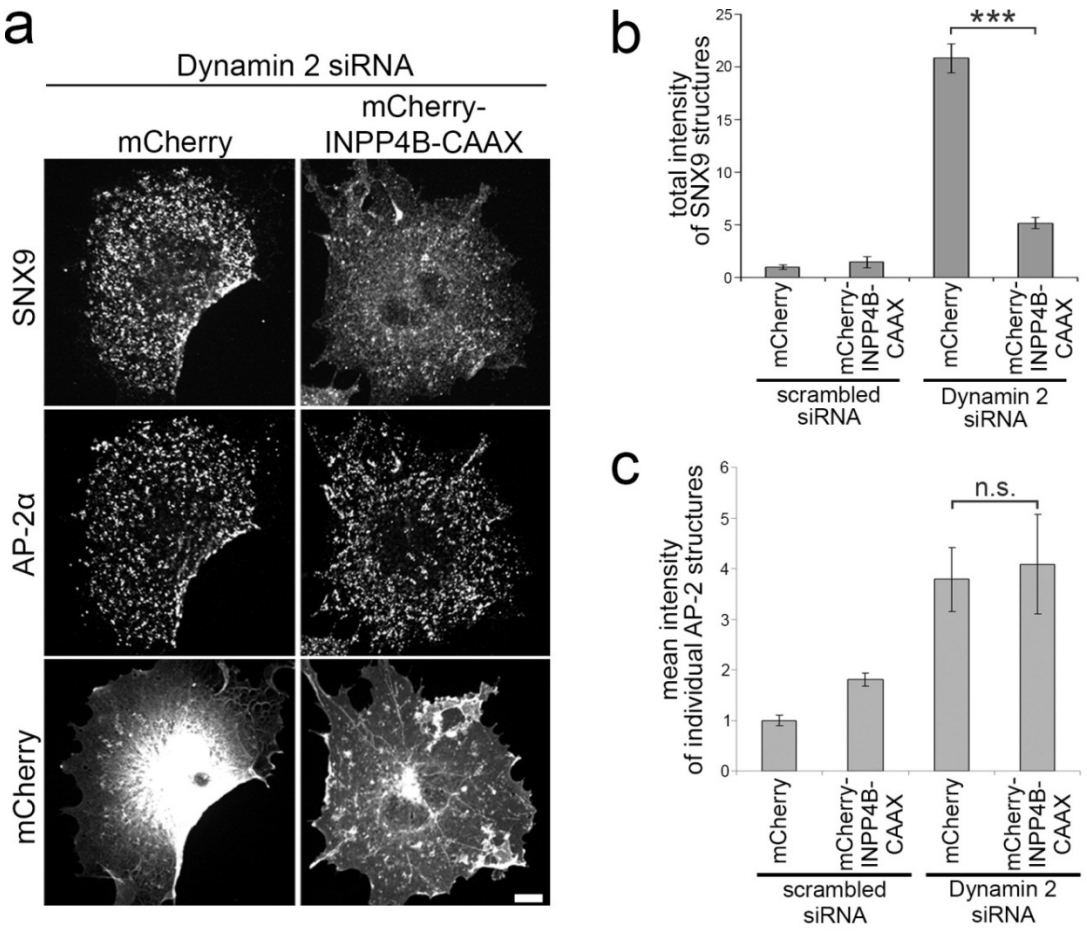

Figure 3-21: PI(3,4)P_2 is required for the accumulation of SNX9 at arrested endocytic intermediates. Cos7 cells deprived of dynamin2 and expressing mCherry (control) or mCherry-INPP4B-CAAX to deplete PI(3,4)P_2 were analyzed for endocytic protein accumulation by confocal microscopy. Depletion of PI(3,4)P_2 prevents accumulation of SNX9 but not of AP-2 at endocytic intermediates. **a)** Scale bar 10 µm. **b)** Quantification of the total intensity of SNX9-stained structures. Quantification of SNX9 levels at endocytic intermediates as shown in a (mean ± s.e.m.; n = 3 independent experiments; * $p < 0.05$, t-test). **c)** Accumulation of AP-2 at arrested CCPs is independent of PI(3,4)P_2. The mean intensity of endocytic AP-2α-containing pits in dynamin2-depleted cells expressing either mCherry or mCherry-INPP4B-CAAX was quantified. Depletion of PI(3,4)P_2 does not alter the extent of AP-2 accumulation at endocytic sites upon depletion of dynamin2 (mean ± s.e.m.; n = 3 independent experiments; t-test).

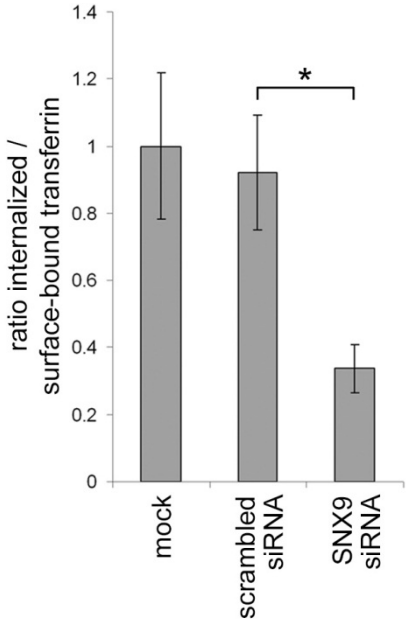

Figure 3-22: Depletion of SNX9 alone inhibits CME in HeLa cells. HeLa cells depleted of SNX9 were assayed for CME of transferrin. Bar diagrams represent the ratio of internalized (10 min, 37°C) to surface transferrin (45 min, 4°C) (mean ± s.e.m.; n = 3 independent experiments; * $p < 0.05$, t-test for scrambled vs. SNX9 siRNA-treated cells).

To further explore the apparent link between local PI(3,4)P_2 synthesis and SNX9 recruitment and function, we asked whether SNX9's role in CME depends on its ability to associate with PIs. To this end, we generated two independent SNX9 PX domain mutants deficient in lipid binding: The RYK mutant (R286A, Y287A, K288A, described in ((Yarar et al., 2008), shown to display proper folding), and the K267N, R327N mutant that was designed on the basis of the PI(3)P-bound PX-BAR domain structure of Pylypenko et al. (Pylypenko et al., 2007). Impaired lipid binding of the K267N, R327N mutant was confirmed in liposome-binding flotation assays (Figure 3-23b). When tested for their ability to reconstitute defective CME in SNX9 and SNX18 double knockdown cells, neither of the lipid binding mutants was able to rescue the phenotype (Figure 3-23c,d). Collectively, these results establish a functional role for SNX9 (and its paralog SNX18) as an effector of PI(3,4)P_2 synthesized by PI3K C2α at sites of CME.

3.4.4 *Spatiotemporal dynamics of SNX9 recruitment*

The results outlined above establish SNX9 as a PI(3,4)P_2-dependent effector of PI3K C2α. A prediction from this finding is that the recruitment of these proteins should be temporally coordinated, i.e. that arrival of PI3K C2α should precede arrival of SNX9. To test this hypothesis, we monitored individual CCPs in live Cos7 cells co-expressing low levels of mCherry-SNX9 and GFP-PI3K C2α by TIRF microscopy. Accumulation of PI3K C2α consistently occurred before SNX9 (Figure 3-24a,b). In

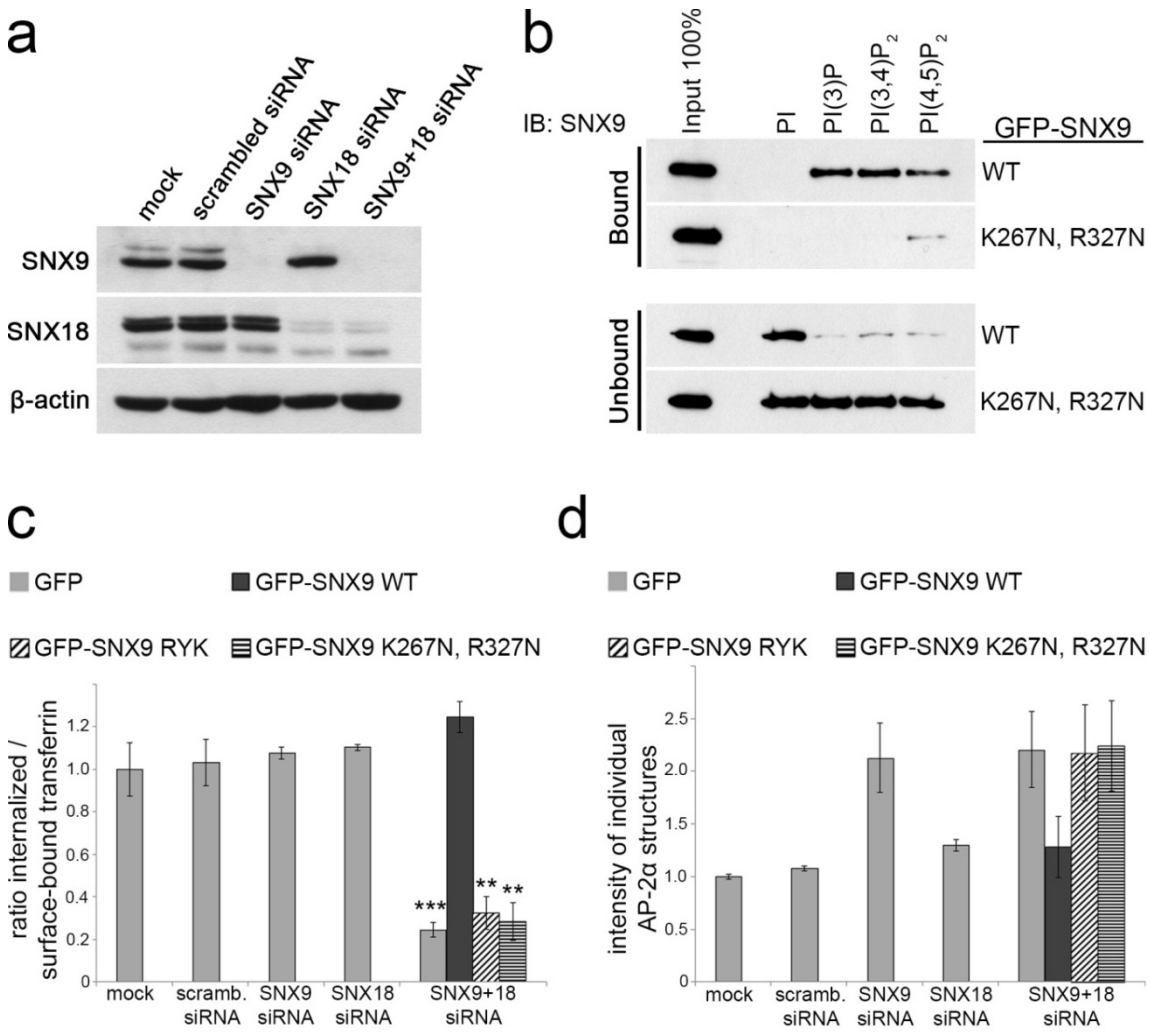

Figure 3-23: SNX9 and SNX18 are redundant and lipid-binding dependent regulators of CME. a) Co-silencing of SNX9 and its close paralog SNX18 in Cos7 cells. Immunoblot analysis of extracts from Cos7 cells depleted of SNX9, SNX18, or both proteins using RNA interference. Detection of β-actin demonstrates equal loading in all lanes. **b)** Mutation of K267N, R327N in the SNX9 PX-domain causes loss of PI-binding. Immunoblot analysis of the association of wild-type (WT) or K267N, R327N mutant eGFP-SNX9 (from cytosolic HEK293 cell extracts) to liposomes containing 5 mol% of the indicated PI in flotation assays. Input shows 100 % of the protein offered in relation to the amount of sample loaded. **c,d)** The lipid-binding deficient mutants of SNX9, RYK (R286A, Y287A, K288;(Yarar et al., 2008)) and K267N,R327N (see b) are unable to reconstitute CME in cells co-silenced for SNX9 and SNX18. **c**, Impaired CME of transferrin in Cos7 cells depleted of SNX9 and SNX18 is rescued by re-expression of WT eGFP-SNX9 but not of PI-binding deficient PX-domain mutants. Bar diagrams represent the ratio of internalized (10 min, 37°C) to surface transferrin (45 min, 4°C) (mean ± s.e.m.; n = 5 independent experiments, except n = 4 [eGFP-SNX9 RYK and K267N, R327N] and n = 2 [SNX18]; ** $p < 0.01$, *** $p < 0.001$, t-test vs. scrambled siRNA). **d**, Accumulation of AP-2α-positive CCPs in Cos7 cells depleted of SNX9 or SNX9 together with SNX18. This phenotype is rescued by re-expression of WT eGFP-SNX9 but not of PI-binding deficient PX-domain mutants. Mean intensity of endocytic AP-2α-containing pits (mean ± s.e.m.; n = 2 independent experiments).

fact, arrival of SNX9 was never observed to precede PI3K C2α, demonstrating tightly controlled recruitment dynamics. To generate a comprehensive picture of protein recruitment to CCPs, these data were directly compared with those shown in Figure 3-10d encompassing clathrin and dynamin. This revealed a precisely defined orchestration of endocytic protein recruitment dynamics (Figure 3-24b): Clathrin arrives first, and with a delay of about 12 s – measured at half maximal intensity –recruits PI3K C2α. This is followed by accumulation of SNX9 ~20 s after PI3K C2α, which slightly precedes the final burst of dynamin accumulation.

We noticed that increasing expression levels of mCherry-SNX9 were associated with constitutive tubulation of cellular membranes, consistent with earlier reports (Shin et al., 2008). Interestingly, when monitoring cells with mildly elevated expression levels of SNX9 that did not display obvious membrane tubulation, we observed dynamic growth of short SNX9 tubules from CCPs immediately prior to fission (Figure 3-24c).

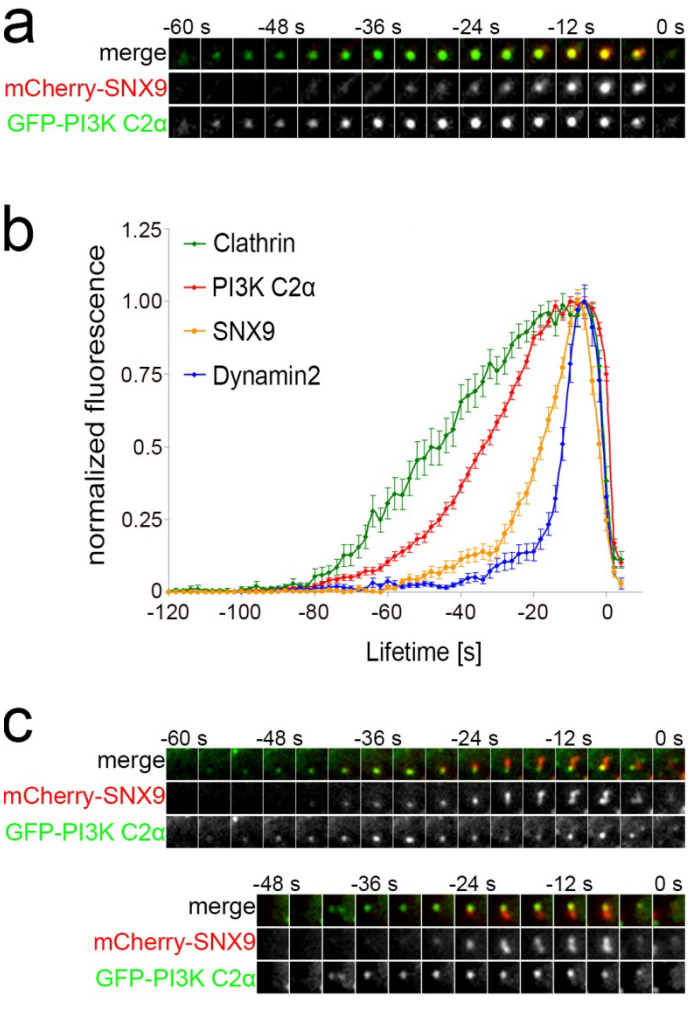

Figure 3-24: Dynamics of SNX9 recruitment to CCPs. a,b) Timing of recruitment of SNX9 and PI3K C2α to CCPs analyzed by TIRF microscopy (low SNX9 expression levels). **a**, Snapshots of eGFP-PI3K C2α and mCherry-SNX9 at single CCPs (fission at t = 0). **b**, Mean time course of relative fluorescence intensity at CCPs. Data represent mean ± s.e.m. (2 independent experiments; total number N of CCPs: N=248 for PI3K C2α, N=100 for SNX9; data for clathrin and dynamin2 are identical to Figure 3-10d). **c**) At moderately high expression levels of mCherry-SNX9, tubule-like structures can be observed to grow from PI3K C2α-positive CCPs. Shown are snapshots of two representative CCPs monitored by TIRF microscopy of GFP-PI3K C2α and mCherry-SNX9 expressing Cos7 cells.

Also in these instances, SNX9 recruitment followed PI3K C2α, and for several seconds both proteins perfectly overlapped at CCPs. This was followed by the growth of tubule-like SNX9-positive structures emanating from PI3K C2α-coated regions that upon fission disappeared together with PI3K C2α. These observations suggested that timed recruitment of mCherry-SNX9 translates into a spatial segregation of the protein from the coated region. In order to assess this on the level of endogenous proteins and to exclude possible overexpression artifacts, we turned to spectral-demixing direct stochastical optical reconstruction microscopy (SD-*d*STORM) imaging of endogenous SNX9 and PI3K C2α (in collaboration with André Lampe, Leibniz Institute for Molecular Pharmacology, Berlin). SD-*d*STORM offers lateral resolution of 20 nm to 30 nm using conventional antibody labeling techniques (Lampe et al., 2012). Whereas clathrin and PI3K C2α displayed very close overlap (Figure 3-25a), SNX9 frequently appeared adjacent to the endocytic protein coat marked by AP-2α, an effect that became overt upon depletion of dynamin2 (Figure 3-25b). The elongated structures seen in these cells most likely correspond to the necks of stalled CCPs. Taken together, these data document the spatiotemporal organization of the late events of CCP formation. The temporally orchestrated recruitment of clathrin, PI3K C2α, and SNX9 results in

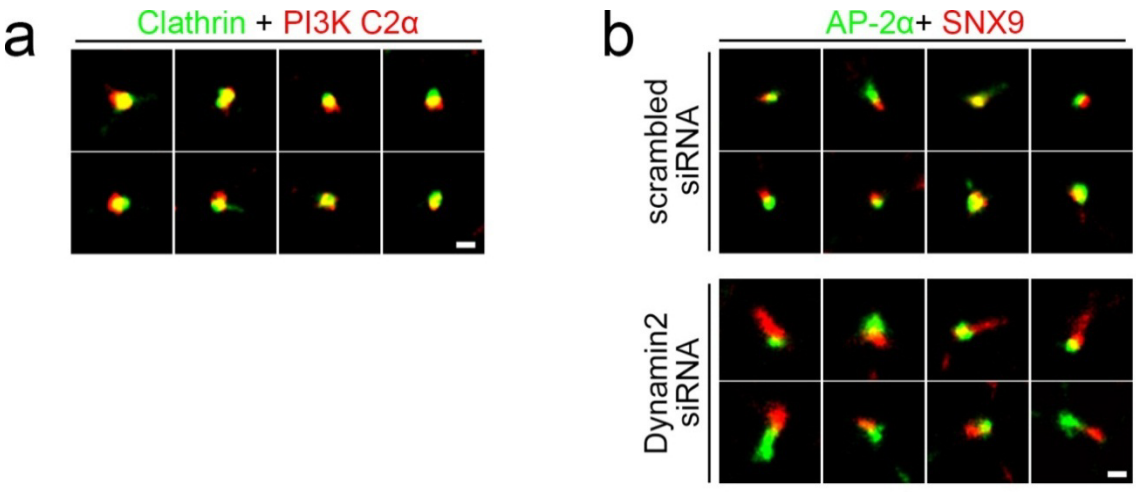

Figure 3-25: Localization of endogenous SNX9 at CCPs using SD-*d*STORM superresolution microscopy. a) Gallery of dual-color SD-*d*STORM images of clathrin and PI3K C2α at endocytic CCPs. **b**) Galleries of dual-color SD-*d*STORM images of endogenous AP-2α and SNX9 at endocytic CCPs in control or in dynamin2-depleted Cos7 cells. Upon depletion of dynamin2, SNX9 is segregated from AP-2α-coated buds towards an elongated structure likely corresponding to the constricted endocytic vesicle neck. Scale bars, 150 nm.

the spatial segregation of SNX9 from the coat, with the time point of SNX9 arrival coinciding with a stage of CCP maturation that requires extensive membrane remodeling as constriction shapes the narrow vesicle neck.

4 Discussion

In the present work, we unravel a novel regulatory role of $PI(3,4)P_2$ in the central cellular pathway of CME and demonstrate that the class II isoform PI3K C2α synthesizes this lipid directly at CCPs. Furthermore, we identify the PX-BAR domain protein SNX9 as an effector protein of $PI(3,4)P_2$ during CME. We provide evidence that $PI(3,4)P_2$ controls the spatiotemporal organization of late maturation stages of CCPs prior to dynamin-mediated vesicle scission. These results have implications for the cellular roles of $PI(3,4)P_2$, the cell physiological functions of class II PI3Ks, and the mechanisms that govern complex regulation of cellular processes by a combination of multiple PI species.

4.1 Spatiotemporal control of CCP maturation by $PI(3,4)P_2$

The formation of CCVs requires the assembly of a protein coat on the cytoplasmic face of the plasma membrane, the gradual invagination from a shallow cavity to a deep pit, the constriction of the membrane-proximal region into a narrow neck, and finally the catalysis of membrane fission at this neck. The succession of events during the nucleation of CCPs has been analyzed in molecular terms with single-molecule resolution (Cocucci et al., 2012). Further, the assembly of the dynamin helix around the constricted neck and the presumptive mechanism of this molecular scission apparatus have been described in molecular and structural detail (Faelber et al., 2012; Ferguson and De Camilli, 2012). In comparison, relatively little is known about the molecular events governing CCP maturation that connect CCP nucleation to the final event of CCV formation. Although membrane remodeling by scaffolding protein assemblies (the clathrin lattice, BAR-domain oligomers) and by proteins inserting amphipathic helices into the inner leaflet of the plasma membrane (N-BAR domains, epsins) have been unraveled (Doherty and McMahon, 2009; Frost et al., 2009), the coordination of these factors during the formation of a narrow neck has remained unclear. In the work reported here, timed synthesis of $PI(3,4)P_2$ is shown to control the temporal and spatial recruitment dynamics of the PX-BAR-domain protein SNX9 to maturing late stage CCPs (Figure 3-19, Figure 3-21, Figure 3-24, Figure 3-25). Failure to recruit SNX9, and potentially other $PI(3,4)P_2$ effectors and associated binding

partners, results in a maturation defect characterized by pits stalled at the pre-constriction stage (Figure 3-10a,b). Absence of SNX9 also renders pits in dynamin-deficient cells partially incapable of forming elongated, narrow necks (Figure 3-20). Based on these findings, we sought to develop a rational understanding of the spatiotemporal control of CCP maturation by $PI(3,4)P_2$. In close collaboration with the group of Dr. Frank Noé (Freie Universitaet Berlin), we applied a mathematical model that simulates the complex protein-lipid dynamics at CCPs.

4.1.1 *A computational model of protein-lipid dynamics at maturing CCPs*

Analysis of SNX9's lipid binding specificity *in vitro* revealed strongest binding to $PI(3,4)P_2$ with only a slight preference over $PI(4,5)P_2$ (Figure 3-18). This was an unexpected observation given the strict dependence of SNX9 recruitment to late-stage CCPs on PI3K C2α and $PI(3,4)P_2$ (Figure 3-19, Figure 3-21) under conditions where levels of $PI(4,5)P_2$ were unaffected (Figure 3-2, Figure 3-12c,d). Why would an effector protein that for its function crucially depends on the ability to bind lipids (Figure 3-23) evolve a lipid binding profile of low specificity?

A key difference between *in vitro* lipid binding experiments and the situation at CCPs *in vivo* is the high local concentration of endocytic proteins that may compete for the same population of PIs. Hence, protein-lipid population dynamics may be complex and cannot be predicted easily based on single binding affinities. To grasp this complexity, Schöneberg and colleagues (Schöneberg et al., 2013) designed a theoretical reaction-diffusion model with single-molecule resolution. This model is based on experimentally determined absolute protein copy numbers in CCVs (Borner et al., 2012), published PI concentrations, and measured binding affinities of major endocytic proteins (Ford et al., 2001; Ford et al., 2002; Henne et al., 2010; Jackson et al., 2010). For the simulation, the two-dimensional projection of a CCP is subdivided into a grid of 217 distinct simulation cells onto which a rigid lattice of clathrin triskelia is superimposed (Figure 4-1a). The binding reactions taken into account for individual protein molecules in each simulation cell are illustrated in Figure 4-1b and encompass membrane association, PI binding, and association with a clathrin-terminal domain. Based on the observed recruitment time course of PI3K C2α to maturing CCPs, the $PI(3,4)P_2$ concentration after an initial stage of "coat assembly" (t = 0 - 10 s) was assumed to rise from zero to the level of $PI(4,5)P_2$ (t = 10 - 15 s; Figure 4-1c, bottom panel). The effects on the concentration of major endocytic PI binding proteins underneath the clathrin coat were then monitored (Figure

4-1c, top and middle panels). Consistently, SNX9 was the only endocytic protein tested that prominently enriched at CCPs concomitant with rising levels of $PI(3,4)P_2$, despite the conservative assumption that it would bind to $PI(3,4)P_2$ and $PI(4,5)P_2$ equally well. Other endocytic PI-binding proteins such as AP-2, FCHo, CALM, or epsin exhibited comparably minor changes during the simulated time course of 20 s (Figure 4-1c). These results indicate that lipid competition amongst different endocytic proteins may indeed be of critical importance for CME. This was confirmed by control simulations in the absence of competing endocytic proteins, which resulted in a much weaker relative response of the SNX9 population to increases in $PI(3,4)P_2$ (Schöneberg et al., 2013). $PI(3,4)P_2$-induced recruitment of SNX9 was observed over a total of 270 different parameter combinations and found to be robust as long as the $PI(3,4)P_2$ levels would rise to about half of those of $PI(4,5)P_2$ (Schöneberg et al., 2013). This is a conservative assumption as based on published turnover numbers of native PI3Ks (Carpenter et al., 1990) and the copy number (Borner et al., 2012) and lifetime (Figure 3-24b) of PI3K C2α at CCPs, $PI(3,4)P_2$ levels can be expected to reach at least the same level as that of $PI(4,5)P_2$. Computational simulation of the protein-lipid dynamics at CCPs thus rationalizes and reconciles the experimental observations of SNX9 lipid binding *in vitro* and lipid-dependent recruitment *in vivo*. However, it appeared plausible that the given lipid binding profile of SNX9 should not only be compatible with the observed behavior in cells but should endow SNX9 with properties advantageous for its functional role in CME. To test this hypothesis, a further control simulation was performed that assumed SNX9 to be fully specific for $PI(3,4)P_2$, i.e. to have only basal affinity for $PI(4,5)P_2$ similar to acidic bulk lipids as phosphatidic acid. Although the relative accumulation of SNX9 in response to the increase in $PI(3,4)P_2$ levels was even stronger, the total protein copy number at simulated CCP was significantly lower than under conditions where SNX9 bound to $PI(4,5)P_2$ (Schöneberg et al., 2013). Mathematical modeling therefore suggests that SNX9's lipid binding abilities are indeed ideally adapted to the competitive environment of a CCP and allow for a stable, yet specifically controlled association of the protein with endocytic sites.

4.1.2 *A spatial model of protein recruitment to CCPs*

Live imaging of SNX9 overexpressing cells and superresolved images of the distribution of endogenous SNX9 at arrested late-stage CCPs (Figure 3-24c, Figure 3-25) suggested a spatial segregation of SNX9 from the endocytic protein coat. As

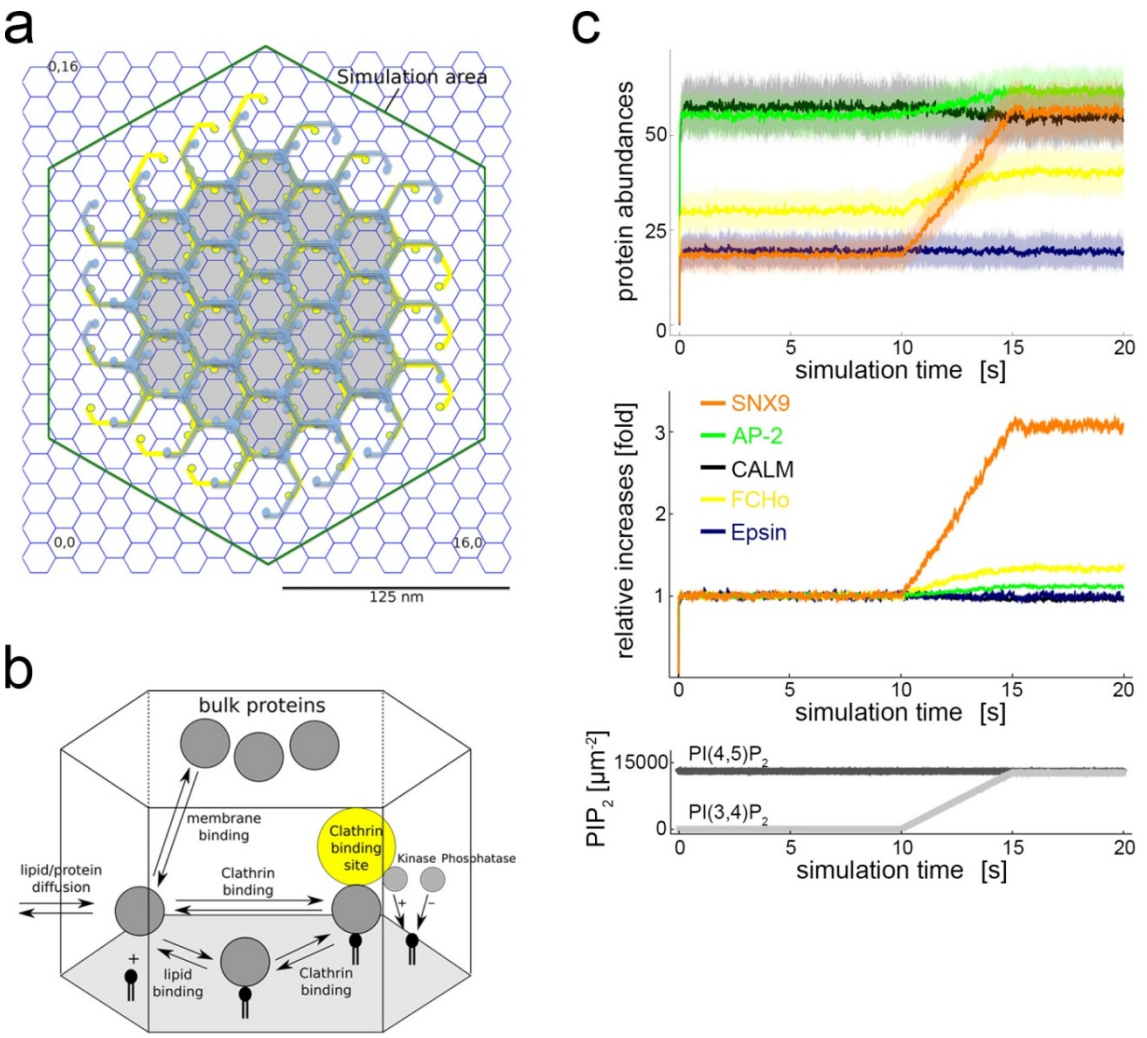

Figure 4-1: Single-particle reaction-diffusion model of protein-lipid dynamics at a CCP. a) Hexagonal simulation grid of a two-dimensional projection of a CCP. The large green hexagon circumscribes the area simulated, consisting of 217 simulation cells (small blue hexagons). The yellow and blue structures represent 54 clathrin triskelia, with hubs shown as larger circles and terminal domains as smaller circles. The shaded gray area is considered to be the area underneath the clathrin coat. **b)** Summary of the reaction and binding processes occurring in each simulation cell. **c)** Simulated endocytic protein abundances underneath the clathrin coat of a 2D-projected CCP over time. Averaged protein copy numbers (solid lines) ± SD (shaded vertical bars; n = 64 simulation runs) are shown (top panel). Ratio of protein copy numbers normalized to those at time t = 10s (middle panel). Concentration profile of $PI(3,4)P_2$ and $PI(4,5)P_2$ (bottom panel). Simulation is divided in 3 phases: equilibration phase (0s - 10s): constant $PI(4,5)P_2$ and zero $PI(3,4)P_2$ level; rising phase (10s-15s): $PI(3,4)P_2$ is elevated to the level of $PI(4,5)P_2$; equilibration phase (15s-20s). SNX9 copy numbers are selectively increased in response to $PI(3,4)P_2$ production to a value sufficient for formation of a hypothetical ring around a CCP neck. Data are taken from (Schöneberg et al., 2013).

factors that are expected to contribute to SNX9 recruitment to maturing CCPs, i.e. PI3K C2α, AP-2, and clathrin, do not show a comparable localization, this behavior was not intuitively comprehensible. For this reason, Schöneberg et al. developed a computational model taking into account protein size (as determined from published crystallographic data) to address the spatial distribution of endocytic proteins within the CCP (Schöneberg et al., 2013). The model starts from the snapshot of a two-dimensional projection of a CCP with a distribution of endocytic proteins as taken from a time point before the onset of $PI(3,4)P_2$ production in the single-particle reaction-diffusion model described above (Figure 4-2a). Then, the random placement of SNX9 dimers into the area of the endocytic coat was probed (Figure 4-2b). The dense protein matrix underneath the clathrin lattice results in space exclusion and, thus, in a predominant recruitment of SNX9 to the CCP rim, as indicated by the high (white on the intensity scale) peripheral recruitment probability density (Figure 4-2b, right panel). When allowing Brownian dynamics, SNX9 remained largely confined to the peripheral region because diffusional paths towards the center of the two-dimensional CCP are blocked (Figure 4-2c). The spatial model thus suggests that the timed recruitment of proteins to CCPs translates into a spatial organization of the maturing endocytic coat. Protein crowding in the center of the pit, at late stages, automatically causes preferential association of newly arriving proteins in the peripheral area of the coat. Transferring the information from this model to a three-dimensional, invaginated CCP, the rim of the clathrin coat corresponds to the membrane-proximal part of the CCP where remodeling of the membrane is required for the formation of a narrow neck. As synthesis of $PI(3,4)P_2$ is delayed compared to clathrin / AP-2 coat assembly, it is tempting to speculate that PI3K C2α-driven $PI(3,4)P_2$ formation constitutes a built-in mechanism to trigger constriction of CCPs upon reaching a certain level of coat maturation. This would require curvature-inducing proteins to be spatiotemporally controlled by $PI(3,4)P_2$, as demonstrated for SNX9 (and SNX18) in this study. However, validation of this hypothesis demands definitive assessment of the mechanism of CCP constriction, the involvement of SNX9 and a systematic evaluation of other proteins contributing to this process.

4.1.3 *The function of SNX9 at CCPs*

The spatiotemporal aspects of SNX9 recruitment dynamics have been analyzed in this study but the precise function of SNX9 at CCPs remains to be ascertained. The

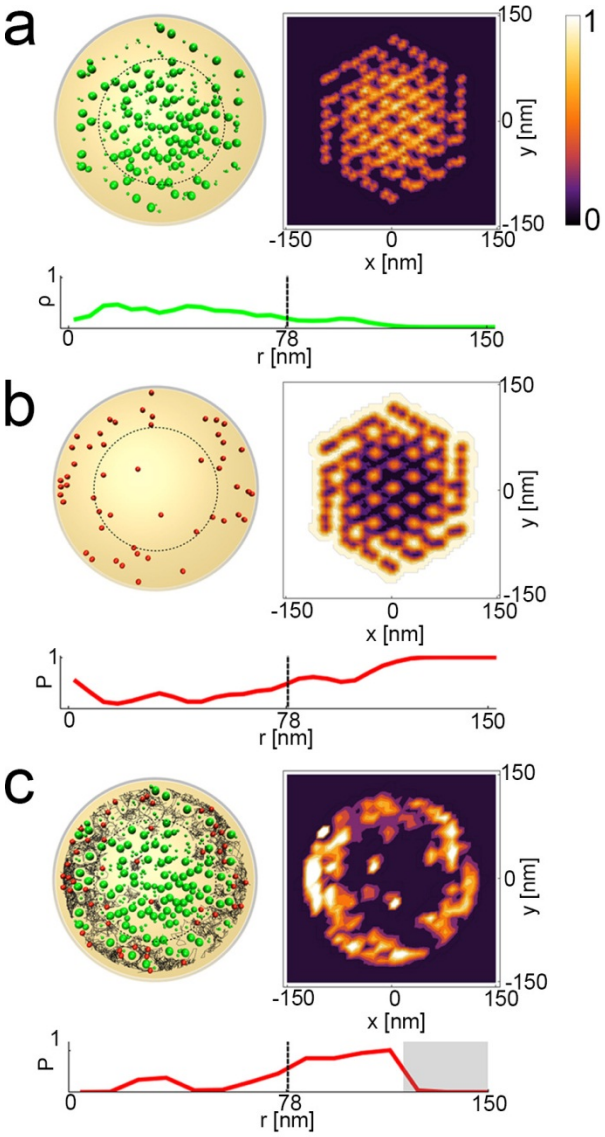

Figure 4-2: A spatial model of protein recruitment to maturing CCPs. a) Sample configuration of all proteins (green) underneath the clathrin coat of a CCP corresponding to a maturation stage before onset of SNX9 recruitment. Dashed line indicates core coat (left). Average density of 100 generated configurations (in [0,1] ~ color scale) (right). Profile of average density, projected onto the radius from the center of the CCP (bottom). **b)** Sample placement of 50 SNX9 (red) in the single protein configuration shown in a (left). Averaged placement probability of SNX9 in the 100 configurations of a, right panel (in [0,1] ~ color scale) (right). Profile of the radius projected placement probability (bottom). **c)** Combined configurations of proteins and SNX9 from a and b. Local mobility of SNX9 is probed by diffusion trajectories (black lines, left). SNX9 residence probability averaged over the diffusion simulation (right). Profile of the radius projected residence probability. Gray shaded regions were not part of the simulation (bottom). Note the higher placement probability of SNX9 towards the rim of the CCP. Data are taken from (Schöneberg et al., 2013).

established properties of SNX9 allow proposing a model of its mechanistic role at late-stage endocytic intermediates.

An important aspect of SNX9 function is the interaction of its SH3 domain with the proline-rich domain of dynamins (Lundmark and Carlsson, 2003) and its potent stimulation of dynamin GTPase-activity (Soulet et al., 2005). The extent of SNX9's contribution to recruiting dynamin to CCPs has been a matter of debate, with an early report showing a strong dependence of dynamin membrane association on SNX9 in HeLa cells (Lundmark and Carlsson, 2004). More recently, a systematic analysis of the contribution of BAR-domain proteins to dynamin recruitment in a skin fibroblast cell line suggested a dominant role of both endophilins and amphiphysins, but no significant

impact of SNX9 (Meinecke et al., 2013). However, in these skin fibroblasts SNX9 depletion did not affect CME of transferrin, indicating that loss of SNX9 is possibly compensated by one of its closely related isoforms, SNX18 or SNX33, proteins expressed only at low levels in HeLa cells (see Figure 3-22, Figure 3-23). Analysis of the accumulating endocytic intermediates in PI3K C2α-depleted cells in this work revealed that dynamin2 was strongly recruited to these structures, whereas SNX9, and by extension likely also SNX18, were not (Figure 3-17). This demonstrates that dynamin association with CCPs does not require SNX9. Taken together, these findings indicate that SNX9 / SNX18 / SNX33 are dispensable for dynamin recruitment, and hence, that this aspect of their function is unlikely to explain their essential role in CME.

A second fundamental property of SNX9 and its homologs is the ability to deform membranes, as evidenced by membrane tubulation both in cells and *in vitro* (Pylypenko et al., 2007; Shin et al., 2008). This activity is believed to involve both amphipathic helix insertion into the inner leaflet and stabilization of membrane curvature by oligomeric assemblies of SNX9 that scaffold the resulting ~20 nm wide membrane tubules (Pylypenko et al., 2007; Yarar et al., 2007). Considering SNX9's time point of recruitment to CCPs and its documented accumulation on elongated necks of CCPs in dynamin-deficient cells (Figure 18; (Ferguson et al., 2009)), this strongly suggests a role for SNX9 in the final membrane remodeling step that generates the narrow neck. Experimental proof for SNX9 mediating CCP constriction has not been published. Examination of endocytic protein recruitment to arrested CCPs in dynamin-depleted cells in this study has provided further support for a role of SNX9 in CCP constriction. As established in (Ferguson et al., 2009), the actin branching and nucleator complex Arp2/3 is one of the components of the actin machinery that is required for the formation of elongated necks at CCPs in dynamin-deficient cells. We have used Arp2/3 as a reporter for the presence of constricted and elongated endocytic necks. Upon depletion of PI3K C2α, the p34 subunit of Arp2/3 was entirely lost from endocytic structures (Figure 3-20). These data indicate that depletion of PI3K C2α or $PI(3,4)P_2$ does not only cause selective loss of SNX9 from late-stage CCPs but rather leads to a failure to form constricted and elongated necks. Depletion of SNX9 resulted in a similar albeit less complete loss of p34 from endocytic structures (Figure 3-20). The residual presence of p34 possibly reflects a partial compensation by SNX18. These findings

argue for a requirement of PI(3,4)P_2-controlled SNX9 recruitment in the constriction of CCPs. Yet, this prediction will have to be confirmed by ultrastructural analyses.

A third major connection links SNX9 to the actin cytoskeleton. Biochemical experiments revealed direct interactions of the SH3 domain of SNX9 with the nucleation-promoting factor N-WASP and of its unstructured linker region with Arp2/3 (Badour et al., 2007; Shin et al., 2008). Furthermore, a stimulating effect of SNX9 binding on the actin-nucleating activity of its interaction partners has been demonstrated (Yarar et al., 2007). The requirement for actin in CME appears to be limited to conditions of membrane stress (Fujimoto et al., 2000; Boulant et al., 2011) and has been assigned to late stages of CCV formation (Taylor et al., 2011). Evidence from ultrastructural analyses suggests that in case actin does participate in CME the generated force is harnessed to promote constriction of CCPs (Boulant et al., 2011; Collins et al., 2011).

Our results argue for a requirement of SNX9 in CCP constriction. In light of this, SNX9's connections with the actin module place it at the core of the membrane remodeling machinery during late CCP maturation. In addition to SNX9's ability to induce curvature via its PX-BAR domain, it may direct the actin cytoskeleton to support membrane constriction by activating N-WASP and Arp2/3. This activity may partially overlap with that of other endocytic SH3 domain proteins such as endophilin and amphiphysin (Otsuki et al., 2003; Yamada et al., 2009). Furthermore, the spatiotemporal control of SNX9 recruitment by PI(3,4)P_2 suggests that, beyond sculpting the membrane itself, SNX9 might serve as a coordinator of membrane remodeling during late stages of CCP maturation. Recent biochemical analyses showed differential regulation of dynamin catalyzed fission by SNX9, endophilin, and amphiphysin (Neumann and Schmid, 2013). Contrasting endophilin and amphiphysin, SNX9 did not synergize with dynamin to release vesicles from supported lipid bilayers, whereas it potently stimulated dynamin GTPase-activity, indicative of enhanced dynamin assembly. These findings suggest a hierarchy of SH3-domain interactions in regulating dynamin, with SNX9 fulfilling an earlier role than the more potent membrane remodeling N-BAR proteins endophilin and amphiphysin (Neumann and Schmid, 2013). Once an increase of membrane curvature has been initialized by SNX9, this may serve as a cue for other curvature-sensitive and curvature-inducing proteins, such as epsins and endophilins, to translocate to the nascent neck, thereby accelerating and completing constriction.

4.2 Concerted regulation of CME by $PI(4,5)P_2$ and $PI(3,4)P_2$

As many other processes at the plasma membrane, CME has been shown to crucially depend on $PI(4,5)P_2$. Most endocytic proteins that directly associate with the membrane display a preference for binding to $PI(4,5)P_2$-enriched membranes. This contributes to defining the plasma membrane as the site of endocytic coat formation and ensures compartmental specificity. The importance of $PI(4,5)P_2$ for the early stages of coat formation has been characterized thoroughly whereas the lipid's role at later stages has remained less clear. After scission, $PI(4,5)P_2$ is hydrolyzed from the membrane in a process that not only triggers uncoating of the newly formed vesicle but also erases plasma membrane identity. In this work, we establish a role for $PI(3,4)P_2$ in regulating a late maturation stage of CCPs, and we demonstrate that $PI(4,5)P_2$ and $PI(3,4)P_2$ are sequentially required for the formation of CCVs (Figure 3-1 - Figure 3-5). Identification of this new lipid requirement of CME calls for a reconsideration of the role of certain PI metabolizing enzymes implicated in CME and allows us to propose a revised model of PI conversion on the early endocytic route.

4.2.1 *Regulation of endocytic coat formation by $PI(4,5)P_2$ and $PI(3,4)P_2$*

The endocytic proteome contains a number of PI metabolizing enzymes. Tracing their mode of association with the endocytic machinery provides an overview of PI conversions that locally take place at CCPs. Members of the $PI(4,5)P_2$-generating enzyme family of type I PIP5Ks associate with and are stimulated by AP-2 (Bairstow et al., 2006; Krauss et al., 2006; Nakano-Kobayashi et al., 2007; Kahlfeldt et al., 2010), but significant enrichment of these kinases at CCPs was never observed. Moreover, PIP5KIγ was shown to be displaced from AP-2 upon clathrin association with the β2-appendage domain (Thieman et al., 2009). Hence, synthesis of $PI(4,5)P_2$ appears to be limited to the nucleation stage of CCPs. The 5-phosphatases SHIP-2 and Sjn 1 have been found to associate with maturing CCPs (Perera et al., 2006; Nakatsu et al., 2010), whereas two other 5-phosphatases, OCRL and the short isoform of Sjn 1, accumulate only during or after fission (Perera et al., 2006; Erdmann et al., 2007). Hydrolysis of $PI(4,5)P_2$ after scission is believed to be required for uncoating. By contrast, the functional significance of 5-phosphatases present at earlier stages of CCP maturation has remained elusive. PI3K C2α has been identified as an interactor of clathrin and as a component of CCVs already earlier (Domin et al., 2000; Gaidarov et al., 2001). We now

show that PI3K C2α accumulates at maturing CCPs and arrives with a delay of about 12 s with respect to clathrin (Figure 3-10c,d).

The complement of phosphatases and kinases within the endocytic protein network thus appears to be designed for a gradual conversion of $PI(4,5)P_2$ to $PI(3,4)P_2$ during CCP maturation and a complete removal of $PI(4,5)P_2$ after scission. At established CCPs, the locally enriched $PI(4,5)P_2$ can be expected to be partially converted to PI(4)P by SHIP-2 and the long isoform of Sjn 1. Towards scission, increasing levels of PI3K C2α will lead to a build-up of $PI(3,4)P_2$, as evidenced by immunolabeling for this lipid, revealing the presence of $PI(3,4)P_2$ at CCPs (Figure 3-1, Figure 3-13b). Notably, only a subpopulation of CCPs was found to be positive for $PI(3,4)P_2$, reflecting the late onset of $PI(3,4)P_2$ production during CCP maturation and possibly also the fact that lipids masked by effector proteins escape antibody detection. The activity of PI3K C2α results in two different pools of PIs being present at maturing CCPs: $PI(4,5)P_2$ dedicated to maintaining membrane association of the endocytic coat and $PI(3,4)P_2$ required for enhanced recruitment of late-stage effector proteins SNX9 / SNX18 and potentially others. During or briefly after membrane fission, the burst of recruitment of OCRL and of the short isoform of Sjn 1 (Perera et al., 2006; Erdmann et al., 2007) will complete conversion of $PI(4,5)P_2$ to PI(4)P, while PI3K C2α may remain active until disassembly of the coat. Newly formed, uncoated endocytic vesicles can thus be expected to be largely devoid of $PI(4,5)P_2$ and enriched in $PI(3,4)P_2$, possibly with remaining amounts of PI(4)P that depend on the 4-phosphatase activity of Sjn 1's Sac domain (Mani et al., 2007). In contrast to earlier concepts of PI conversion during constitutive CME, this model results in endocytic vesicles that contain 3-phosphorylated PIs and are thus poised for fusion with the endosomal compartment. The precise role of PI3K C2α and $PI(3,4)P_2$ after scission of the vesicle from the plasma membrane remains uncertain. Is their function limited to the final maturation stage of CCPs or do PI3K C2α and / or $PI(3,4)P_2$ serve additional purposes on newly formed endocytic vesicles? PI3K C2α has been reported to interact with the dynein component dynactin (Zhao et al., 2007), implicating the kinase in microtubule-based motility. Whether PI3K C2α may thereby contribute to a retrograde, inward movement of endocytic vesicles remains to be determined.

4.2.2 *Phosphoinositide conversion en route to endosomes*

Compartmental identity is in part defined by the PI species present in the membrane of an organelle (Behnia and Munro, 2005). Consequently, membrane carriers travelling in between compartments need to undergo PI conversion that deletes the PI identity of the donor membrane and allows the membrane to acquire the identity of the receiving organelle. On the endocytic route, this corresponds to conversion of plasma membrane PI(4,5)P_2 to endosomal PI(3)P. Previously, PIs were assumed to be largely degraded to phosphatidylinositol during late stages of vesicle formation and uncoating. Class III PI3K hVps34, an effector of the endosomal key regulator Rab5, would then synthesize PI(3)P from phosphatidylinositol and hence create early endosomal membrane identity *de novo* (Zerial and McBride, 2001; Gruenberg, 2003). Our findings of PI(3,4)P_2 synthesis by PI3K C2α during CCP maturation (Figure 3-7, Figure 3-8, Figure 3-10, Figure 3-14) are rather compatible with a continuous conversion mechanism operating along the endocytic route. Amongst the effector proteins of GTP-bound Rab5 is the PI(3,4)P_2-4-phosphatase INPP4A (Ivetac et al., 2005; Shin et al., 2005) so that, upon acquisition of Rab5, PI(3,4)P_2-containing endocytic vesicles are likely to be converted to PI(3)P-positive endosomes.

According to this model, PI3K C2α-derived PI(3,4)P_2 would feed into an early endosomal pool of PI(3)P that previously has been attributed to hVps34 and, to a minor extent, to class I PI3K activity (Shin et al., 2005; Di Paolo and De Camilli, 2006; Sorkin and von Zastrow, 2009). In fact, evidence for a non-essential role of hVps34 in early endosomal biogenesis and maintenance has been presented but has received only limited attention. Johnson et al. analyzed the effects of hVps34-depletion on the endolysosomal system of cultured fibroblasts and in accordance with earlier reports (Futter et al., 2001) described a defect in MVB formation accompanied by the accumulation of large cytoplasmic vacuoles with late endosomal or lysosomal identity (Johnson et al., 2006). Strikingly, the PI(3)P-dependent early endosomal tethering factor EEA1 and the PI(3)P-binding FYVE-domain displayed only minor alterations in Vps34-depleted cells. Even more, the authors reported that in wild-type cells treatment with 100 nM wortmannin, inhibiting class I and class III PI3Ks as wells as PI3K C2β, did not perturb EEA1 localization. By contrast, 1 µM wortmannin, a concentration that also blocks PI3K C2α activity, caused a dispersal of EEA1 (Johnson et al., 2006). Thus, hVps34 appears to be of central importance for MVB formation and also autophagy (Simonsen and Tooze, 2009) but may be dispensable for early endosome biogenesis and

maintenance. Taken together, these findings strongly support a model of continuous PI conversion on the endocytic route with PI3K C2α significantly contributing to early endosomal PI(3)P. This is corroborated by a recent study analyzing the role of PI3K C2α in sphingosine-1-phosphate receptor signaling, which reports a marked reduction in FYVE-domain labeled PI(3)P-positive endosomes in PI3K C2α-depleted cells but not in hVps34-depleted cells (Biswas et al., 2013).

The β isoform of class II PI3Ks has been reported to associate with clathrin and to localize to CCPs as well (Wheeler and Domin, 2006; Nakatsu et al., 2010). Initial experiments did not reveal an endocytic defect in PI3K C2β-depleted cells (data not shown), yet contribution of PI3K C2β to PI(3,4)P_2-synthesis during CME cannot be excluded. Although PI3K C2β has been proposed to elevate PI(3)P levels in response to LPA-stimulation at the plasma membrane (Maffucci et al., 2005) and to contribute to endosomal PI(3)P (Razidlo et al., 2011), the direct lipid product of PI3K C2β and its contribution to total cellular PI pools remain unclear.

In summary, available evidence suggests that the different pools of 3-PIs generated on the endocytic route are dedicated to preparing subsequent steps in the pathway. Class II PI3K-derived PI(3)P, at least in part resulting from plasma membrane PI(3,4)P_2, may be of importance for generating the early endosomal compartment. By contrast, class III PI3K-dependent pools of the lipid generated on endosomes appear to be primarily required for degradative trafficking.

4.3 A novel and constitutive role for $PI(3,4)P_2$

Research on 3-phosphorylated PIs has so far been focusing on the roles of PI(3)P in organizing endosomal membrane traffic and the crucial importance of $PI(3,4,5)P_3$ as a signaling molecule regulating cell survival and proliferation (Engelman et al., 2006; Vanhaesebroeck et al., 2010). The discovery of class I PI3K-dependent $PI(3,4,5)P_3$ formation and the high incidence of constitutively activating mutations in the catalytic and regulatory subunits of the α and β isoforms of class I PI3Ks across almost all types of human cancers have fuelled investigations of this branch of PI metabolism over the past two decades (Vanhaesebroeck et al., 2012). Formation of $PI(3,4)P_2$ by the 5-phosphatases SHIP-1/2 as a secondary consequence of class I PI3K activity has long been recognized (Bunney and Katan, 2010). However, clear implications of this conversion for the development of cancer have not been described until very recently (Gewinner et al., 2009), leaving $PI(3,4)P_2$ in the shadow of its precursor $PI(3,4,5)P_3$.

The identification of $PI(3,4)P_2$ as the main lipid product of the class II PI3K C2α under basal conditions (Figure 3-12, Figure 3-13) requires the revision of previous concepts concerning this PI species. The activity of PI3K C2α during the constitutive process of CME is independent of extracellular stimuli, suggesting that PI3K C2α may generate a pool of $PI(3,4)P_2$ that is independent of growth factor receptor activation. This is in agreement with our observation that the canonical PI3K inhibitor wortmannin completely abolishes EGF-induced class I PI3K-dependent $PI(3,4,5)P_3$ synthesis while only moderate affects on $PI(3,4)P_2$ levels under basal conditions are observed (Figure 3-5). The identification of PI3K C2α, a wortmannin-resistant kinase, as a main regulator of $PI(3,4)P_2$ levels explains these observations. Thus, it appears that instead of being limited to the role of a degradation product of a stimulation-induced second messenger, $PI(3,4)P_2$ fulfills class I PI3K- and $PI(3,4,5)P_3$-independent regulatory functions in cell physiology.

4.3.1 *Class I and class II PI3K-dependent pools of $PI(3,4)P_2$*

The precise relative contributions of class I PI3Ks and PI3K C2α to the total pool of $PI(3,4)P_2$ remain to be established. In serum-starved and synchronously stimulated cell populations – a commonly used but artificial scenario for assessing cellular effects of extracellular stimuli – class I PI3Ks may well be the indirect source of

the vast majority of PI(3,4)P_2. In continuous presence of low levels of growth factors, e.g. under basal culture conditions, the constitutive nature of CME and hence of PI3K C2α activity is likely to cause a significant contribution to the total PI(3,4)P_2 pool. In fact, when monitoring mRFP-2xTAPP1-PH membrane association by ratiometric TIRF / epifluorescence imaging we observed comparable effects of wortmannin-treatment (0.73 ± 0.02 of untreated control, mean ± s.e.m., n = 4 independent experiments) and siRNA-mediated depletion of PI3K C2α (0.80 ± 0.04, see Figure 3-12c) on plasma membrane PI(3,4)P_2 levels. Moreover, treatment of PI3K C2α-depleted cells with wortmannin caused an additional loss of mRFP-2xPH-TAPP1 membrane association (0.59 ± 0.02, mean ± s.e.m., n = 4 independent experiments), corroborating the co-existence of similarly sized class I and class II PI3K-dependent pools of PI(3,4)P_2. Of note, TIRF / epifluorescence ratios do not provide absolute values of remaining membrane association as even a completely cytosolic protein remains detectable by TIRF. Hence, TIRF / epifluorescence signal ratios express relative degrees of membrane association compared to a control. For example, expression of soluble mRFP resulted in a ratio of 0.38 ± 0.03 normalized to mRFP-2xPH-TAPP1 in control cells (mean ± s.e.m., n = 4 independent experiments). Further, effects of wortmannin treatment need to be interpreted with care as this inhibitor may, in addition to class I PI3Ks, also affect PI3K C2β, a class II isoform not resistant to wortmannin inhibition. Although PI3K C2β has not been experimentally analyzed with respect to substrate specificity, its activation loop sequence and hence its predicted substrate specificity are identical to those of PI3K C2α.

4.3.2 *The lipid product of PI3K C2α*

The extensive controversy about the lipid product of PI3K C2α – PI(3)P or PI(3,4)P_2 – ((Falasca et al., 2007; Leibiger et al., 2010; Yoshioka et al., 2012) and this work) suggests that PI3K C2α may indeed generate different lipids under different cellular conditions. Given PI3K C2α's clear preference for PI(4)P *in vitro* (Figure 3-12a,b), substrate availability in different subcellular locations may determine the respective product. At the plasma membrane, PI(4)P is abundant (Hammond et al., 2012; Nakatsu et al., 2012) and can thus be expected to be the preferred substrate. On endosomal membranes, PI(4)P is believed to be rare so that phosphatidylinositol, which is present in all cytoplasmic membrane leaflets, may be accepted as a substrate. To address this hypothesis, experimental means of distinguishing between PI3K C2α's

ability to produce either of the two lipid species are needed. As shown in Figure 3-14, the class III-like activation loop mutant of PI3K C2α has selectively lost its PI(3,4)P_2-synthesizing activity while PI(3)P-production is unaffected. Hence, by using this new tool, future reconstitution experiments in PI3K C2α-deficient cells should allow us to discern between PI(3)P and PI(3,4)P_2 synthesis by PI3K C2α in the context of distinct cellular processes.

4.4 Outlook

The description of $PI(3,4)P_2$ as a novel lipid regulator of CME and the identification of the class II PI3K C2α as the enzyme to synthesize this lipid constitute significant contributions to the understanding of the regulation of membrane traffic, the roles of class II PI3Ks, and the physiological functions of $PI(3,4)P_2$. In addition to addressing unresolved issues such as the functionally and mechanistically unexplored presence of PI3K C2α in CCVs, these findings raise new questions and may direct us towards future avenues of research.

CME is a ubiquitous cellular pathway that is essential for a multitude of physiological processes. Amongst these, the synaptic vesicle cycle and the maintenance of neurotransmission are of outstanding interest. Synaptic communication relies on the Ca^{2+}-triggered fusion of neurotransmitter-containing synaptic vesicles (SVs) with the presynaptic plasma membrane and continued excitability of synapses requires the recovery of the exocytosed SV proteins and SV membrane by endocytosis (Haucke et al., 2011). Endocytic proteins are frequently expressed at high levels in the brain. Consequently, perturbation of numerous components of the CME machinery results in synaptic phenotypes (Saheki and De Camilli, 2012). Although synaptic vesicle endocytosis displays some distinct features when compared to CME in non-neuronal cells, such as the kinetics (faster), the size of resulting vesicles (smaller), or different isoforms of the same protein, the general machinery operating in the two processes is largely identical. Whether PI3K C2α participates in CME at the synapse and whether synaptic vesicle endocytosis underlies the same requirement for $PI(3,4)P_2$ as CME in non-neuronal cells is an open question. PI3K C2α is expressed in the brain of mice (data not shown) and CCV preparations from calf brain display a strong enrichment of the enzyme (Figure 3-6b). However, localization of PI3K C2α to presynaptic boutons has not been analyzed. It hence appears likely, though not proven, that CME at the synapse involves $PI(3,4)P_2$ formation by PI3K C2α. Given the strong kinetic delay of CME upon $PI(3,4)P_2$ depletion, as opposed to full block of CME seen upon $PI(4,5)P_2$ depletion (Figure 3-3, Figure 3-4), investigation of a putative modulatory role of PI3K C2α in SV endocytosis might prove a fruitful area of research.

Class II PI3Ks have so far remained in the shadow of their class I family members but are now attracting increasing interest. A recent study reported the first PI3K C2α gene knockout, with ensuing embryonic lethality in constitutive homozygous knockout mice (Yoshioka et al., 2012). Further, PI3K C2a was shown to have an

essential function in sprouting angiogenesis and vascular maturation that caused embryonic lethality also in an endothelial cell-specific knockout. These results promise to raise interest in the class II PI3K subfamily, also in light of the cell biologically poorly defined mechanistic basis of the angiogenic phenotype of PI3K C2α knockouts (Yoshioka et al., 2012). In general, the potential involvement of $PI(3,4)P_2$ in processes controlled by class II PI3Ks gives rise to a host of new possibilities. These range from conceivable effects of $PI(3,4)P_2$ on the actin cytoskeleton to class I PI3K-independent $PI(3,4)P_2$-signaling. Additionally, class II PI3Ks may produce PI(3)P on endosomal membranes, i.e. in absence of PI(4)P as preferred substrate. PI3K C2α was identified as a component of the autophagy interaction network and as a positive regulator of autophagy in a recent proteomic screen (Behrends et al., 2010). The functional significance of this finding remains elusive.

Lastly, the mechanistic insight into a complex protein interaction network that is regulated by the consecutive synthesis of two distinct PI species may influence our future understanding of lipid-regulated processes. It appears likely that multiple PI species are simultaneously present at a given subcellular site. Hence, the concerted regulation of protein ensembles by two PI species at the same time may be a more common theme than previously anticipated. Competition mechanisms distinguishing between proteins capable of associating with one, the other, or both PIs offer yet more diverse possibilities of organizing the complexity of processes found in eukaryotic cells.

5 Bibliography

Arcaro, A., Zvelebil, M.J., Wallasch, C., Ullrich, a., Waterfield, M.D., and Domin, J. (2000). Class II phosphoinositide 3-kinases are downstream targets of activated polypeptide growth factor receptors. *Mol Cell Biol* **20**, 3817-3830.

Axelrod, D. (1981). Cell-substrate contacts illuminated by total internal reflection fluorescence. *J Cell Biol*, 141-145.

Badour, K., McGavin, M.K.H., Zhang, J., Freeman, S., Vieira, C., Filipp, D., et al. and Siminovitch, K.a. (2007). Interaction of the Wiskott-Aldrich syndrome protein with sorting nexin 9 is required for CD28 endocytosis and cosignaling in T cells. *Proc Natl Acad Sci USA* **104**, 1593-1598.

Bae, Y.H., Ding, Z., Das, T., Wells, A., Gertler, F., and Roy, P. (2010). Profilin1 regulates PI(3,4)P2 and lamellipodin accumulation at the leading edge thus influencing motility of MDA-MB-231 cells. *Proc Natl Acad Sci USA* **107**, 21547-21552.

Bairstow, S.F., Ling, K., Su, X., Firestone, A.J., Carbonara, C., and Anderson, R.a. (2006). Type Igamma661 phosphatidylinositol phosphate kinase directly interacts with AP2 and regulates endocytosis. *J Biol Chem* **281**, 20632-20642.

Behnia, R., and Munro, S. (2005). Organelle identity and the signposts for membrane traffic. *Nature* **438**, 597-604.

Behrends, C., Sowa, M.E., Gygi, S.P., and Harper, J.W. (2010). Network organization of the human autophagy system. *Nature* **466**, 68-76.

Biswas, K., Yoshioka, K., Asanuma, K., Okamoto, Y., Takuwa, N., Sasaki, T., and Takuwa, Y. (2013). Essential role of class II phosphatidylinositol-3-kinase-C2α in sphingosine 1-phosphate receptor-1-mediated signaling and migration in endothelial cells. *J Biol Chem* **288**, 2325-2339.

Böcking, T., Aguet, F., Harrison, S.C., and Kirchhausen, T. (2011). Single-molecule analysis of a molecular disassemblase reveals the mechanism of Hsc70-driven clathrin uncoating. *Nat Struct Mol Biol* **18**, 295-301.

Borner, G.H.H., Antrobus, R., Hirst, J., Bhumbra, G.S., Kozik, P., Jackson, L.P., et al. and Robinson, M.S. (2012). Multivariate proteomic profiling identifies novel accessory proteins of coated vesicles. *J Cell Biol* **197**, 141-160.

Borner, G.H.H., Harbour, M., Hester, S., Lilley, K.S., and Robinson, M.S. (2006). Comparative proteomics of clathrin-coated vesicles. *J Cell Biol* **175**, 571-578.

Boucrot, E., Pick, A., Çamdere, G., Liska, N., Evergren, E., McMahon, Harvey T., and Kozlov, Michael M. (2012). Membrane Fission Is Promoted by Insertion of Amphipathic Helices and Is Restricted by Crescent BAR Domains. *Cell* **149**, 124-136.

Boulant, S., Kural, C., Zeeh, J.-C., Ubelmann, F., and Kirchhausen, T. (2011). Actin dynamics counteract membrane tension during clathrin-mediated endocytosis. *Nat Cell Biol* **13**, 1-10.

Brown, R.A., Domin, J., Arcaro, A., Waterfield, M.D., and Shepherd, P.R. (1999). Insulin Activates the alpha Isoform of Class II Phosphoinositide 3-Kinase. *J Biol Chem* **274**, 14529-14532.

Bunney, T.D., and Katan, M. (2010). Phosphoinositide signalling in cancer: beyond PI3K and PTEN. *Nat Rev Cancer* **10**, 342-352.

Campbell, C., Squicciarini, J., Shia, M., Pilch, P.F., and Fine, R.E. (1984). Identification of a protein kinase as an intrinsic component of rat liver coated vesicles. *Biochemistry* **23**, 4420-4426.

Carpenter, C.L., Duckworth, B.C., Auger, K.R., Cohen, B., Schaffhausen, B.S., and Cantley, L.C. (1990). Purification and characterization of phosphoinositide 3-kinase from rat liver. *J Biol Chem* **26**, 19704-19711.

Chappie, J.S., Acharya, S., Leonard, M., Schmid, S.L., and Dyda, F. (2010). G domain dimerization controls dynamin's assembly-stimulated GTPase activity. *Nature* **465**, 435-440.

Cocucci, E., Aguet, F., Boulant, S., and Kirchhausen, T. (2012). The First Five Seconds in the Life of a Clathrin-Coated Pit. *Cell* **150**, 495-507.

Collins, A., Warrington, A., Taylor, K.a., and Svitkina, T. (2011). Structural Organization of the Actin Cytoskeleton at Sites of Clathrin-Mediated Endocytosis. *Curr Biol* **21**, 1167-1175.

Conner, S.D., and Schmid, S.L. (2003). Regulated portals of entry into the cell. *Nature* **422**, 37-44.

Cremona, O., Di Paolo, G., Wenk, M.R., Lüthi, a., Kim, W.T., Takei, K., et al. and De Camilli, P. (1999). Essential role of phosphoinositide metabolism in synaptic vesicle recycling. *Cell* **99**, 179-188.

Cullen, P.J. (2008). Endosomal sorting and signalling: an emerging role for sorting nexins. *Nat Rev Mol Cell Biol* **9**, 574-582.

Cullen, P.J., and Korswagen, H.C. (2012). Sorting nexins provide diversity for retromer-dependent trafficking events. *Nat Cell Biol* **14**, 29-37.

Dannhauser, P.N., and Ungewickell, E.J. (2012). Reconstitution of clathrin-coated bud and vesicle formation with minimal components. *Nat Cell Biol* **14**, 1-8.

De Matteis, M.A., and Godi, A. (2004). PI-loting membrane traffic. *Nat Cell Biol* **6**, 487-492.

Di Paolo, G., and De Camilli, P. (2006). Phosphoinositides in cell regulation and membrane dynamics. *Nature* **443**, 651-657.

DiNitto, J.P., Cronin, T.C., and Lambright, D.G. (2003). Membrane recognition and targeting by lipid-binding domains. *Science STKE* **2003**, re16-re16.

Dippold, H.C., Ng, M.M., Farber-Katz, S.E., Lee, S.-K., Kerr, M.L., Peterman, M.C., et al. and Field, S.J. (2009). GOLPH3 bridges phosphatidylinositol-4- phosphate and actomyosin to stretch and shape the Golgi to promote budding. *Cell* **139**, 337-351.

Diril, M.K., Wienisch, M., Jung, N., Klingauf, J., and Haucke, V. (2006). Stonin 2 is an AP-2-dependent endocytic sorting adaptor for synaptotagmin internalization and recycling. *Dev Cell* **10**, 233-244.

Doherty, G.J., and McMahon, H.T. (2009). Mechanisms of endocytosis. *Annu Rev Biochem* **78**, 857-902.

Domin, J., Gaidarov, I., Smith, M.E., Keen, J.H., and Waterfield, M.D. (2000). The class II phosphoinositide 3-kinase PI3K-C2alpha is concentrated in the trans-Golgi network and present in clathrin-coated vesicles. *J Biol Chem* **275**, 11943-11950.

Domin, J., Pages, F., Volinia, S., Rittenhouse, S.E., Zvelebil, M.J., Stein, R.C., and Waterfield, M.D. (1997). Cloning of a human phosphoinositide 3-kinase with a C2 domain that displays reduced sensitivity to the inhibitor wortmannin. *Biochem J* **326**, 139-139.

Dominguez, V., Raimondi, C., Somanath, S., Bugliani, M., Loder, M.K., Edling, C.E., et al. and Maffucci, T. (2011). Class II phosphoinositide 3-kinase regulates exocytosis of insulin granules in pancreatic beta cells. *J Biol Chem* **286**, 4216-4225.

Doray, B., Lee, I., Knisely, J., Bu, G., Kornfeld, S., and Louis, S. (2007). The γ/σ-1 and α/σ-2 Hemicomplexes of Clathrin Adaptors AP-1 and AP-2 Harbor the Dileucine Recognition Site. *Mol Biol Cell* **18**, 1887-1896.

Dowler, S., Currie, R.a., Campbell, D.G., Deak, M., Kular, G., Downes, C.P., and Alessi, D.R. (2000). Identification of pleckstrin-homology-domain-containing proteins with novel phosphoinositide-binding specificities. *Biochem J* **351**, 19-31.

Edeling, M.a., Smith, C., and Owen, D. (2006). Life of a clathrin coat: insights from clathrin and AP structures. *Nat Rev Mol Cell Biol* **7**, 32-44.

Engelman, J.a., Luo, J., and Cantley, L.C. (2006). The evolution of phosphatidylinositol 3-kinases as regulators of growth and metabolism. *Nat Rev Genet* **7**, 606-619.

Erdmann, K.S., Mao, Y., McCrea, H.J., Zoncu, R., Lee, S., Paradise, S., et al. and De Camilli, P. (2007). A role of the Lowe syndrome protein OCRL in early steps of the endocytic pathway. *Dev Cell* **13**, 377-390.

Faelber, K., Held, M., Gao, S., Posor, Y., Haucke, V., Noé, F., and Daumke, O. (2012). Structural insights into dynamin-mediated membrane fission. *Structure* **20**, 1621-1628.

Faelber, K., Posor, Y., Gao, S., Held, M., Roske, Y., Schulze, D., et al. and Daumke, O. (2011). Crystal structure of nucleotide-free dynamin. *Nature* **477**, 556-560.

Falasca, M., Hughes, W.E., Dominguez, V., Sala, G., Fostira, F., Fang, M.Q., et al. and Maffucci, T. (2007). The role of phosphoinositide 3-kinase C2alpha in insulin signaling. *J Biol Chem* **282**, 28226-28236.

Ferguson, S., Raimondi, A., Paradise, S., Shen, H., Mesaki, K., Ferguson, A., et al. and De Camilli, P. (2009). Coordinated actions of actin and BAR proteins upstream of dynamin at endocytic clathrin-coated pits. *Dev Cell* **17**, 811-822.

Ferguson, S.M., and De Camilli, P. (2012). Dynamin, a membrane-remodelling GTPase. *Nat Rev Mol Cell Biol* **13**, 75-88.

Fili, N., Calleja, V., Woscholski, R., Parker, P.J., and Larijani, B. (2006). Compartmental signal modulation: Endosomal phosphatidylinositol 3-phosphate controls endosome morphology and selective cargo sorting. *Proc Natl Acad Sci USA* **103**, 15473-15478.

Ford, M.G., Pearse, B.M., Higgins, M.K., Vallis, Y., Owen, D.J., Gibson, a., et al. and McMahon, H.T. (2001). Simultaneous binding of PtdIns(4,5)P2 and clathrin by AP180 in the nucleation of clathrin lattices on membranes. *Science* **291**, 1051-1055.

Ford, M.G.J., Mills, I.G., Peter, B.J., Vallis, Y., Praefcke, G.J.K., Evans, P.R., and McMahon, H.T. (2002). Curvature of clathrin-coated pits driven by epsin. *Nature* **419**, 361-366.

Fotin, A., Cheng, Y., Grigorieff, N., Walz, T., Harrison, S.C., and Kirchhausen, T. (2004). Structure of an auxilin-bound clathrin coat and its implications for the mechanism of uncoating. *Nature* **432**, 649-653.

Frost, A., Unger, V.M., and De Camilli, P. (2009). The BAR domain superfamily: membrane-molding macromolecules. *Cell* **137**, 191-196.

Fujimoto, L.M., Roth, R., Heuser, J.E., and Schmid, S.L. (2000). Actin assembly plays a variable, but not obligatory role in receptor-mediated endocytosis in mammalian cells. *Traffic* **1**, 161-171.

Futter, C.E., Collinson, L.M., Backer, J.M., and Hopkins, C.R. (2001). Human VPS34 is required for internal vesicle formation within multivesicular endosomes. *J Cell Biol* **155**, 1251-1264.

Gaidarov, I., Smith, M.E., Domin, J., and Keen, J.H. (2001). The class II phosphoinositide 3-kinase C2alpha is activated by clathrin and regulates clathrin-mediated membrane trafficking. *Mol Cell* **7**, 443-449.

Gaidarov, I., Zhao, Y., and Keen, J.H. (2005). Individual phosphoinositide 3-kinase C2alpha domain activities independently regulate clathrin function. *J Biol Chem* **280**, 40766-40772.

Gewinner, C., Wang, Z.C., Richardson, A., Teruya-Feldstein, J., Etemadmoghadam, D., Bowtell, D., et al. and Cantley, L.C. (2009). Evidence that inositol polyphosphate 4-

phosphatase type II is a tumor suppressor that inhibits PI3K signaling. *Cancer Cell* **16**, 115-125.

Godi, A., Di Campli, A., Konstantakopoulos, A., Di Tullio, G., Alessi, D.R., Kular, G.S., et al. and De Matteis, M.A. (2004). FAPPs control Golgi-to-cell-surface membrane traffic by binding to ARF and PtdIns(4)P. *Nat Cell Biol* **6**, 393-404.

Goh, L.K., Huang, F., Kim, W., Gygi, S., and Sorkin, A. (2010). Multiple mechanisms collectively regulate clathrin-mediated endocytosis of the epidermal growth factor receptor. *J Cell Biol* **189**, 871-883.

Grant, B.D., and Donaldson, J.G. (2009). Pathways and mechanisms of endocytic recycling. *Nat Rev Mol Cell Biol* **10**, 597-608.

Gruenberg, J. (2003). Lipids in endocytic membrane transport and sorting. *Curr Opin Cell Biol* **15**, 382-388.

Håberg, K., Lundmark, R., and Carlsson, S.R. (2008). SNX18 is an SNX9 paralog that acts as a membrane tubulator in AP-1-positive endosomal trafficking. *J Cell Sci* **121**, 1495-1505.

Hammond, G.R.V., Fischer, M.J., Anderson, K.E., Holdich, J., Koteci, A., Balla, T., and Irvine, R.F. (2012). PI4P and PI(4,5)P2 Are Essential But Independent Lipid Determinants of Membrane Identity. *Science* **727**, 2-6.

Harris, D.P., Vogel, P., Wims, M., Moberg, K., Humphries, J., Jhaver, K.G., et al. and Oravecz, T. (2011). Requirement for class II phosphoinositide 3-kinase C2alpha in maintenance of glomerular structure and function. *Mol Cell Biol* **31**, 63-80.

Haucke, V., Neher, E., and Sigrist, S.J. (2011). Protein scaffolds in the coupling of synaptic exocytosis and endocytosis. *Nat Rev Neurosci* **12**, 127-138.

Heilemann, M., van de Linde, S., Schüttpelz, M., Kasper, R., Seefeldt, B., Mukherjee, A., et al. and Sauer, M. (2008). Subdiffraction-resolution fluorescence imaging with conventional fluorescent probes. *Angew Chem Int Ed* **47**, 6172-6176.

Henne, W.M., Boucrot, E., Meinecke, M., Evergren, E., Vallis, Y., Mittal, R., and McMahon, H.T. (2010). FCHo proteins are nucleators of clathrin-mediated endocytosis. *Science* **328**, 1281-1284.

Henne, W.M., Buchkovich, N.J., and Emr, S.D. (2011). The ESCRT pathway. *Dev Cell* **21**, 77-91.

Henne, W.M., Kent, H.M., Ford, M.G.J., Hegde, B.G., Daumke, O., Butler, P.J.G., et al. and McMahon, H.T. (2007). Structure and analysis of FCHo2 F-BAR domain: a dimerizing and membrane recruitment module that effects membrane curvature. *Structure* **15**, 839-852.

Heuser, J. (1980). Three-dimensional visualization of coated vesicle formation in fibroblasts. *J Cell Biol* **84**, 560-583.

Ho, C.Y., Alghamdi, T.a., and Botelho, R.J. (2012). Phosphatidylinositol-3,5-bisphosphate: no longer the poor PIP2. *Traffic* **13**, 1-8.

Hokin, L.E., and Hokin, M.R. (1958). Phosphoinositides and protein secretion in pancreas slices. *J Biol Chem* **233**, 805-810.

Hokin, M.R., and Hokin, L.E. (1953). Enzyme secretion and the incorporation of P32 into phospholipides of pancreas slices. *J Biol Chem* **203**, 967-977.

Höning, S., Ricotta, D., Krauss, M., Späte, K., Spolaore, B., Motley, A., et al. and Owen, D.J. (2005). Phosphatidylinositol-(4,5)-bisphosphate regulates sorting signal recognition by the clathrin-associated adaptor complex AP2. *Mol Cell* **18**, 519-531.

Ivetac, I., Munday, A.D., and Kisseleva, M.V. (2005). The type Iα inositol polyphosphate 4-phosphatase generates and terminates phosphoinositide 3-kinase signals on endosomes and the plasma membrane. *Mol Biol Cell* **16**, 2218-2233.

Jackson, L.P., Kelly, B.T., McCoy, A.J., Gaffry, T., James, L.C., Collins, B.M., et al. and Owen, D.J. (2010). A large-scale conformational change couples membrane recruitment to cargo binding in the AP2 clathrin adaptor complex. *Cell* **141**, 1220-1229.

Johnson, E.E., Overmeyer, J.H., Gunning, W.T., and Maltese, W.a. (2006). Gene silencing reveals a specific function of hVps34 phosphatidylinositol 3-kinase in late versus early endosomes. *J Cell Sci* **119**, 1219-1232.

Kahlfeldt, N., Vahedi-Faridi, A., Koo, S.J., Schäfer, J.G., Krainer, G., Keller, S., et al. and Haucke, V. (2010). Molecular basis for association of PIPKI gamma-p90 with clathrin adaptor AP-2. *J Biol Chem* **285**, 2734-2749.

Keen, J.H., Willingham, M.C., and Pastan, I.H. (1979). Clathrin-coated vesicles: isolation, dissociation and factor-dependent reassociation of clathrin baskets. *Cell* **16**, 303-312.

Kim, Y.J., Guzman-hernandez, M.L., and Balla, T. (2011). A Highly Dynamic ER-Derived Phosphatidylinositol-Synthesizing Organelle Supplies Phosphoinositides to Cellular Membranes. *Dev Cell* **21**, 813-824.

Kok, K., Geering, B., and Vanhaesebroeck, B. (2009). Regulation of phosphoinositide 3-kinase expression in health and disease. *Trends Biochem Sci* **34**, 115-127.

Koo, S.J., Markovic, S., Puchkov, D., Mahrenholz, C.C., Beceren-Braun, F., Maritzen, T., et al. and Haucke, V. (2011). SNARE motif-mediated sorting of synaptobrevin by the endocytic adaptors clathrin assembly lymphoid myeloid leukemia (CALM) and AP180 at synapses. *Proc Natl Acad Sci USA* **108**, 13540-13545.

Krause, M., Leslie, J.D., Stewart, M., Lafuente, E.M., Valderrama, F., Jagannathan, R., et al. and Gertler, F.B. (2004). Lamellipodin, an Ena/VASP ligand, is implicated in the regulation of lamellipodial dynamics. *Dev Cell* **7**, 571-583.

Krauss, M., and Haucke, V. (2007). Phosphoinositide-metabolizing enzymes at the interface between membrane traffic and cell signalling. *EMBO Rep* **8**, 241-246.

Krauss, M., Kukhtina, V., Pechstein, A., and Haucke, V. (2006). Stimulation of phosphatidylinositol kinase type I-mediated phosphatidylinositol (4,5)-bisphosphate synthesis by AP-2 μ – cargo complexes. *Proc Natl Acad Sci USA* **103**, 11934-11939.

Laemmli, U.K. (1970). Cleavage of structural proteins during the assembly of the head of bacteriophage T4. *Nature* **227**, 680-685.

Laketa, V., Zarbakhsh, S., Morbier, E., Subramanian, D., Dinkel, C., Brumbaugh, J., et al. and Schultz, C. (2009). Membrane-permeant phosphoinositide derivatives as modulators of growth factor signaling and neurite outgrowth. *Chem Biol* **16**, 1190-1196.

Lampe, A., Haucke, V., Sigrist, S.J., Heilemann, M., and Schmoranzer, J. (2012). Multi-colour direct STORM with red emitting carbocyanines. *Biol Cell* **104**, 229-237.

Laplante, M., and Sabatini, D.M. (2012). mTOR signaling in growth control and disease. *Cell* **149**, 274-293.

Leibiger, B., Moede, T., Uhles, S., Barker, C.J., Creveaux, M., Domin, J., et al. and Leibiger, I.B. (2010). Insulin-feedback via PI3K-C2alpha activated PKBalpha/Akt1 is required for glucose-stimulated insulin secretion. *FASEB* **24**, 1824-1837.

Lemmon, M.a. (2008). Membrane recognition by phospholipid-binding domains. *Nat Rev Mol Cell Biol* **9**, 99-111.

Lodish, H., Berk, A., Matsudaira, P., Kaiser, C.A., Krieger, M., Scot, M.P., et al. and Darnell, J. (2003). Molecular Cell Biology, Fifth Edition edn (New York: W.H. Freeman).

Loerke, D., Mettlen, M., Yarar, D., Jaqaman, K., Jaqaman, H., Danuser, G., and Schmid, S.L. (2009). Cargo and dynamin regulate clathrin-coated pit maturation. *PLoS Biol* **7**, e57-e57.

Lundmark, R., and Carlsson, S.R. (2003). Sorting nexin 9 participates in clathrin-mediated endocytosis through interactions with the core components. *J Biol Chem* **278**, 46772-46781.

Lundmark, R., and Carlsson, S.R. (2004). Regulated membrane recruitment of dynamin-2 mediated by sorting nexin 9. *J Biol Chem* **279**, 42694-42702.

Lundmark, R., and Carlsson, S.R. (2009). SNX9 - a prelude to vesicle release. *J Cell Sci* **122**, 5-11.

MacDougall, L.K., Domin, J., and Waterfield, M.D. (1995). A family of phosphoinositide 3-kinases in Drosophila identifies a new mediator of signal transduction. *Curr Biol* **5**, 1404-1415.

Maffucci, T., Cooke, F.T., Foster, F.M., Traer, C.J., Fry, M.J., and Falasca, M. (2005). Class II phosphoinositide 3-kinase defines a novel signaling pathway in cell migration. *J Cell Biol* **169**, 789-799.

Malecz, N., McCabe, P.C., Spaargaren, C., Qiu, R., Chuang, Y., and Symons, M. (2000). Synaptojanin 2, a novel Rac1 effector that regulates clathrin-mediated endocytosis. *Curr Biol* **10**, 1383-1386.

Mani, M., Lee, S.Y., Lucast, L., Cremona, O., Di Paolo, G., De Camilli, P., and Ryan, T.a. (2007). The dual phosphatase activity of synaptojanin1 is required for both efficient synaptic vesicle endocytosis and reavailability at nerve terminals. *Neuron* **56**, 1004-1018.

Massol, R.H., Boll, W., Griffin, A.M., and Kirchhausen, T. (2006). A burst of auxilin recruitment determines the onset of clathrin-coated vesicle uncoating. *Proc Natl Acad Sci USA* **103**, 10265-10270.

McLaughlin, S., Wang, J., Gambhir, A., and Murray, D. (2002). PIP(2) and proteins: interactions, organization, and information flow. *Annu Rev Biophys Biomol Struct* **31**, 151-175.

McMahon, H.T., and Boucrot, E. (2011). Molecular mechanism and physiological functions of clathrin-mediated endocytosis. *Nat Rev Mol Cell Biol* **12**, 517-533.

McMahon, H.T., and Gallop, J.L. (2005). Membrane curvature and mechanisms of dynamic cell membrane remodelling. *Nature* **438**, 590-596.

Meinecke, M., Boucrot, E., Camdere, G., Hon, W.-C., Mittal, R., and McMahon, H.T. (2013). Cooperative recruitment of dynamin and BIN/amphiphysin/Rvs (BAR) domain-containing proteins leads to GTP-dependent membrane scission. *J Biol Chem* **288**, 6651-6661.

Merrifield, C.J., Feldman, M.E., Wan, L., and Almers, W. (2002). Imaging actin and dynamin recruitment during invagination of single clathrin-coated pits. *Nat Cell Biol* **4**, 691-698.

Meunier, F.A., Osborne, S.L., Hammond, G.R.V., Cooke, F.T., Parker, P.J., Domin, J., and Schiavo, G. (2005). Phosphatidylinositol 3-kinase C2alpha is essential for ATP-dependent priming of neurosecretory granule exocytosis. *Mol Biol Cell* **16**, 4841-4851.

Michell, R.H. (2008). Inositol derivatives: evolution and functions. *Nat Rev Mol Cell Biol* **9**, 151-161.

Miele, A.E., Watson, P.J., Evans, P.R., Traub, L.M., and Owen, D.J. (2004). Two distinct interaction motifs in amphiphysin bind two independent sites on the clathrin terminal domain beta-propeller. *Nat Struct Mol Biol* **11**, 242-248.

Milosevic, I., Giovedi, S., Lou, X., Raimondi, A., Collesi, C., Shen, H., et al. and De Camilli, P. (2011). Recruitment of Endophilin to Clathrin-Coated Pit Necks Is Required for Efficient Vesicle Uncoating after Fission. *Neuron* **72**, 587-601.

Nakano-Kobayashi, A., Yamazaki, M., Unoki, T., Hongu, T., Murata, C., Taguchi, R., et al. and Kanaho, Y. (2007). Role of activation of PIP5Kγ661 by AP-2 complex in synaptic vesicle endocytosis. *EMBO J* **26**, 1105-1116.

Nakatsu, F., Baskin, J.M., Chung, J., Tanner, L.B., Shui, G., Lee, S.Y., et al. and De Camilli, P. (2012). PtdIns4P synthesis by PI4KIIIα at the plasma membrane and its impact on plasma membrane identity. *J Cell Biol* **199**, 1003-1016.

Nakatsu, F., Perera, R.M., Lucast, L., Zoncu, R., Domin, J., Gertler, F.B., et al. and De Camilli, P. (2010). The inositol 5-phosphatase SHIP2 regulates endocytic clathrin-coated pit dynamics. *J Cell Biol* **190**, 307-315.

Neumann, S., and Schmid, S.L. (2013). Dual role of BAR domain-containing proteins in regulating dynamin-2 catalyzed vesicle release. *J Biol Chem* advance online publication. **doi:** 10.1074/jbc.M113.490474

Nielsen, E., Christoforidis, S., Uttenweiler-Joseph, S., Miaczynska, M., Dewitte, F., Wilm, M., et al. and Zerial, M. (2000). Rabenosyn-5, a novel Rab5 effector, is complexed with hVPS45 and recruited to endosomes through a FYVE finger domain. *J Cell Biol* **151**, 601-612.

Ohya, T., Miaczynska, M., Coskun, U., Lommer, B., Runge, A., Drechsel, D., et al. and Zerial, M. (2009). Reconstitution of Rab- and SNARE-dependent membrane fusion by synthetic endosomes. *Nature* **459**, 1091-1097.

Oikawa, T., Itoh, T., and Takenawa, T. (2008). Sequential signals toward podosome formation in NIH-src cells. *J Cell Biol* **182**, 157-169.

Otsuki, M., Itoh, T., and Takenawa, T. (2003). Neural Wiskott-Aldrich syndrome protein is recruited to rafts and associates with endophilin A in response to epidermal growth factor. *J Biol Chem* **278**, 6461-6469.

Park, J., Kim, Y., Lee, S., Park, J.J., Park, Z.Y., Sun, W., et al. and Chang, S. (2010). SNX18 shares a redundant role with SNX9 and modulates endocytic trafficking at the plasma membrane. *J Cell Sci* **123**, 1742-1750.

Patel, K.M., and Watson, M.L. (2005). Differential sensitivity of class II phosphoinositide 3-kinase (PI3K) isoforms to broad spectrum P13K inhibitors. *Pa2 Online* **2**, 294002-294002.

Pearse, B.M. (1976). Clathrin: a unique protein associated with intracellular transfer of membrane by coated vesicles. *Proc Natl Acad Sci USA* **73**, 1255-1259.

Perera, R.M., Zoncu, R., Lucast, L., De Camilli, P., and Toomre, D. (2006). Two synaptojanin 1 isoforms are recruited to clathrin-coated pits at different stages. *Proc Natl Acad Sci USA* **103**, 19332-19337.

Pirola, L., Zvelebil, M.J., Bulgarelli-Leva, G., Van Obberghen, E., Waterfield, M.D., and Wymann, M.P. (2001). Activation loop sequences confer substrate specificity to phosphoinositide 3-kinase alpha (PI3Kalpha). Functions of lipid kinase-deficient PI3Kalpha in signaling. *J Biol Chem* **276**, 21544-21554.

Prior, I.a., and Clague, M.J. (1999). Localization of a class II phosphatidylinositol 3-kinase, PI3KC2alpha, to clathrin-coated vesicles. *Mol Cell Biol Res Comm* **1**, 162-166.

Pylypenko, O., Lundmark, R., Rasmuson, E., Carlsson, S.R., and Rak, A. (2007). The PX-BAR membrane-remodeling unit of sorting nexin 9. *EMBO J* **26**, 4788-4800.

Rameh, L.E., and Cantley, L.C. (1999). The role of phosphoinositide 3-kinase lipid products in cell function. *J Biol Chem* **274**, 8347-8350.

Razidlo, G.L., Katafiasz, D., and Taylor, G.S. (2011). Myotubularin regulates Akt-dependent survival signaling via phosphatidylinositol 3-phosphate. *J Biol Chem* **286**, 20005-20019.

Rohde, G., Wenzel, D., and Haucke, V. (2002). A phosphatidylinositol (4, 5)-bisphosphate binding site within μ2-adaptin regulates clathrin-mediated endocytosis. *J Cell Biol*.

Roth, T.F., and Porter, K.R. (1964). Yolk protein uptake in the oocyte of the mosquito Aedes aegypti. L. *J Cell Biol*, 313-332.

Roux, A., Koster, G., Lenz, M., Sorre, B., Manneville, J.-B., Nassoy, P., and Bassereau, P. (2010). Membrane curvature controls dynamin polymerization. *Proc Natl Acad Sci USA* **107**, 4141-4146.

Roux, A., Uyhazi, K., Frost, A., and De Camilli, P. (2006). GTP-dependent twisting of dynamin implicates constriction and tension in membrane fission. *Nature* **441**, 528-531.

Saheki, Y., and De Camilli, P. (2012). Synaptic vesicle endocytosis. *Cold Spring Harbor Persp Biol* **4**, a005645-a005645.

Saiki, R.K., Gelfand, D.H., Stoffel, S., Scharf, S.J., Higuchi, R., Horn, G.T., et al. and Erlich, H.a. (1988). Primer-directed enzymatic amplification of DNA with a thermostable DNA polymerase. *Science* **239**, 487-491.

Santiago-Tirado, F.H., and Bretscher, A. (2011). Membrane-trafficking sorting hubs: cooperation between PI4P and small GTPases at the trans-Golgi network. *Trends Cell Biol* **21**, 515-525.

Schlossman, D.M., Schmid, S.L., Braell, W.a., and Rothman, J.E. (1984). An enzyme that removes clathrin coats: purification of an uncoating ATPase. *J Cell Biol* **99**, 723-733.

Schneider, C.a., Rasband, W.S., and Eliceiri, K.W. (2012). NIH Image to ImageJ: 25 years of image analysis. *Nat Meth* **9**, 671-675.

Schöneberg, J., Ullrich, A., Posor, Y., Haucke, V., and Noé, F. (2013). Spatiotemporal model of a key step in endocytosis: SNX9 recruitment via phosphoinositides. *arXiv preprint*. **arXiv:**1307.4614

Shin, H.-W., Hayashi, M., Christoforidis, S., Lacas-Gervais, S., Hoepfner, S., Wenk, M.R., et al. and Zerial, M. (2005). An enzymatic cascade of Rab5 effectors regulates phosphoinositide turnover in the endocytic pathway. *J Cell Biol* **170**, 607-618.

Shin, N., Ahn, N., Chang-Ileto, B., Park, J., Takei, K., Ahn, S.-G., et al. and Chang, S. (2008). SNX9 regulates tubular invagination of the plasma membrane through interaction with actin cytoskeleton and dynamin 2. *J Cell Sci* **121**, 1252-1263.

Simonsen, A., Lippe, R., Christoforidis, S., Gaullier, J.M., Brech, A., Callaghan, J., et al. and Stenmark, H. (1998). EEA1 links PI (3) K function to Rab5 regulation of endosome fusion. *Nature* **394**, 2-6.

Simonsen, A., and Tooze, S.a. (2009). Coordination of membrane events during autophagy by multiple class III PI3-kinase complexes. *J Cell Biol* **186**, 773-782.

Soda, K., and Balkin, D.M. (2012). Role of dynamin, synaptojanin, and endophilin in podocyte foot processes. *J Clin Invest* **122**.

Sorkin, A., and von Zastrow, M. (2009). Endocytosis and signalling: intertwining molecular networks. *Nat Rev Mol Cell Biol* **10**, 609-622.

Soulet, F., Yarar, D., Leonard, M., and Schmid, S.L. (2005). SNX9 regulates dynamin assembly and is required for efficient clathrin-mediated endocytosis. *Mol Biol Cell* **16**, 2058-2067.

Stachowiak, J.C., Schmid, E.M., Ryan, C.J., Ann, H.S., Sasaki, D.Y., Sherman, M.B., et al. and Hayden, C.C. (2012). Membrane bending by protein-protein crowding. *Nat Cell Biol* **14**, 944-949.

Stahelin, R.V., Karathanassis, D., Bruzik, K.S., Waterfield, M.D., Bravo, J., Williams, R.L., and Cho, W. (2006). Structural and membrane binding analysis of the Phox homology domain of phosphoinositide 3-kinase-C2alpha. *J Biol Chem* **281**, 39396-39406.

Subramanian, D., Laketa, V., Müller, R., Tischer, C., Zarbakhsh, S., Pepperkok, R., and Schultz, C. (2010). Activation of membrane-permeant caged PtdIns(3)P induces endosomal fusion in cells. *Nat Chem Biol* **6**, 324-326.

Szentpetery, Z., Várnai, P., and Balla, T. (2010). Acute manipulation of Golgi phosphoinositides to assess their importance in cellular trafficking and signaling. *Proc Natl Acad Sci USA* **107**, 8225-8230.

Taylor, M.J., Perrais, D., and Merrifield, C.J. (2011). A high precision survey of the molecular dynamics of mammalian clathrin-mediated endocytosis. *PLoS Biol* **9**, e1000604-e1000604.

Ter Haar, E., C Harrison, S., and Kirchhausen, T. (2000). Peptide-in-groove interactions link target proteins to the beta-propeller of clathrin. *Proc Natl Acad Sci USA* **97**, 1096-1100.

Thieman, J.R., Mishra, S.K., Ling, K., Doray, B., Anderson, R.a., and Traub, L.M. (2009). Clathrin regulates the association of PIPKIgamma661 with the AP-2 adaptor beta2 appendage. *J Biol Chem* **284**, 13924-13939.

Traub, L.M. (2009). Tickets to ride: selecting cargo for clathrin-regulated internalization. *Nat Rev Mol Cell Biol* **10**, 583-596.

Umasankar, P.K., Sanker, S., Thieman, J.R., Chakraborty, S., Wendland, B., Tsang, M., and Traub, L.M. (2012). Distinct and separable activities of the endocytic clathrin-coat components Fcho1/2 and AP-2 in developmental patterning. *Nat Cell Biol* **14**, 488-501.

Ungewickell, E., Ungewickell, H., Holstein, S.E.H., Lindner, R., Prasad, K., Barouch, W., et al. and Eisenberg, E. (1995). Role of auxillin in uncoating clathrin-coated vesicles. *Nature* **378**, 632-635.

van den Bogaart, G., Meyenberg, K., Risselada, H.J., Amin, H., Willig, K.I., Hubrich, B.E., et al. and Jahn, R. (2011). Membrane protein sequestering by ionic protein–lipid interactions. *Nature*, 4-7.

van Meer, G., Voelker, D.R., and Feigenson, G.W. (2008). Membrane lipids: where they are and how they behave. *Nat Rev Mol Cell Biol* **9**, 112-124.

Vanhaesebroeck, B., Guillermet-Guibert, J., Graupera, M., and Bilanges, B. (2010). The emerging mechanisms of isoform-specific PI3K signalling. *Nat Rev Mol Cell Biol* **11**, 329-341.

Vanhaesebroeck, B., Stephens, L., and Hawkins, P. (2012). PI3K signalling: the path to discovery and understanding. *Nat Rev Mol Cell Biol* **13**, 195-203.

Varnai, P., Thyagarajan, B., Rohacs, T., and Balla, T. (2006). Rapidly inducible changes in phosphatidylinositol 4,5-bisphosphate levels influence multiple regulatory functions of the lipid in intact living cells. *J Cell Biol* **175**, 377-382.

Wang, Y.J., Wang, J., Sun, H.Q., Martinez, M., Sun, Y.X., Macia, E., et al. and Yin, H.L. (2003). Phosphatidylinositol 4 phosphate regulates targeting of clathrin adaptor AP-1 complexes to the Golgi. *Cell* **114**, 299-310.

Wen, P.J., Osborne, S.L., and Meunier, F.a. (2011). Dynamic control of neuroexocytosis by phosphoinositides in health and disease. *Prog Lipid Res* **50**, 52-61.

Wen, P.J., Osborne, S.L., Morrow, I.C., Parton, R.G., Domin, J., and Meunier, F.A. (2008). Ca2+-regulated pool of phosphatidylinositol-3-phosphate produced by phosphatidylinositol 3-kinase C2alpha on neurosecretory vesicles. *Mol Biol Cell* **19**, 5593-5603.

Wheeler, M., and Domin, J. (2006). The N-terminus of phosphoinositide 3-kinase-C2beta regulates lipid kinase activity and binding to clathrin. *J Cell Physiol* **206**, 586-593.

Wieffer, M., Haucke, V., and Krauss, M. (2012). Regulation of phosphoinositide-metabolizing enzymes by clathrin coat proteins. *Meth Cell Biol* **108**, 209-225.

Wieffer, M., Maritzen, T., and Haucke, V. (2009). SnapShot: endocytic trafficking. *Cell* **137**, 382.e381-383.

Wolter, S., Schüttpelz, M., Tscherepanow, M., Van De Linde, S., Heilemann, M., and Sauer, M. (2010). Real-time computation of subdiffraction-resolution fluorescence images. *J Micrsoc* **237**, 12-22.

Wu, M., Huang, B., Graham, M., Raimondi, A., Heuser, J.E., Zhuang, X., and De Camilli, P. (2010). Coupling between clathrin-dependent endocytic budding and F-BAR-dependent tubulation in a cell-free system. *Nat Cell Biol* **12**, 902-908.

Wymann, M.P., and Schneiter, R. (2008). Lipid signalling in disease. *Nat Rev Mol Cell Biol* **9**, 162-176.

Yamada, H., Padilla-Parra, S., Park, S.-J., Itoh, T., Chaineau, M., Monaldi, I., et al. and Takei, K. (2009). Dynamic interaction of amphiphysin with N-WASP regulates actin assembly. *J Biol Chem* **284**, 34244-34256.

Yarar, D., Surka, M.C., Leonard, M.C., and Schmid, S.L. (2008). SNX9 activities are regulated by multiple phosphoinositides through both PX and BAR domains. *Traffic* **9**, 133-146.

Yarar, D., Waterman-Storer, C.M., and Schmid, S.L. (2005). A dynamic actin cytoskeleton functions at multiple stages of clathrin-mediated endocytosis. *Mol Biol Cell* **16**, 964-975.

Yarar, D., Waterman-Storer, C.M., and Schmid, S.L. (2007). SNX9 couples actin assembly to phosphoinositide signals and is required for membrane remodeling during endocytosis. *Dev Cell* **13**, 43-56.

Yoshioka, K., Yoshida, K., Cui, H., Wakayama, T., Takuwa, N., Okamoto, Y., et al. and Takuwa, Y. (2012). Endothelial PI3K-C2α, a class II PI3K, has an essential role in angiogenesis and vascular barrier function. *Nat Med*.

Zeigerer, A., Gilleron, J., Bogorad, R.L., Marsico, G., Nonaka, H., Seifert, S., et al. and Zerial, M. (2012). Rab5 is necessary for the biogenesis of the endolysosomal system in vivo. *Nature* **485**, 465-470.

Zerial, M., and McBride, H. (2001). Rab proteins as membrane organizers. *Nat Rev Mol Cell Biol* **2**, 107-117.

Zhao, Y., Gaidarov, I., and Keen, J.H. (2007). Phosphoinositide 3-kinase C2alpha links clathrin to microtubule-dependent movement. *J Biol Chem* **282**, 1249-1256.

Zoncu, R., Perera, R.M., Balkin, D.M., Pirruccello, M., Toomre, D., and De Camilli, P. (2009). A phosphoinositide switch controls the maturation and signaling properties of APPL endosomes. *Cell* **136**, 1110-1121.

Zoncu, R., Perera, R.M., Sebastian, R., Nakatsu, F., Chen, H., Balla, T., et al. and De Camilli, P.V. (2007). Loss of endocytic clathrin-coated pits upon acute depletion of phosphatidylinositol 4,5-bisphosphate. *Proc Natl Acad Sci USA* **104**, 3793-3798.

6 Appendix

6.1 Appendix A: Abbreviations

ABP	actin-binding proteins
AM	acetoxymethylester
AP-2	adaptor protein complex 2
Arf1	ADP-ribosylation factor 1
BAR	Bin1 / amphiphysin / Rvs
BSA	bovine serum albumine
BSE	bundle signaling element
CCP	Clathrin-coated pit
CCV	clathrin-coated vesicle
CHC	clathrin heavy chain
CI	catalytically inactive
cl.III mut	class III-like mutant
CLASP	clathrin-associated sorting protein
CLC	clathrin light chain
CME	clathrin-mediated endocytosis
CTD	clathrin terminal domain
DAG	diacylglycerol
EGF	epidermal growth factor
EM	electron microscopy
ENTH	epsin N-terminal homology
ER	endoplasmic reticulum
ESCRT	endosomal complex required for transport
EtBr	ethidium bromide
FCHo	Fer/Cip4 homology domain-only proteins
FERM	band4.1 / Ezrin / Radixin / Moesin
FRAP	Fluorescence recovery after photobleaching
FYVE	Fab1, YOTB, Vac1, EEA1
GPCR	G-protein coupled receptor
GSDB	goat serum dilution buffer
Hsc70	heat shock cognate 70
INPP4B	type II inositol 3,4-bisphosphate 4-phosphatase
IP_3	inositol-1,4,5-trisphosphate
KO	knockout
MEF	Mouse embryonic fibroblast
MTM1	Myotubularin 1
mTOR	mammalian target of rapamycin
MVB	multi-vesicular body

N-BAR	N-terminal amphipathic helix BAR
PDGF	platelet-derived growth factor
PH	pleckstrin-homology
PI	phosphoinositide
PI(3)P	phosphatidylinositol-3-phosphate
$PI(3,4)P_2$	phosphatidylinositol-3,4-bisphosphate
$PI(3,4,5)P_3$	phosphatidylinositol-3,4,5-trisphosphate
$PI(3,5)P_2$	phosphatidylinositol-3,5-bisphosphate
PI(4)P	phosphatidylinositol-4-phosphate
$PI(4,5)P_2$	phosphatidylinositol-4,5-bisphosphate
PI3K	phosphoinositide-3-kinase
PI4K	phosphatidylinositol-4-kinase
PIP5K	phosphatidylinositol-4-phosphate 5-kinases
PKC	protein kinase C
PLC	phosphoinositide-specific phospholipase C
PRD	proline rich domain
PTEN	phosphatase and tensin homologue deleted on chromosome 10
PX	phox homology
REN	Restriction endonuclease
RTK	receptor tyrosine kinase
SD-*d*STORM	spectral demixing direct stochastic optical reconstruction microscopy
SH3	src homology 3
SHIP	SH2 domain-containing inositol 5-phosphatase
siRNA	small interfering RNA
Sjn	synaptojanin
SNX	sorting nexin
SNX9	sorting nexin 9
SV	synaptic vesicle
TGN	*trans*-Golgi network
TIRF	Total internal reflection fluorescence
TLC	thin layer chromatography
TSC1/2	tuberous sclerosis proteins 1/2
WASP	Wiskott-Aldrich syndrome protein
WAVE	WASP family verprolin homologous protein
WT	wild-type

6.2 Appendix B: List of Figures

6.3 Appendix C: Primers (DNA oligonucleotides)

Table 6-1: List of all primers used in this study. Primers are mostly named according to the following pattern: [amplificate name] [position of first 5' nucleotide in the cDNA, numbering starting at the initiator methionine codon] [forward/reverse] [restriction endonuclease site in primer overhang].

Primer name	Sequence 5' to 3'	Amplificate
PC2a nt1 fw SpeI	agtc actagt atggctcagatatttagcaacagcgg	human PI3K C2α
PC2a 1383 rev EcoRI	agtc GAATTC gtcatcatgtacccagcaaagggc	human PI3K C2α
PC2a 1233 int NdeI fw	cacagcgcaaagaaacatatgcggag	human PI3K C2α
PC2a 1356 Fusion fw	gcaagccctttgctgggtacatgatga	human PI3K C2α
PC2a 2290 rev EcoRI	agtc GAATTC gagtaaggtgaagaactgattctaatggc	human PI3K C2α
PC2a 2222 fw SpeI	agtc actagt gggatgaactaatcatttttcctatcca	human PI3K C2α
PC2a 5061 rev EcoRI	agtc GAATTC ttacaagtatgttgccgcagtcagc	human PI3K C2α
PC2a 2851 fw seq	gctgatcaggaagtaagatccc	human PI3K C2α
PC2a 3521 fw seq	gtctctcaactggcagagatc	human PI3K C2α
PHtapp fw EcoRI	agtc gaattc tttactcctaaaccacctcaagatagt	PH domain of TAPP1 aa 182-303
PHtapp rev	gggatgctcagaagacgcag	PH domain of TAPP1 aa 182-304
PHtapp Fus fw	gatctgcgtcttctgagcatccctttactcctaaaccacctcaagatag	PH domain of TAPP1 aa 182-305
PHtapp revstop NotI	agtc gcggccgc tcagggatgctcagaagacgc	PH domain of TAPP1 aa 182-306
PC2a K1138A	ggagaagaaattaatgtcatgtttgctgttggtgaagatcttcgg	vector PCR human PI3K C2α
PC2a D1157A	cagatgataaagattatggctaagatctggcttaaagaagg	vector PCR human PI3K C2α
PC2a D1250A	cctatgttttaggcatctgtgctcgacacaatgac	vector PCR human PI3K C2α
PC2a 1 fw EcoRI	agtc GAATTC atggctcagatatttagcaacagcgg	human PI3K C2α
PC2a 990 rev XhoI	agtc ctcgag TCA cacagaaagggattttccattcacc	human PI3K C2α
PC2a 1978 fw EcoRI	agtc GAATTC gcaaattctggtaggagtcctacag	human PI3K C2α
PC2a 3180 rev XhoI	agtc ctcgag TCA tgctactcctcctaaaagctgtacaag	human PI3K C2α
PC2a D1157Aalter	gctttacagatgataaagattatggctaagatctggc	vector PCR human PI3K C2α
PC2a 5061 R NotI	agtc gcggccgc ttacaagtatgttgccgcagtcagc	human PI3K C2α
PC2a D1157A rev	gccagatcttagccataatctttatcatctgtaaagc	vector PCR human PI3K C2α
PC2a K1138A rev	ccgaagatcttcaccaacagcaaacatgacattaatttcttctcc	vector PCR human PI3K C2α
PC2a D1250A rev	gtcattgtgtcgagcacagatgcctaaaacatagg	vector PCR human PI3K C2α
PC2a 298 fw EcoRI	agtc GAATTC cttgagaaactattgctggatgacagtttcg	human PI3K C2α
PC2a 945 rev XhoI	agtc ctcgag TCA tgctgtcgatctctcttcaagaagaacag	human PI3K C2α
PC2a 1999 fw EcoRI	agtc GAATTC acagactgtgcccaaagtagcaag	human PI3K C2α
PC2a 2202 rev XhoI	agtc ctcgag TCA attcttgtaagtgccaaccttctttgattg	human PI3K C2α

Primer name	Sequence 5' to 3'	Amplificate
PC2a 2955 rev XhoI	agtc ctcgag TCA ttcatatttcaaagcttgtacaaactgtgg	human PI3K C2α
PC2a 4221 rev XhoI	agtc ctcgag TCA gggctcatcattagaaggaagacc	human PI3K C2α
mCherry fw KpnI	agtc ggtacc atggtgagcaagggcgaggagg	mCherry
mCherry rev BamHI	agtc ggatcc cttgtacagctcgtccatgccgc	mCherry
APPL1 rev NotI	agtc gcggccgc ttatgcttctgattctctcttctttcctcc	human APPL1 FL
PC2a 4 fw EcoRI	agtc GAATTC gctcagatatttagcaacagcgg	human PI3K C2α
PC2a 1095 rev XhoI	agtc ctcgag TCA tggcaaactactggtcccatttgg	human PI3K C2α
PC2a 702 rev XhoI	agtc ctcgag TCA tgatgtactagctattttgtcaaatagttttgc	human PI3K C2α
PC2 B 1 fw EcoRI	agtc GAATTC atgtcttcgactcagggcaatggg	human PI3K C2β
PC2 B 4905 R NotI	agtc gcggccgc tcacaaggtgccatgacttcgagatc	human PI3K C2β
PC2 B 819 rev XhoI	agtc ctcgag TCA gggttttccagaggtgtctttgctg	human PI3K C2β
DhcSP#2 RES F	ccaatcacc ggacgaacccgggttattt gttaagtcc	vector PCR human PI3K C2α
DhcSP#2 RES R	ggacttaac aaataacccgggttcgtcc ggtgattgg	vector PCR human PI3K C2α
Ambion RES F	ggaaa agatctattcaaaccgatt caatcaaagaaggttggc	vector PCR human PI3K C2α
Ambion RES R	gccaaccttctttgattg aatcggtttgaatagatct tttcc	vector PCR human PI3K C2α
p85 iSH2 F KpnI	agtc GGTACC ATG aaataccaacaggatcaagttgtcaaagaag	p85 inter-SH2 domain
p85 iSH2 R BamHI	agtc GGATCC TCA gggcaaatcttcatcatcttccacc	p85 inter-SH2 domain
rat Dnm2 siR#2 F	ctgaacca gcaattgacaaaccatatc cgggag	vector PCR rat Dynamin 2
rat Dnm2 siR#2 R	ctcccg gatatggtttgtcaattgc tggttcag	vector PCR rat Dynamin 2
rat Dnm2 804 F	ggctgaccgcatgggtac	rat Dynamin 2
rat Dnm2 2197 R	gcgcttccttgagtgcatgg	rat Dynamin 2
PC2aΔcore 2019R	cgatcgggatcccttaag gctactttgggcacagtctgtagg	5' fragment of ΔCore mutant
PC2aΔcore 4201F	gcccaaagtagc cttaagggatcccgatcg cttccttctaatgatgagcccatcc	3' fragment of ΔCore mutant
p110α 967F AflII	agct cttaag tctacaaaatccctttgggttataaatagagc	p110α catalytic domain
p110α 3204R PvuI	agct cgatcg gttcaatgcatgctgtttaattgtgtgg	p110α catalytic domain
SHIP2 1267F AflII	agct cttaag atgatctcagtcttcataggcacctgg	SHIP2 phosphatase domain
SHIP2 2205R PvuI	agct cgatcg ggagatgaactgggaggtaactcc	SHIP2 phosphatase domain
PTEN 40 F AflII	agct cttaag aggagatatcaagaggatggattcg	PTEN phosphatase domain
PTEN 555 R PvuI	agct cgatcg atgattctttaacaggtagctataataatacac	PTEN phosphatase domain
p110α 634 F seq	gctcaaagcaatttctacacgagatc	p110α catalytic domain
p110a 967F PvuI	agct cgatcg tctacaaaatccctttgggttataaatagagc	p110α catalytic domain
SHIP2 1267F PvuI	agct cgatcg atgatctcagtcttcataggcacctgg	SHIP2 phosphatase domain

Primer name	Sequence 5' to 3'	Amplificate
PTEN 40 F PvuI	agct cgatcg aggagatatcaagaggatggattcg	PTEN phosphatase domain
CALM 1 F EcoRI	agtc GAATTC atgtccggccagagcctgacg	human CALM ANTH domain
CALM 459 R fuse	cctcatctgtcacctccagg ccatcagcccctctcttcacttttg	CALM ANTH domain for fusion with Hip1R
Hip1R 457 F fuse	gtgaagagaggggctgat ggcctggaggtgacagatgagg	Hip1RΔANTH for fusion with CALM ANTH
Hip1R 3297 R NotI	agtc gcggccgc ctagtagttcacgagttgagctggg	Hip1RΔANTH
INPP4B 1 F XhoI	agtc ctcgag atggaaattaaagaggaaggggcatc	human INPP4B
INPP4B 2775 R KpnI	agtc ggtacc ttaggtgtcagcttttccataagtcc	human INPP4B
INPP4B 724 F	cccacatctgacaataagtgg	human INPP4B
INPP4B 1462 F	cctaagagcagcacagagg	human INPP4B
PC2a3843 cImutR	gctgcc cttcgtcttgaa atgtcccaaaaactttccaaagtcaatg	PI3K C2α class I activation loop mutant 5` fragment
PC2a 3822 cIII R	gggtggcaggggcttggggtccct tcccaaaaactttccaaagtcaatgtg	PI3K C2α class III activation loop mutant 5` fragment
PC2a 3862 cIII F	agggaccccaagcccctgccaccc ccttttgtgctgacctctgatatg	PI3K C2α class III activation loop mutant 3` fragment
PC2a 3849 cIII.2 R	ggagcgggcaggggtttgaagctgcc aaacatctgtgc	PI3K C2α class III.2 activation loop mutant 5` fragment
PC2a 3859 cIII.2 F	ggcagcttcaaacccctgcccgctcc ttttgtgctgacctctg	PI3K C2α class III.2 activation loop mutant 3` fragment
PC2a3843 cI.2 R	gctgcccttcttcttcttatggtccaaaaactttcc aaagtcaatgtg	PI3K C2α class I.2 activation loop mutant 5` fragment
PC2a3808 cI.2 F	ggaaagtttttggaccataagaagaagaagggcagc ttcaaaagggatc	PI3K C2α class I.2 activation loop mutant 3` fragment
INPP4B 1 F EcoRV	agtc gatatc atggaaattaaagaggaaggggcatc	human INPP4B
INPP4B 2775 R NotI	agtc gcggccgc cggtgtcagcttttccataagtcc	human INPP4B
INPP4B2775RNot.2	agtc gcggccgc ggtgtcagcttttccataagtcc	human INPP4B
SNX9 1 F EcoRI	agtc gaattc atggccaccaaggctcgggttatg	human SNX9
SNX9 612 F EcoRI	agtc gaattc ccccttaacaaatttcctggatttgcgaaacc	human SNX9
SNX9 1785 R NotI	agtc gcggccgc ctacatcactggaaagcggctgagg	human SNX9
SNX9 741 F EcoRI	agtc gaattc cctacctctacttttgactgtgtgg	human SNX9
SNX9 1124 R NotI	agtc gcggccgc cta ctcatctctctcggccttcc	human SNX9
INPP4B C842A 2506F	Ggtattcgtttcacctgcgcaaaaagtgccaaagacaggacatcg	INPP4B catalytically inactive 3' fragment
INPP4B C842A 2550R	Cgatgtcctgtctttggcacttttgcgcaggtgaaacgaatacc	INPP4B catalytically inactive 5' fragment
L3 FKBP Xho-out F NotI	agtc gcggccgc gggagcaggaggagcagcacgagc	L3-FKBP-L4

Primer name	Sequence 5' to 3'	Amplificate
L4 FKBP Xho-out R XhoI	agtc CTCGAG tta tcctcctgctcccgctgctgcgcctctagcttcc	L3-FKBP-L4
PC2a +CAAX R EcoRI	agtc GAATTC tta cataattacacactttgtctttgactt caagtatgttgccgcagtcagc	human PI3K C2a-CAAX box[Ras]
hMTM1 1 F EcoRV	agtc gatatc atggcttctgcatcaacttctaaatataattcac	hMTM1 FL
hMTM1 1809R NotI	agtc gcggccgc gaagtgagtttgcacatggggc	hMTM1 FL w/o STOP
hPTEN 1 F EcoRI	agtc GAATTC atgacagccatcatcaaagagatcg	hPTEN FL
hPTEN 1212R NotI	agtc gcggccgc gacttttgtaatttgtgtatgctgatcttcatc	hPTEN FL w/o STOP
INPP5E 640F EcoRV	agtc gatatc tcggatcttgcagactacaagctcc	INPP5E 5-Ptase domain
INPP5E 1932R NotI	agtc gcggccgc agaaacggagcagatggtgctgg	INPP5E 5-Ptase domain w/o STOP
SNX9 1F EcoRI loT_m	agtc gaattc atggccaccaaggctcggg	human SNX9
SNX9 1785R NotI loT_m	agtc gcggccgc ctacatcactggaaagcggctg	human SNX9
SNX9 873R RYK	gtcaaagtgcgcagcctg gtggtttacagatcgattagtgttagtagg	human SNX9
SNX9 841F RYK	cgatctgtaaaccaccaggctgcg cactttgactggttatatgagcgtc	human SNX9
SNX9 811R K267Q	cgatgtagctg tttagaccatacattttggagcctttcc	human SNX9
SNX9 778F K267Q	ggctccaaaatgtatggtctaaac agctacatcgaatatcagc	human SNX9
SNX9 999R R327Q	ggcctgaagtctctccatgtt cattttgataaattcctcttcaaagcggc	human SNX9
SNX9 963F R327Q	ggaatttatcaaaatgaac atggagagacttcaggcctgg	human SNX9

6.4 Appendix D: Publications

Wieffer, M., Cibrian Uhalte, E., **Posor, Y.**, Otten, C., Branz, K., Schütz, I., Mössinger, J., Schu, P., Abdelilah-Seyfried, S., Krauss, M., Haucke, V. (2013). PI4K2β/AP-1-based TGN-endosomal sorting regulates Wnt signaling. *Current Biology* **23***,* 2185-2190.

Posor, Y., Eichhorn-Gruenig, M., Puchkov, D., Schöneberg, J., Ullrich, A., Lampe, A., Müller, R., Zarbakhsh, S., Gulluni, F., Hirsch, E., Krauss, M., Schultz, C., Schmoranzer, J., Noé, F., Haucke, V. (2013). Spatiotemporal control of endocytosis by phosphatidylinositol-3,4-bisphosphate. *Nature* **499**, 233-237.

Schöneberg, J., Ullrich, A., **Posor, Y.**, Haucke, V., and Noé, F. (2013). Spatiotemporal model of a key step in endocytosis: SNX9 recruitment via phosphoinositides. *arXiv preprint*. **arXiv:1307.4614v1**

Faelber, K., Gao, S., Held, M., **Posor, Y.**, Haucke, V., Noé, F., Daumke, O. (2013). Oligomerization of dynamin superfamily proteins in health and disease. *Progress in Molecular Biology and Translational Science* **117**, 411-43.

Faelber, K., Held, M., Gao, S., **Posor, Y.**, Haucke, V., Noé, F., Daumke, O. (2012). Structural insights into dynamin-mediated membrane fission. *Structure* **20**, 1621-8.

Faelber, K., **Posor, Y.**, Gao, S., Held, M., Roske, Y., Schulze, D., Haucke, V., Noé, F., Daumke, O. (2011). Crystal structure of nucleotide-free dynamin. *Nature* **477,** 556-60.